HIRIS

High-Resolution Imaging Spectrometer:
Science Opportunities for the 1990s

## Volume IIc

EARTH OBSERVING SYSTEM

Instrument Panel Report

NASA

National Aeronautics and
Space Administration

HIRIS

High-Resolution Imaging Spectrometer:
Science Opportunities for the 1990s

EARTH OBSERVING SYSTEM
Volume IIc

ATMOSPHERE

SOLID EARTH

CRYOSPHERE

HYDROSPHERE

INSTRUMENT PANEL REPORT

NASA

National Aeronautics and
Space Administration

1987

EARTH OBSERVING SYSTEM REPORTS

HIGH-RESOLUTION IMAGING SPECTROMETER INSTRUMENT PANEL FOR THE EARTH OBSERVING SYSTEM

Alexander F. H. Goetz, Chairman
Michael Abrams, Executive Secretary
Jeff Dozier, HIRIS Project Scientist
Mark Abbott
John D. Aber
John B. Adams
Arden Albee
James E. Anderson
Kendall L. Carder
Siegfried A. W. Gerstl
Laveen N. Kanal
Hugh Kieffer
Dan Kimes
David A. Landgrebe
John MacDonald
James A. MacMahon
John M. Melack
Lawrence C. Rowan
Philip N. Slater
James A. Smith
Richard H. Waring

Ex Officio
William Barnes

Contributors
Vincent Abreu
Ray Arvidson
Marion Baumgardner
James Coakley
Joseph Conley
Curtiss O. Davis
David J. Diner
Larry Esposito
Robert Fraser
Michael Griggs
Mark Herring
John Martonchik
Helen N. Paley
Jerry E. Solomon
Gregg A. Vane

COVER PHOTOGRAPH:
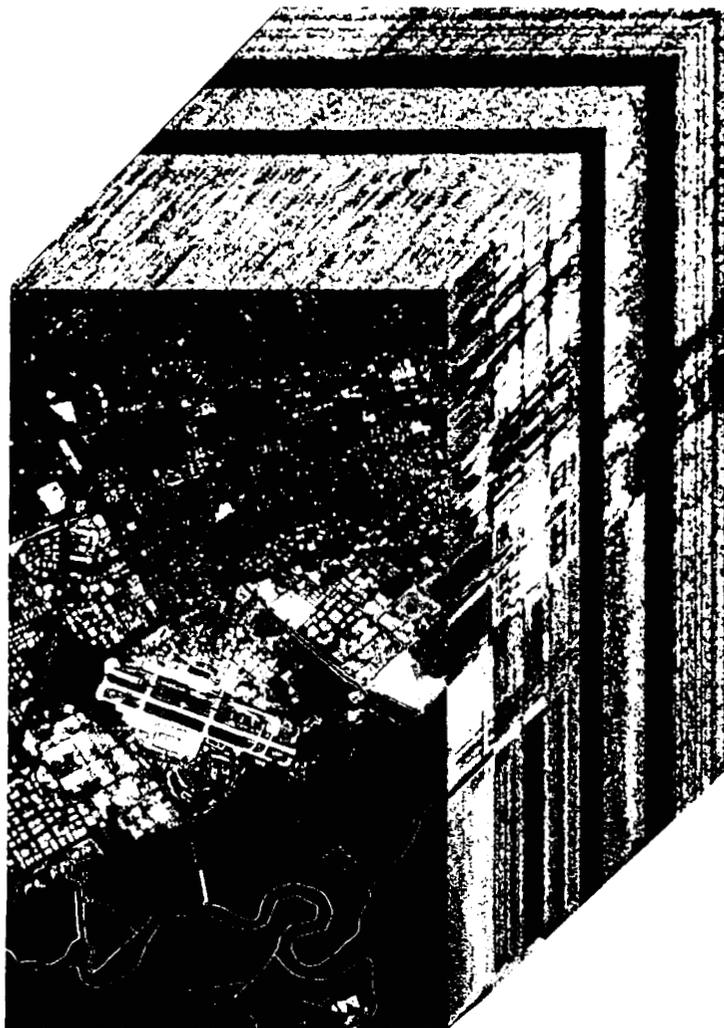
The image on the cover is a portion of a scene centered on the Ames Research Center, California acquired by the Airborne Visible and Infrared Imaging Spectrometer (AVIRIS) aboard the NASA U-2 at an elevation of 20 km. AVIRIS collects images over an 11 km swath in 224 spectral bands simultaneously. The image portion of the figure is a color infrared composite of three 10 nm-wide bands centered at 544, 663, and 803 nm. In order to convey to the viewer a sense of the high dimensionality of the data, the faces of the parallelepiped in the figure show the color-coded, relative reflectance spectra for each of the 358 pixels along the top and 614 pixels along the right-hand edge of the image. Each spectrum covers the 0.4 to 2.45 μm region from front to back. Black and blue represent low values, and red and white represent high values of reflectance. The two black stripes fall in the 1.4 and 1.9 μm atmospheric water vapor absorption bands. North is to the right. (Processed by the Center for the Study of Earth from Space, University of Colorado, Boulder.)

EXECUTIVE SUMMARY

A recent emphasis in the natural sciences is the attempt to understand the Earth as an integrated system. Traditionally, Earth science has advanced through studies within its various disciplines of individual components—atmosphere, oceans, snow and ice, water, vegetation, soils, crust, and interior. Models of these components have not been specifically designed to mesh with one another. Ecological and hydrological models, for example, usually require data and produce results over relatively small areas, whereas global climate models use a coarse spatial grid and cannot easily incorporate finer-scale data or model calculations.

Modern Earth science, however, is beginning to examine interactions among the different terrestrial components at all temporal and spatial scales. Such a global perspective requires an integrated remote sensing program, Eos, the Earth Observing System, which uses instruments throughout the electromagnetic spectrum to collect data about the Earth's surface, oceans, and atmosphere over a range of selected scales. With such an integrated program, we can plan a rational sampling strategy for measurements needed to produce and verify models of Earth-system processes. Further, if we understand the scale dependencies involved, such as those between global climate models and smaller scale models produced by specific disciplines, we can use the output of one type of model as input to another, and we can explore the relations between models to predict plausible environmental changes. Studies of specific processes by individual investigators will require remote sensing data at spatial, spectral, and temporal resolutions appropriate to the scale of the research.

At the finest scales, we will require instruments capable of detailed sampling both spatially and spectrally. We have designed the High-Resolution Imaging Spectrometer (HIRIS) to acquire simultaneous images in 192 spectral bands in the dominant wavelengths of the solar spectrum, 0.4 to 2.5 micrometers, at a spectral sampling interval of 10 nanometers. The ground instantaneous field-of-view (GIFOV) will be 30 meters over a 30-kilometer swath. A pointing capability will allow image acquisition up to +60 degrees/-30 degrees down-track and ±24 degrees or more cross-track. Thus we will be able to study surface spectral bidirectional reflectance properties and variations in atmospheric attenuation with viewing angle. The cross-track pointing will also allow multiple viewing opportunities during one orbital revisit cycle, nominally 16 days.

Observing reflected solar illumination with this detailed spectral resolution will make possible: (1) direct identification of virtually all diagnostic absorption features in minerals and soils, (2) examination of suspended sediments and phytoplankton in coastal and inland waters, (3) estimation of the grain size of snow and its contamination by absorbing impurities, and (4) study of biochemical processes in vegetation canopies. With our current spaceborne broadband sensors, we have not been able to adequately measure or investigate any of these essential attributes.

The temporal variations of many of Earth's surface processes necessitate global coverage every few days. This can be accomplished by Eos instruments with broad swath widths, such as the Moderate-Resolution Imaging Spectrometer (MODIS) in the visible, near-infrared, and thermal infrared wavelengths and the various passive microwave instruments that comprise the High-Resolution Multifrequency Microwave Radiometer (HMMR). HIRIS, the Eos instrument with high spatial and spectral resolution in the visible and near infrared, is also essential to allow understanding of processes at regional and global scales; it will be complemented by a Synthetic Aperture Radar (SAR) in the active microwave and a Thermal Infrared Multispectral Scanner (TIMS). Such high-resolution instruments will permit analysis and interpretation of specific areas and detailed sampling within scenes produced by instruments with lower spatial or spectral resolution. Because HIRIS is designed for targeting rather than for continuous data acquisition, the raw internal rate at which it can produce data is extremely high, about 512 megabits per second.

This multistage sampling capability of Eos is necessary for two reasons:

1. The spectral response from sensors with low spatial resolution is a mixture of signals from a diversity of surfaces within a picture element (pixel). To understand fully the radiance averaged over resolution cells larger than several tens of meters, we need to investigate reflectance characteristics of their components at a spatial resolution that allows recognition of features and analysis of the mixing process.

2. Some processes that are important at the global scale are manifested in surface features with dimensions on the order of tens of meters. Examples include upwelling and mixing along fronts in coastal waters; anthropogenic damage to vegetation, which first appears in patches; forest clearing, which dramatically affects the Earth's carbon cycling and which in parts of the tropics occurs in small, noncontiguous areas; land-use change and desertification, where boundaries may not move far enough to be detected by low-resolution sensors; and alpine snow and ice, which play an important role in the Earth's hydrology, climate, and sea level.

HERITAGE OF HIRIS

There are two types of instruments whose construction and use have provided the scientific and engineering experience necessary to produce HIRIS: (1) satellite sensors with high spatial resolution but low spectral resolution, and (2) airborne imaging spectrometers with both high spatial and high spectral resolution.

The Landsat Thematic Mapper (TM), first launched in 1982 on Landsat-4, has demonstrated the benefits of 30 meter GIFOV and seven spectral bands, one in the thermal wavelength region, for a variety of scientific disciplines. Its excellent radiometric calibration has also yielded considerable scientific benefit, and its wavelength bands in the "short-wave infrared" region (1.1 to 2.5 micrometers) have been used for radiation studies of clouds, snow-cloud discrimination in alpine areas, detection of stress in vegetation due to dehydration, and identification of some groups of hydrothermally altered minerals.

The High-Resolution Visible instrument on the French satellite SPOT (Systeme Probatoire d'Observation de la Terre), launched in 1986, has three spectral bands in the 0.5 to 0.9 micrometer range at 20 meter GIFOV and one panchromatic band at 10 meter GIFOV. It also has the ability to point ±27 degrees cross-track, allowing both stereophotogrammetry and multiple views during an orbital revisit cycle. This capability for multiple views has proven invaluable for data collection during the intensive field campaigns of the first field experiments of the International Satellite Land Surface Climatology Project (ISLSCP).

The Airborne Imaging Spectrometers (AIS-1 and AIS-2) were flown from 1983 to 1987, collecting images 32 and 64 pixels wide, respectively, in 128 spectral bands from 1.2 to 2.4 micrometers at a GIFOV of 10 meters. Although they were designed primarily to test area-array infrared detectors, they obtained significant scientific results in geologic identification and plant-canopy biochemistry.

The next-generation airborne instrument, the Airborne Visible and Infrared Imaging Spectrometer (AVIRIS), has become operational in 1987. AVIRIS covers the 0.4 to 2.5 micrometer region, the same spectral range as HIRIS, in 10 nanometer increments. The GIFOV is 20 meters. Current research with AVIRIS is testing its data quality and scientific benefit in several disciplines.

The first spaceborne imaging spectrometer proposed was the Shuttle Imaging Spectrometer Experiment (SISEX). Because of the Challenger accident and subsequent delays in the Space Shuttle program, the SISEX project has been expanded to include many features of the planning and design of HIRIS.

SCIENTIFIC OBJECTIVES

Imaging spectrometry can acquire continuous reflectance spectra for each pixel at a spectral resolution sufficient to extract virtually all information available in the return signal. The prospect of acquiring such useful data leads to a new look at the applications of remote sensing to several areas in Earth science.

Geologic Units

Imaging spectrometry makes possible the direct identification of many minerals on the Earth's surface based on their diagnostic electronic and vibrational transitions. Over 1,000 minerals bearing Fe^{2+}, Fe^{3+}, OH, CO_3, and SO_4 have unique spectral characteristics in the 0.4 to 2.5 micrometer region. The ability to identify these minerals in surface rocks and soils is necessary to characterize and map the surface materials important in global study: the bedrock units of whatever origin that have been subject to tectonism and magmatism and exposed by subsequent erosion. The outcrop patterns of rocks produced by various sedimentary, magmatic, and tectonic processes are the fundamental record of Earth's history. Moreover, most of our nonrenewable resources occur within the continental crust; a better understanding of the nature and distribution of crustal units will increase our understanding of the deformational history of the Earth and improve our ability to locate nonrenewable resources. Other economic and scientific benefits will result from the use of imaging spectrometry to study surficial materials and landforms. These record geologically recent processes on the Earth's surface that are significant not only in themselves but also as indicators of processes that operated earlier in geologic time.

Oceans and Inland Waters

The increased spectral resolution of HIRIS over that of existing instruments such as the Coastal Zone Color Scanner (CZCS) will make possible the separation of components of suspended matter (sediment versus phytoplankton) in near-surface waters. Moreover, the HIRIS bands in the near infrared can be used to remove atmospheric effects over waters with higher sediment or pigment concentration than the open ocean, where CZCS was designed to operate. The high spectral resolution and continuous channels of HIRIS also permit selective mapping of various continental and maritime aerosols over clear water, improving our ability to correct for the atmospheric effect in nearby land scenes. HIRIS will enable the study of near-shore or inland waters, which can visibly fluoresce and which contain suspended sediments and organic material not correlated with chlorophyll pigments.

Inland waters have several distinctive characteristics that require special attention if remote sensing of those ecosystems is to succeed: (1) sizes of water bodies are moderate to small, 1 to 100 kilometers long; (2) interfaces between land and water may be long and complex; (3) optical conditions can vary widely during short intervals of time; and (4) strong

horizontal and vertical gradients in geological, physical, and chemical conditions are common. Current remote sensing methodology has had only modest success in the examination of inland waters. Improvement will require the higher spectral and spatial resolution of HIRIS.

Soils

Although aerial photography has been used to map soils for more than a half-century, spectral characteristics of soils are less well understood. Soil reflectance is a cumulative property, which derives from inherent spectral behavior of a soil's heterogeneous combination of minerals, organic material, and water. Moreover, the remotely sensed signal usually contains both soil and vegetation components. The high-resolution spectral data from HIRIS will allow extraction of the components of the signal from a pixel, allowing the characteristics of the soil and vegetation to be evaluated separately.

Vegetation

Modern studies using remote sensing of vegetation concentrate on biogeochemical processes, including the biogeochemical cycles. Inventories of vegetation characteristics such as biomass and water content of leaves, as well as physiological processes such as photosynthetic activity, productivity, and transpiration, are essential to these studies. High-resolution spectral measurements of vegetation reflectance can be used to map stress associated with excesses or deficiencies in soils that lead to subtle shifts in the chlorophyll absorption spectrum. At a larger scale, total net primary productivity by plant communities is related to measurable parameters such as total leaf area or total foliar nitrogen. Lignin and nitrogen in leaves have spectral signals that will be detectable in HIRIS data, although the spectral absorption bands are not as clear as those for minerals. If these components can be reliably identified, carbon and nitrogen turnover through decomposition can be estimated.

We can also gain information from the capability of HIRIS to view the surface from an off-nadir angle. The angular distribution of reflection from vegetation is sensitive to leaf orientation, leaf density, and the distance between plants; off-nadir viewing provides superior information on canopy characteristics. The total albedo of the canopy can be better estimated with carefully chosen off-nadir viewing orientations.

Atmosphere

Although HIRIS will be used mainly to observe the surface, it will also provide valuable information on the atmosphere, which in the visible wavelengths can account for more than half the total signal. Because of its spectral resolution and off-nadir viewing capability, HIRIS can measure key attributes of

the atmosphere, such as aerosol loading and composition. These determinations are of intrinsic scientific value as well as necessary for correcting surface scenes for atmospheric perturbations. HIRIS data will also provide information on cloud characteristics useful for calculating their climatic effects.

Snow and Ice

Reflectance of snow can be characterized by its grain size and absorbing impurities, from which the albedo over the entire solar spectrum can be estimated. However, our current satellite sensors are not well designed for estimating these attributes. The most common use of remote sensing in snow hydrology has been to monitor snow-covered areas with broadband sensors. Selected wavelength bands from HIRIS, along with off-nadir viewing, can be used to estimate surface characteristics of snow that are necessary for calculation of the surface radiation balance. HIRIS data will also allow discrimination between snow and clouds, even in alpine areas.

INSTRUMENT REQUIREMENTS

HIRIS will be tailored to scientific objectives. The sensor is intended to be a targeting instrument that will acquire data at specified times and places, as opposed to one that acquires data continuously. It complements MODIS and HMMR by providing higher spectral and spatial resolution and more complete spectral coverage at the cost of less ground coverage. HIRIS, therefore, is at an intermediate level in a multistage sampling program between *in situ* field data and global mapping instruments.

Based on experience with Landsat Thematic Mapper, the equivalent spatial resolution was chosen: a GIFOV of 30 meters. This pixel size, or smaller, is necessary in studies of forest ecosystems, where changes in vegetation structure and function are linked to the size of gaps created by tree death, windfall, and other disturbances. Arguments can be made for even higher spatial resolution in geological mapping, because some key marker beds may have only a few meters of horizontal surface exposure. However, a higher spatial resolution in all bands would extract too large a penalty in data rates, and the disadvantages of a spectral resolution degradation to overcome this problem would outweigh information gained by smaller pixels.

The choice of spectral coverage was dictated by both the scientific requirements and the technological capabilities. The 0.4 to 2.5 micrometer region contains almost all the surface information that can be derived by passive sensors from reflected solar energy. In this wavelength region, diagnostic information is obtainable for water, vegetation, and minerals and soils. A wavelength band near 1.6 micrometers, in combination with information in the visible wavelengths, allows discrimination between clouds and snow and other surface covers. Important spectral information about geological materials also

lies in thermal infrared wavelengths, 3 to 5 micrometers and 8 to 12 micrometers, but these data should be acquired with a separate instrument, such as the TIMS.

The requirements for spectral resolution are determined by water and vegetation studies in the visible and near-infrared regions and by the need for mineralogical mapping in the short-wave infrared. A major advance in understanding biological activity in water will result from direct identification of constituents and concentrations. Absorption spectra of algal pigments exhibit features whose detections require 10 nanometer sampling, as do the spectral changes associated with canopy biochemistry. Most minerals can be detected by 10 nanometer sampling; increasing the sampling interval to 20 nanometers results in a significant degradation in our ability to identify certain minerals; for example, certain magnesium-bearing minerals would not be distinguishable with 20 nanometer sample intervals.

Frequency requirements of coverage are directly related to the dynamic nature of the problem to be studied. Water and snow/ice studies need frequent measurements, vegetation studies less frequent ones. Although the frequency of measurements needed for geological studies is much lower, data must be obtained at optimal lighting and visibility conditions, when the surface is not covered by vegetation or obscured by clouds. HIRIS will not acquire continuous coverage, but will sample sites. By pointing cross-track up to ±24 degrees, the maximum time between potential acquisitions is 5 to 6 days at the Equator. Within the 16-day orbital revisit period determined by the sun-synchronous Eos orbit at 824-kilometer altitude, a site at the Equator could be imaged three to four times and a site at 40 degrees north or south latitude four to five times.

Pointing is therefore a necessary requirement. In addition to cross-track pointing, down-track pointing is necessary to estimate the bidirectional reflectance-distribution function (BRDF) of surfaces, to remove atmospheric attenuation, and to implement image motion compensation to increase signal-to-noise ratio for dark targets. The atmosphere measurements require +60 degrees/-30 degrees down-track capability.

Requirements for encoding (number of bits per pixel) depend on the dynamic range and the smallest reflectance interval to be observed. Great dynamic range is required for snow, which for wavelengths of 0.4 to 0.8 micrometers is one of the brightest natural substances. Moreover, for estimates of the energy balance of snow surfaces, it is important to discriminate between albedo differences of, for example, 0.92 and 0.90, because the difference in absorption is 20 percent. Therefore, a dynamic range that encompasses the full solar irradiance is necessary, and the quantization must be fine enough to distinguish minor differences, at least 10 bits per pixel. Because signal summation by image motion compensation is necessary to acquire adequate signal-to-noise ratios

(S/N) for water studies, 12-bit encoding will be required. For some other studies, 8-bit quantization will be adequate.

The calibration requirements for HIRIS are ambitious, but the benefits to science increase significantly if stable, reliable calibration can be achieved. In addition to pre-launch laboratory calibration, three in-flight methods will be used to achieve 0.5 percent band-to-band relative response accuracy and 5 percent absolute accuracy, with 1 percent as a goal. These methods are semiannual lunar viewing, the use of a solar diffuser, and annual, well-instrumented, field-calibration campaigns. In addition, HIRIS will be carefully cross-calibrated with MODIS.

CURRENT INSTRUMENT DESIGN

The current HIRIS concept is based on the parameters and assumptions described above and summarized in the following table.

Orbit altitude	824 km
Swath width	30 km
Ground instantaneous field-of-view	30 m
Spectral coverage	0.4–2.5 μm, 192 bands
0.4–1.0 μm	9.4 nm
1.0–2.5 μm	11.7 nm
Focal ratio	f/3.8
Image motion compensation	gain states of 1 (off), 2, 4, or 8
Pointing	
Down-track	+60°/–30°
Cross-track	±24°
Encoding	12 bits/pixel
Maximum data rate	
Internal	512 Mbits/sec
Output	300 Mbits/sec
Operating temperature	
Optics	270 K
Detector	130 K
Mass	987 kg (705 kg + 40% contingency)
Power	
Peak	870 W
Average	<300 W

The HIRIS sensor consists of a broadband, pushbroom spectrometer utilizing silicon and hybrid mercury-cadmium-telluride (HgCdTe) charge-coupled device (CCD) area-array detectors. Incident radiation passing through a slit at the front of the fore-optics is collimated, separated into two bands, and dispersed and reimaged onto separate detector arrays: silicon for visible and near-infrared wavelengths and HgCdTe for short-wave infrared wavelengths. Singal-to-noise ratios range from 50 to 200 in most regions of the spectrum. Current mass of the instrument is projected at an upper limit of 987 kilograms; several design modifications may reduce the mass.

DATA HANDLING AND DATA PRODUCTS

The planned HIRIS data system will allow maximum flexibility in the number of bits and number of bands transmitted to the surface, within constraints imposed by the available data rate. Possible modes in which data can be edited include spectral selection, whereby only some of the available bands are transmitted; selected encoding, whereby 8 or 10 bits per band, rather than 12, are transmitted; and spatial editing, either by pixel averaging or a narrower swath. In addition, information-preserving data-compression schemes are under study; possibilities include amplitude compression, bandwidth compression, and encoding. The statistical properties and the entropy of data of high spectral resolution are not yet well known. Experience with scientific use of AVIRIS data will allow evaluation of the possible success of data compression schemes.

The large volume of HIRIS data will require a disciplined approach to data processing. The downlink and telemetry formats will be such that the required ancillary data (attitude and ephemeris) from the spacecraft are readily available and of sufficient accuracy to permit routine cartographic correction of images. Investigators will be able to request data acquisition via an online user interface, including specification of bands to be acquired and precise swath to be covered. They will also be able to request output products via the same mechanism. The distribution medium is not yet defined, but it will conform to format and media standards to be established for Eos. Within the framework of the data-level definitions of the Eos Data Panel, we expect the following data products to be available. Level 1B data will be the standard product. It is probable that coded algorithms will be distributed to allow users to generate their own higher-level products.

Level 1A—HIRIS instrument data augmented with ancillary data for geographic location and radiometric conversion.

Level 1B—Level 1A data converted to radiometric units; equalization between detectors will be included.

Level 2— Geophysical parameters derived from Level 1B data. Examples of possible products include identification of specific minerals, leaf area indices, coastal phytoplankton, aerosols, snow cover, and bioluminescence.

Level 3A—Level 1B or 2 data mapped to geographic data base by means of satellite ephemeris information.

Level 3B—Level 1B or 2 data mapped to geographic data base by means of ephemeris information and ground control points.

Level 4—Model output or results from analyses of lower-level data, possibly augmented by ground measurements, multitemporal HIRIS data, and data from other sensors or satellites. An example of a possible product is surface reflectance corrected for atmospheric scattering and absorption.

Preliminary-look data for two spectral bands, 0.65 micrometers and 1.6 micrometers, available for field experiments having critical time requirements.

SUMMARY

HIRIS is an Eos sensor developed for high spatial and high spectral resolution. It can acquire more information in the 0.4 to 2.5 micrometer spectral region than any other sensor yet envisioned. Its capability for critical sampling at high spatial resolution makes it an ideal complement to MODIS and HMMR, lower-resolution sensors designed for repetitive coverage. With HIRIS we can observe transient processes in a multistage remote sensing strategy for Earth observations on a global scale.

CONTENTS

LIST OF TABLES

LIST OF FIGURES

LIST OF FIGURES (continued)

ACRONYMS

AIS	Airborne Imaging Spectrometer
AMSR	Advanced Mechanically Scanned Radiometer
AMSU	Advanced Microwave Sounding Unit
AVHRR	Advanced Very High Resolution Radiometer
AVIRIS	Airborne Visible and Infrared Imaging Spectrometer
BRDF	Bidirectional Reflectance-Distribution Function
CCD	Charge-Coupled Device
CZCS	Coastal Zone Color Scanner
DMSP	Defense Meteorological Satellite Program
EFL	Effective Focal Length
Eos	Earth Observing System
EosDIS	Eos Data and Information System
ERB	Earth Radiation Budget
ESTAR	Electronically Scanned Thinned Array Radiometer
FET	Field Effect Transistor
FOV	Field-of-View
FWC	Full Well Capacity
GIFOV	Ground Instantaneous Field-of-View
GLRS	Geodynamics Laser Ranging System
GOES	Geosynchronous Operational Environmental Satellite
HIRIS	High-Resolution Imaging Spectrometer
HMMR	High-Resolution Multifrequency Microwave Radiometer
IFOV	Instantaneous Field-of-View
IMC	Image Motion Compensation
ISLSCP	International Satellite Land Surface Climatology Project
ISSAG	Imaging Spectrometer Science Advisory Group
JPL	Jet Propulsion Laboratory
LAI	Leaf Area Index
LASA	Lidar Atmospheric Sounder and Altimeter
LFC	Large Format Camera
LMT	Local Meridian Time
MODIS	Moderate-Resolution Imaging Spectrometer
MODIS-N	MODIS Nadir
MODIS-T	MODIS Tilt
MOMS	Modular Optoelectronic Multispectral Scanner
MSS	Multispectral Scanning System
MTF	Modulation Transfer Function
NASA	National Aeronautics and Space Administration
NOAA	National Oceanic and Atmospheric Administration
PFA	Principal Factor Analysis
pixel	Picture Element
ppmw	Parts Per Million by Weight
REE	Rare Earth Elements

ACRONYMS (continued)

rms	Root Mean Square
SAR	Synthetic Aperture Radar
SCAT	Scatterometer
SCS	Soil Conservation Service
SISEX	Shuttle Imaging Spectrometer Experiment
SMIRR	Shuttle Multispectral Infrared Radiometer
S/N	Signal-to-Noise Ratio
SPAM	Spectral Analysis Manager
SPOT	Systeme Probatoire d'Observation de la Terre
SST	Sea Surface Temperature
SWIR	Short-Wave Infrared Wavelengths (1.1 to 2.5 μm)
TIMS	Thermal Infrared Multispectral Scanner
TM	Thematic Mapper
USGS	U.S. Geological Survey
VNIR	Visible and Near-Infrared Wavelengths (0.4 to 1.1 μm)

I. IMAGING SPECTROMETRY FROM SPACE

INTRODUCTION

Important global-scale research in oceanography, geology, limnology, hydrology, glaciology, and terrestrial ecology is just beginning to be addressed with the most advanced kinds of sensors now available on satellites. A new generation of optical sensors, called imaging spectrometers, is flying on aircraft and is slated to fly aboard the polar-orbiting space platform in the mid-1990s as part of the Earth Observing System (Eos). These new generation sensors are the Airborne Visible and Infrared Imaging Spectrometer (AVIRIS), the High-Resolution Imaging Spectrometer (HIRIS), and the Moderate-Resolution Imaging Spectrometer (MODIS). MODIS is described in a separate advisory group report. The purposes of this report on HIRIS are: (1) to establish scientific observational requirements for high-resolution imaging spectrometer data, (2) to outline the characteristics of the Eos instrument that can obtain the necessary data sets, and (3) to show how these data can be used synergistically with other Eos data sets in various geoscientific disciplines.

SCOPE

This document justifies the need and describes the basic features of the HIRIS instrument required to meet critical needs of the scientific community representing oceanography and inland waters, geology and soils, and terrestrial ecology and related fields of vegetation, snow and ice, and atmospheric studies. It is the result of the joint efforts of the members of the Imaging Spectrometer Science Advisory Group (ISSAG) formed in January 1985 to advise NASA on the scientific questions to be addressed with the new technology of imaging spectrometry, as well as to advise on the requirements for a sensor to be flown on the space platform as part of the Eos instrument complement. The membership consists of researchers in the main disciplines in the geosciences whose problems will be addressed with surface remote sensing using imaging spectrometers. Representatives from the information sciences were also involved to help devise concepts for efficiently extracting information from imaging spectrometer data.

The Eos concept envisions the synergistic use of a number of remote sensing instruments such as HIRIS, SAR, MODIS, LASA, HMMR/AMSR, GLRS, and others (see Acronyms). These instruments, along with an advanced data management system, are expected to provide the global data sets for the 1990s to further our understanding of geological and glaciological processes, the hydrologic cycle, oceans and inland waters, and biogeochemical cycles, among others. Various instrument panels, including the ISSAG, have articulated the data needs and specified the instrument designs to meet those needs. The ISSAG has addressed these problems and, in addition, has considered the intermediate steps necessary to prepare users for the satellite data sets. HIRIS will provide spectral reflectance measurements with sufficient resolution to identify surface materials. The data analysis requirements and synergistic use of these data with those produced by other remote sensing instruments are discussed in this report.

THE ROLE OF HIRIS IN THE EARTH OBSERVING SYSTEM

Recent reports from the National Academy of Sciences (1982, 1985, 1986a) and NASA (1986) have articulated sets of goals necessary for an interdisciplinary understanding of the Earth's geology, hydrology, climate, oceans, and biota at regional and global scales. This emphasis on a global perspective for a variety of scientific problems demands an integrated remote sensing program, Eos, that utilizes instruments collecting data over the entire electromagnetic spectrum at a range of spatial and temporal scales. The utility of remote sensing instruments with both high spectral and spatial resolution has been demonstrated for numerous applications involving specific analyses of small areas, and many examples of such accomplishments are described and cited in this report.

Instruments like HIRIS also contribute in essential ways to our understanding of processes operating at regional and global scales, for two reasons:

1. The spectral response from sensors with low spatial resolution is produced by the reflection from a diversity of surfaces. Few, if any, areas of the Earth's land surface are uniform over these dimensions, so in order to fully understand the radiance averaged over the resolution of Eos sensors with kilometer-scale resolution, we need a high-resolution instrument for multistage sampling, intermediate between the scale of field measurements and low- or medium-resolution satellite sensors that would provide frequent temporal coverage.

2. Some processes of importance at global scales are manifested in surface features with dimensions on the order of tens or hundreds of meters, whose optical properties would be difficult to detect with kilometer-scale sensors. Examples include upwelling along oceanic fronts, where considerable nutrient cycling occurs; anthropogenic damage to vegetation from pollution, which first appears in patches; forest clearing, which dramatically affects the Earth's carbon cycling

and which in the tropics occurs in small, discontinuous areas; land-use change and desertification, where boundaries may not move far enough to be detected by low-resolution sensors; and alpine snow and ice, which play an important role in the Earth's hydrology, climate, and sea level.

HIRIS is not intended to be an instrument for repetitive operational mapping of large areas. Such mapping is better accomplished with an instrument of lower spatial resolution, such as MODIS. Instead HIRIS, like SAR, is a targeting instrument to be used for analysis and interpretation of specific areas and for detailed subsampling within scenes produced by instruments with lower spatial or spectral resolution—for example, MODIS or HMMR. It will measure spectral reflectance of the surface at high spatial resolution, while SAR will measure active microwave properties. HIRIS will combine detailed spectral information with a spatial resolution equal to that of the Landsat Thematic Mapper (TM), down- and cross-track pointing capability, excellent absolute calibration, and a dynamic range and sensitivity suitable for both dark and bright surfaces. Therefore, investigators will be able to interpret properties of the Earth's surface cover at a level of detail unmatched by any previous satellite instrument. Specific examples of its possible applications for research in oceanography, coastal and inland waters, snow and ice, geology, soils, forestry, and terrestrial ecology are summarized in the chapters that follow. In addition, there is a chapter detailing synergism with other Eos instruments.

IMAGING SPECTROMETER SYSTEMS

The concept of imaging spectrometry is shown in Figure 1. Instead of acquiring images in a few separate spectral bands of various widths, as with Landsat, imaging spectrometry makes possible the simultaneous collection of images in a hundred or more contiguous spectral bands. The result is a continuous reflectance spectrum for each picture element (pixel) in the image. In the 0.4 to 2.5 μm region, a 10 nm spectral sampling interval is required to describe salient features in the reflectance spectra of rocks and minerals, plants, and organic particles suspended in water. The design of the imaging spectrometer allows all possible spectral data to be collected and presents the possibility of transmitting the subset most relevant to a particular investigation. No longer will it be necessary to form committees to pick the "best possible bands" for a multispectral imager.

The need for high spectral resolution reflectance data in the 0.4 to 2.5 μm region was recognized soon after data from the first Landsat Multispectral Scanning System (MSS) had been analyzed. Spectra acquired in the field (Goetz et al., 1975; Rowan et al., 1974) and in the laboratory (Hunt, 1977) showed that direct identification of mineral constituents could be made if continuous spectra could be acquired. In 1976 a proposal was made to fly a multichannel radiometer in orbit aboard the shuttle to test the hypothesis that direct identification of some minerals could be made in spite of variable atmospheric attenuation. The Shuttle Multispectral Infrared Radiometer

EACH PIXEL HAS
AN ASSOCIATED
CONTINUOUS SPECTRUM
THAT CAN BE USED TO
IDENTIFY THE SURFACE
MATERIALS

IMAGES TAKEN
SIMULTANEOUSLY
IN 100-200 SPECTRAL BANDS,
INHERENTLY REGISTERED

R

0.4   2.5
WAVELENGTH (μm)
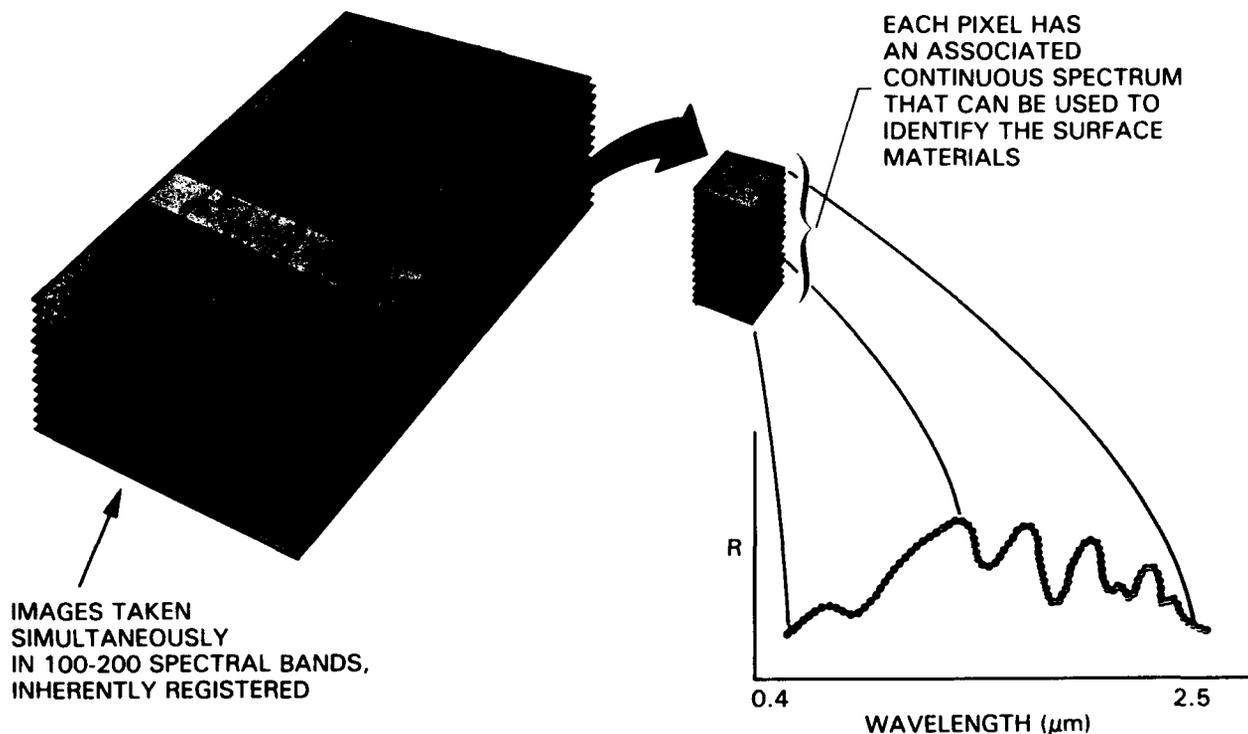
Figure 1. Schematic definition of imaging spectrometry.

(SMIRR) flew on Challenger in 1981 and demonstrated that mineral phases can be identified from space (Goetz et al., 1982).

Simultaneous imaging in many contiguous spectral bands requires a new approach to sensor design. Sensors such as the Landsat MSS or TM are optical mechanical systems in which discrete, fixed detector elements are scanned across the surface of the Earth perpendicular to the flight path by a mirror, and these detectors convert the reflected solar photons from each pixel in the scene into an electronic signal (Figure 2a). The detector elements are placed behind filters that pass broad portions of the spectrum. The MSS has four such filters and detectors, whereas TM has seven. The primary limitation of this approach is the short residence time of the detector in each instantaneous field-of-view (IFOV). To achieve adequate signal-to-noise ratio (S/N) without sacrificing spatial resolution, such a sensor must operate in broad spectral bands (100 nm or greater) or must use optics with unrealistically small ratios of focal length to aperture (i.e., low f-numbers).

One approach to increasing the residence time of a detector in each IFOV is to use line arrays of detector elements (Figure 2b). In this configuration there is a dedicated detector element for each cross-track pixel, which increases the residence, or integration, time to the interval required to move one IFOV along the track. Such an experimental, two-spectral channel instrument, called the Modular Optoelectronic Multispectral Scanner (MOMS), has been carried aboard the space shuttle. A French satellite sensor (the Systeme Probatoire d'Observation de la Terre, or SPOT), launched in 1986, also uses line array detectors. The SPOT system provides stereoscopic image capability in three spectral bands for wavelengths less than 1.0 μm.

There are limitations and trade-offs associated with the use of multiple line arrays, each having their own spectral band pass filter. If all the arrays are placed in the focal plane of the telescope, then the same ground locations are not imaged simultaneously in each spectral band. If beam splitters are used to facilitate simultaneous data acquisition, the signal is reduced by 50 percent or more for each additional spectral band acquired in a given spectral region. Furthermore, instrument complexity increases substantially if more than 6 to 10 spectral bands are desired.

Two other approaches to imaging spectrometry are shown in Figures 2c and 2d. The line array approach (Figure 2c) is analogous to the scanner ap-

(a)

(b)

(c)

(d)
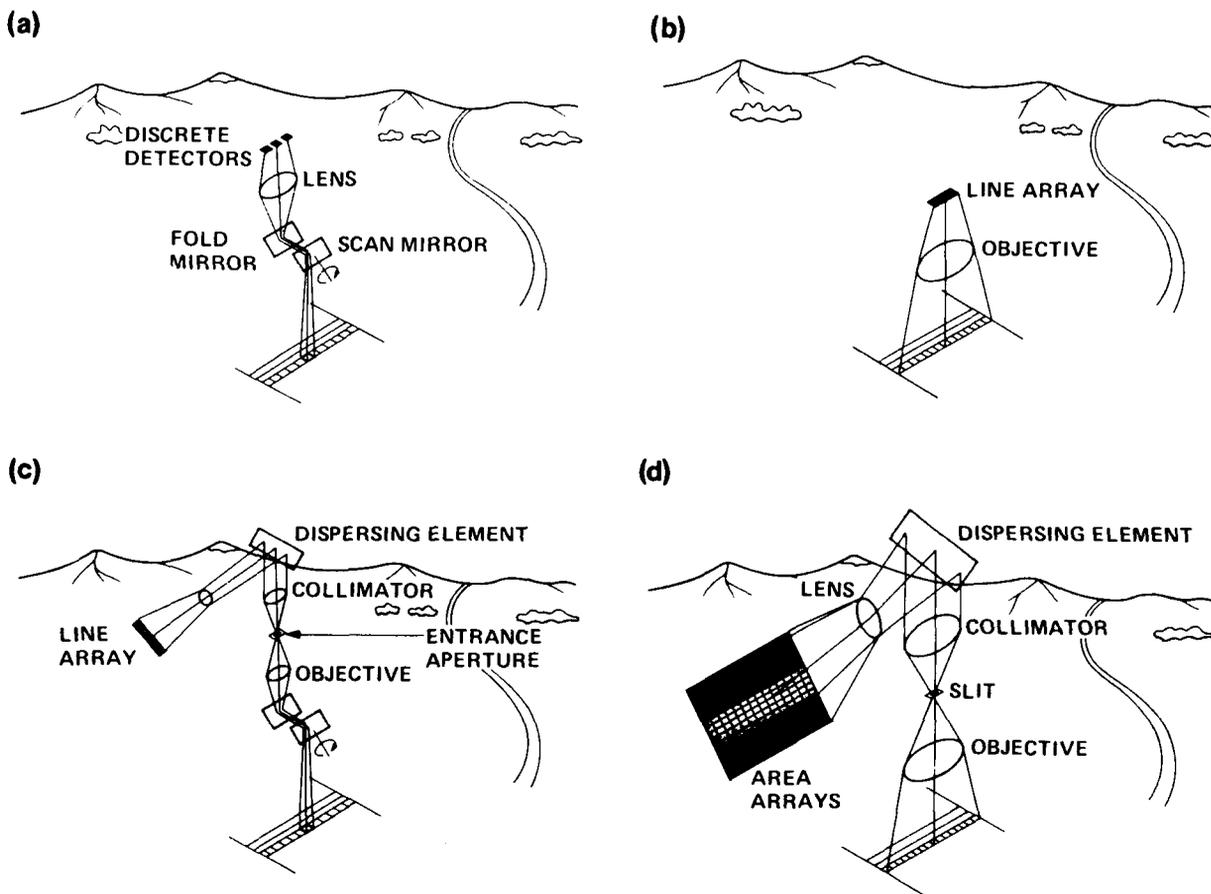
Figure 2. Four approaches to sensors for multispectral imaging: (a) multispectral imaging with discrete detectors; (b) multispectral imaging with line arrays; (c) imaging spectrometry with line arrays; and (d) imaging spectrometry with area arrays.

proach used for the MSS or TM except that light from a pixel is passed into a spectrometer where it is dispersed and focused onto a line array. Thus, each pixel is simultaneously sensed in as many spectral bands as there are detector elements in the line array. For high spatial resolution imaging (ground IFOVs of 10 to 30 m), this approach is suited only to an airborne sensor that flies slowly enough that the readout time of the detector array is a small fraction of the integration time. Because of the high spacecraft velocities, imaging spectrometers designed for Earth orbit require the use of two-dimensional area arrays of detectors at the focal plane of the spectrometer (Figure 2d), thereby obviating the need for the optical scanning mechanism. In this configuration there is a dedicated column of spectral detector elements for each cross-track pixel in the scene.

The key to imaging spectrometry is the detector array. Line arrays of silicon, sensitive to radiation at wavelengths from 0.35 to 1.1 μm, are available commercially in dimensions up to 5,000 elements in length. Area arrays of up to 800×800 elements of silicon were developed for the Galileo Jupiter camera and for the Space Telescope wide-field and planetary camera. However, the state of infrared array development for wavelengths beyond 1.1 μm is not yet so advanced. Line arrays are available in several materials up to a few hundred detector elements in length. Two of the most attractive materials are mercury-cadmium-telluride (HgCdTe) and indium antimonide (InSb). InSb arrays of 512 elements having very high quantum efficiency and detectors with similar element-to-element responsivity have been developed. InSb arrays respond to wavelengths from about 0.7 to 5.2 μm.

For area arrays, 64×64 element devices of HgCdTe sandwiched with a silicon charged-coupled device (CCD) multiplexer have been made successfully, and 64×64 element devices, which can be abutted on opposite sides, are under development (Wellman et al., 1983). These devices can be mosaicked to form focal plane arrays of $64 \times 64 \times n$ elements in dimension, where n represents the number of devices in the mosaic. Although development of 64×64 element devices is progressing, the 32×32 element array represented the state-of-the-art in infrared area arrays in 1983 when the first airborne sensor was being tested.

DEVELOPMENT OF IMAGING SPECTROMETERS

In 1981 NASA Headquarters began funding the imaging spectrometer program at the Jet Propulsion Laboratory (JPL) with the purpose of developing high spectral resolution imaging sensors, first for aircraft and later for use aboard the shuttle and on satellites. The program evolved into the development of two aircraft systems, the Airborne Imaging Spectrometer (AIS) and the Airborne Visible and Infrared Imaging Spectrometer (AVIRIS), a Shuttle Imaging Spectrometer Experiment (SISEX), and a further development of SISEX called the High-Resolution Imaging Spectrometer (HIRIS) for the Eos mission. Figure 3 shows the capabilities of the four sensors. Because of the Challenger accident and subsequent

	SPECTRAL REGION (μm)	No. BANDS	WIDTH (nm)	SWATH	IFOV
AIS	1.2 - 2.4	128	9.6	320 m	10 m
AVIRIS	0.4 - 2.4	224	9.6	11 km	20 m
SISEX	0.4 - 2.5	192	11	12 km	30 m
HIRIS	0.4 - 2.5	192	11	30 km	30 m
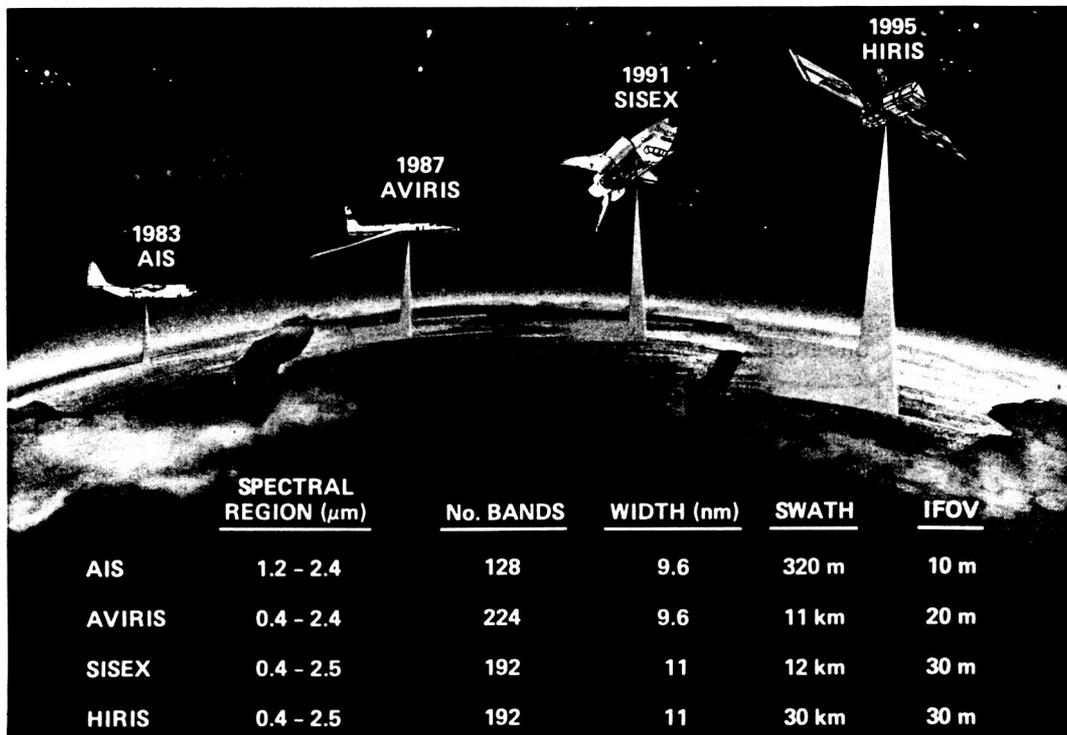
Figure 3. Imaging spectrometer program sensors, as originally proposed. Because of the Challenger accident, SISEX has been postponed.

delays in the Space Shuttle Program, the development of an instrument for the shuttle as a precursor to HIRIS has been postponed. The SISEX project has been expanded to incorporate many features of the planning and design into HIRIS.

Airborne Imaging Spectrometer (AIS)

AIS was built to test the imaging spectrometer concept with infrared area arrays (Vane *et al.*, 1984b). This instrument operates in the mode shown in Figure 2d. Two versions of the instrument have been flown; their characteristics are summarized in Table 1. The spectral coverage of the instrument is 0.8 to 1.6 μm and 1.2 to 2.4 μm, in contiguous bands that are about 10 nm wide. This sampling interval is sufficient to completely describe the absorption features for minerals in this wavelength region. Continuous strip images 32 pixels wide (AIS-1) or 64 pixels wide (AIS-2) in up to 128 spectral bands are acquired from the NASA C-130 aircraft. The 128 spectral bands are acquired by stepping the spectrometer grating through several positions during the time it takes to fly forward 1 pixel width on the ground. The area array is read out in each grating position and the data are recorded on the aircraft with a high-density, analog tape recorder. The IFOV of AIS is 2.0 mrad, which produces a ground pixel size of approximately 12×12 m from a typical operating altitude of 6 km. To aid in locating the AIS ground track, a bore-sited 35 mm camera acquires black and white, wide field-of-view (FOV) photography.

Figure 4 shows AIS-1 images acquired over Van Nuys, California, on the first engineering flight in November 1982. The images cover the area outlined in black lines on the aerial photograph. Identifiable features include the field in the lower portion of the image, the condominium complex in the center, and a school in the upper left of the image. On this test flight images were acquired in only one grating position, in 32 contiguous spectral bands in the region from 1.2 to 1.5 μm. A mosaic of the 32 AIS-1 images, each in a 9.3-nm spectral band and each 32 pixels wide, is shown below the photograph. The most obvious feature in the mosaic is the loss of detail in the 1.4 μm atmospheric water absorption band. However, there is considerable detail visible in the adjacent spectral images. Details associated with reflected variations are identified with arrows. The reflectance of a well-watered courtyard lawn inside the school grounds (location a) dropped significantly beyond 1.4 μm in comparison with the reflectance of the unwatered field (location b).

In order to test the capability of imaging spectrometry for mineral identification with the AIS, the Cuprite mining district of Nevada was chosen for study. The Cuprite area contains both hydrothermally altered and unaltered rocks, well exposed and nearly devoid of vegetation. The altered rocks overflown in this study contain secondary quartz, opal, alunite, and clay minerals (Abrams *et al.*, 1977), and the area has been subject to extensive study with broadband multispectral images in the visible, reflective infrared, and emissive infrared regions (Kahle and Goetz, 1983). Several minerals that have diagnostic absorption features in the 2.0 to 2.4 μm region occur in the Cuprite area. The narrow spectral band sampling possible with an imaging spectrometer therefore allows these minerals to be identified.

Figure 5a shows the central region of the Cuprite district overflown with AIS-1 in 1983. The bright areas are the result of trenching operations that break through the dark stained surface crust and expose materials consisting of almost pure silica. The bottom curve in Figure 5b shows a raw 128 channel spectrum of a 5×5 pixel area in the AIS coverage outlined in Figure 5a. The major features are the broad atmospheric water bands centered at 1.4 and 1.9 μm, and the solar irradiance curve, which ex-

Table 1. Performance Characteristics of AIS-1 and AIS-2

Parameter	AIS-1	AIS-2
IFOV	1.91 mrad	2.05 mrad
GIFOV (at 6 km altitude)	11.4 m	12.3 m
FOV	3.7°	7.3°
Swath width (at 6 km altitude)	365 m	787 m
Spectral sampling interval	9.3 nm	10.6 nm
Data rate	394 kbit/sec	1,670 kbit/sec
Spectral sampling "Tree" mode	0.9–2.1 μm	0.8–1.6 μm
"Rock" mode	1.2–2.4 μm	1.2–2.4 μm

Note: AIS-1 was flown in 1982, 1983, 1984, and 1985. It was replaced by AIS-2 in 1986.
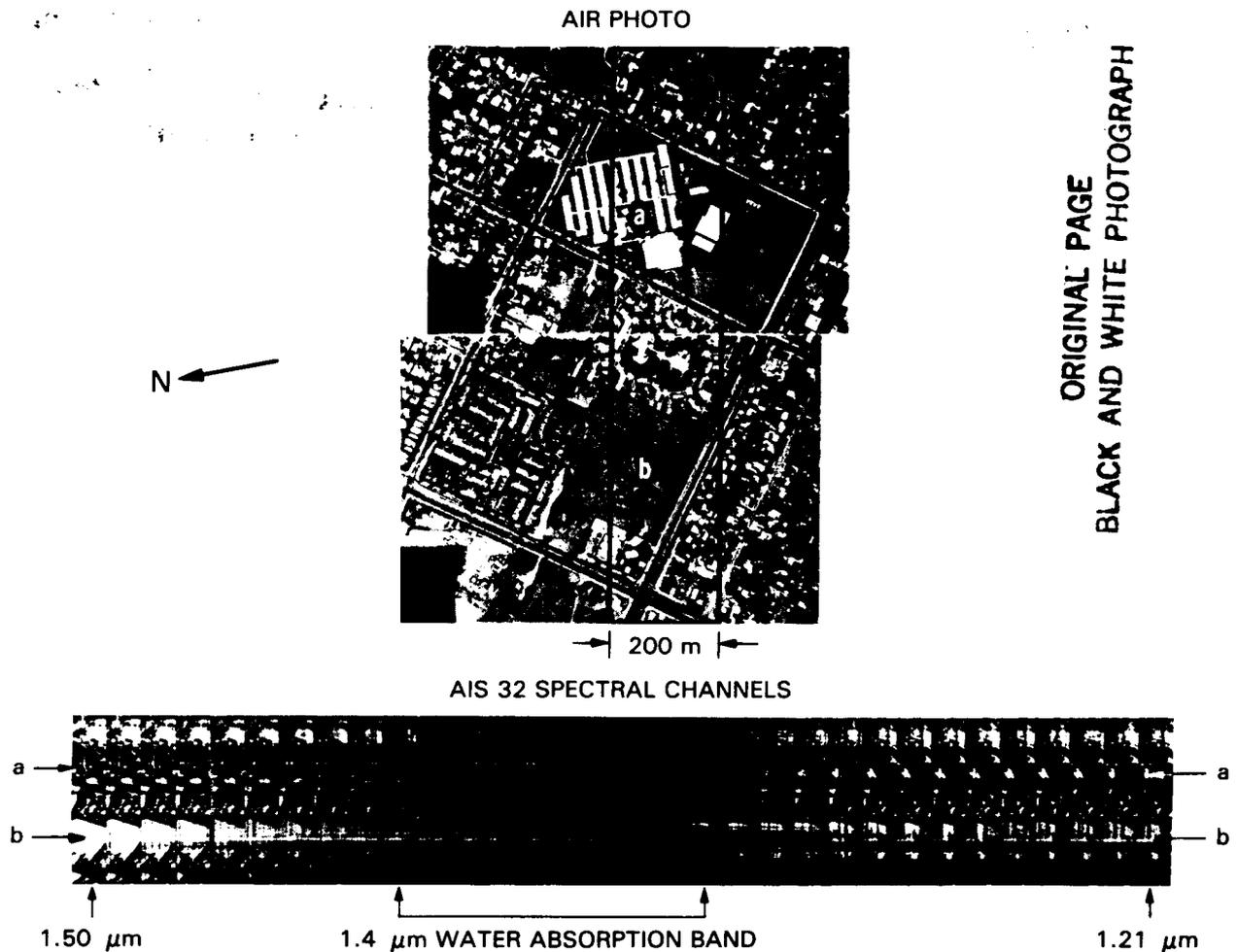
ORIGINAL PAGE
BLACK AND WHITE PHOTOGRAPH

N ◄——

—►| 200 m |◄—

AIS 32 SPECTRAL CHANNELS

a ——►   ——— a

b ——►   ——— b

↑   ↑_____↑   ↑
1.50 μm   1.4 μm WATER ABSORPTION BAND   1.21 μm

Figure 4. Air photo of an area in Van Nuys, California, showing (a) a school courtyard, and (b) an open field. The black traces outline the coverage of the 32-pixel-wide AIS-1 images taken in 32 spectral bands between 1.5 and 1.21 μm. The individual AIS images taken in 9.3-nm-wide, contiguous spectral intervals are shown at the bottom. The spectral reflectance behavior of the well-watered courtyard and the open field are quite different and reflect the irrigation practices.

hibits a rapid falloff toward longer wavelengths. An approximate compensation for atmospheric and insolation effects can be made if one normalizes the data to an area in the image having little or no topographic relief and uniform, known spectral reflectance characteristics. The top curve in Figure 5b is the result of this normalization procedure. Spectral features in the surface material become more apparent in the normalized spectrum because the removal of systematic effects makes it possible to display the full radiometric resolution of the data. Enhanced 32-channel images covering the 2.03 to 2.32 μm wavelength region, and acquired in the area outlined in Figure 5a, are shown in Figure 5c. Surface features having absorption bands can be recognized by changes in contrast with respect to their surroundings.

Spectra can be derived on a pixel-by-pixel basis from any point on the AIS image. Figure 6 shows a single 9.3-nm-wide channel image at 2.03 μm taken from Figure 5c and the reflectance spectra derived from averages of 3 × 3 pixel areas from all 32 images.

Three general spectral classes are seen. The spectra taken from the hill in the lower portion of the image contain an absorption doublet that matches that of the clay kaolinite $[Al_2(Si_2O_5)(OH)_4]$. A laboratory spectrum of a field sample is shown superimposed. Other spectra show a single, broad absorption feature centered at 2.17 μm indicative of alunite $[KAl_3(SO_4)(OH)_6]$, a mineral associated with altered feldspathic rocks. A laboratory reflectance spectrum of a field sample is superimposed. The spectra obtained from the top of the image are devoid of absorption features because this surface material consists of almost pure quartz, which does not exhibit spectral absorption features in this wavelength region.

Airborne Visible and Infrared Imaging Spectrometer (AVIRIS)

The AIS instrument was designed primarily as an engineering test bed for detector development, but it has been used successfully for data acquisition
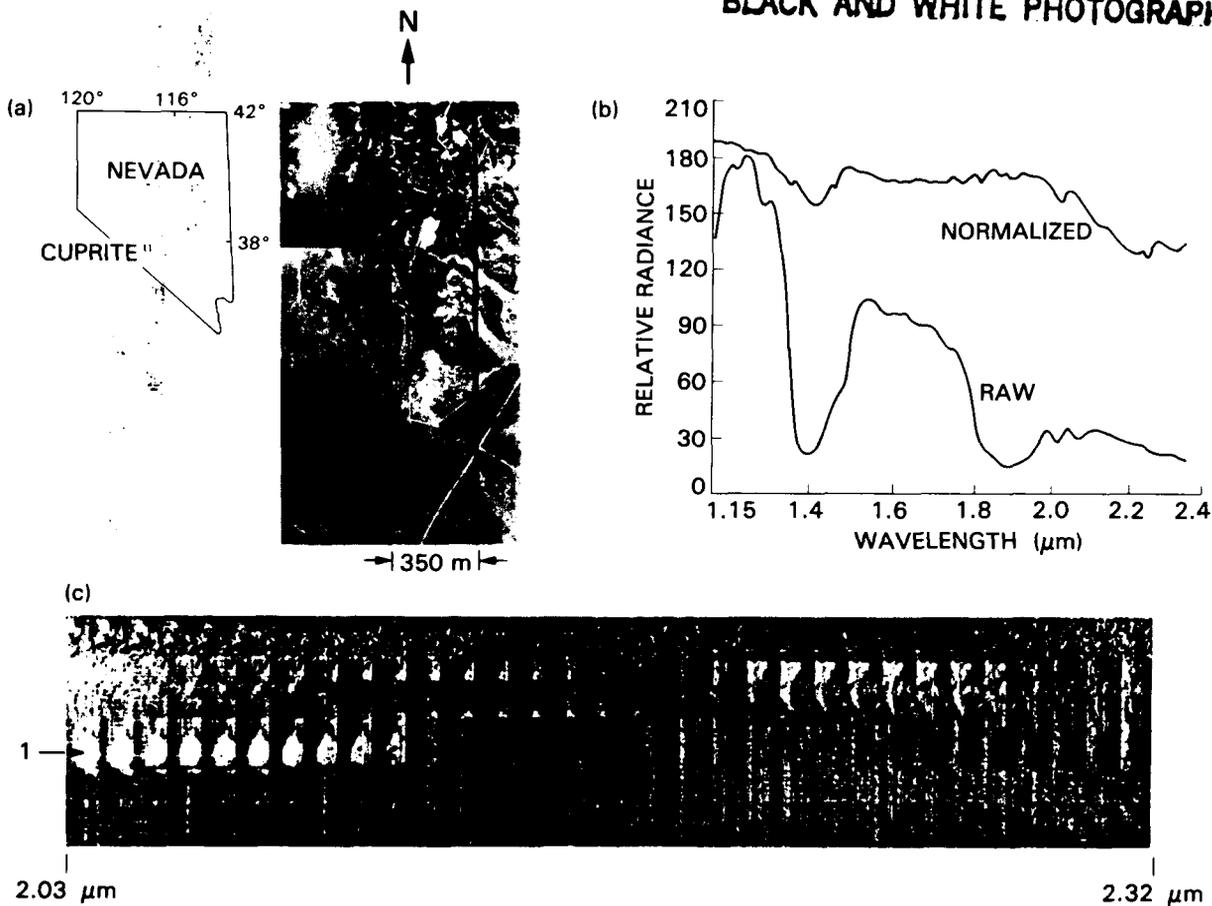
Figure 5. (a) Air photo of a portion of the Cuprite mining district in Nevada, superimposed with the AIS coverage. (b) Spectra (128 channels) derived from a 5×5 pixel area in the AIS-1 image of the Cuprite mining district. The normalized spectrum approximates the ground spectral reflectance. (c) A set of 32 AIS spectral images over Cuprite taken at 9.3-nm intervals between 2.03 and 2.32 μm in which each pixel spectrum has been normalized to produce an equal area under the reflectance curve. The differing reflectance characteristics as a function of wavelength are clearly visible (location 1).

and supportive research in remote sensing. However, to acquire data with greater spectral and spatial coverage, a new instrument called the AVIRIS has been developed (Vane et al., 1984a).

AVIRIS covers the visible and near infrared, as well as the short-wavelength infrared, imaging in the mode shown in Figure 2c. Using line arrays of silicon and indium antimonide, images 550 pixels across in 224 contiguous spectral bands from 0.41 to 2.45 μm are acquired by the instrument as it is flown 20 km above the Earth aboard a NASA ER-2 aircraft. From that altitude, the AVIRIS swath width is about 11 km, and the GIFOV is 20 m. The functional parameters for AVIRIS are summarized in Table 2. Figure 7 shows the conceptual layout of the instrument. In addition to thorough ground calibration of AVIRIS, the instrument also has an onboard calibrator that allows collection of dark current, spectral and radiometric calibration information during image acquisition.

An integral part of the AVIRIS program at JPL is the data handling system (Vane et al., 1984a),

Table 2. AVIRIS Observational Parameters

IFOV	1 mrad
GIFOV (at 20 km altitude)	20 m
FOV	30°
Swath width (at 20 km altitude)	11 km
Spectral coverage	0.41–2.45 μm
Number of spectral bands	224
Digitization	10 bits
Data rate	17 Mbits/sec

Spectrometer	Wavelength Range (μm)	Number of Samples	Sampling Interval (nm)
1	0.4–0.72	31	9.7
2	0.69–1.30	63	9.6
3	1.25–1.87	63	8.8
4	1.84–2.45	63	11.6

7

WAVELENGTH (μm)
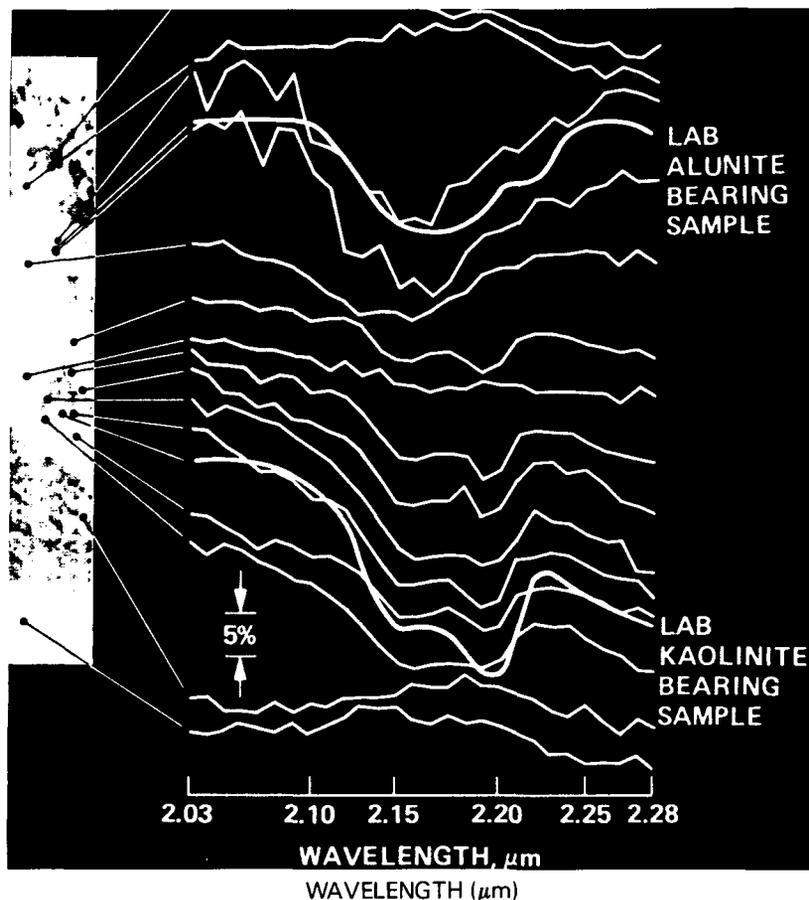
Figure 6. AIS image from cuprite, Nevada showing 3×3 pixel spectra of three representative surface units. Direct identification of the dominant minerals in each area, kaolinite and alunite, can be made on the basis of the 2.0 to 2.3 μm spectral response. Laboratory spectra of field-collected samples are also shown (yellow lines), and they verify the AIS results.

which is dedicated to converting the raw data recorded on high-density tapes aboard the aircraft to geometrically and radiometrically corrected data that are written onto computer-compatible tapes for subsequent analysis and information extraction. The system has been sized to allow a 2-week turnaround time from receipt of the raw data from an 11×11 km scene to completion of the radiometric and geometric processing.

AVIRIS system checkout aboard the ER-2 began in early 1987. Allowing the early months of 1987 for final system adjustments, AVIRIS became operational in the summer of 1987 to support scientific studies consistent with the goals of the NASA Earth Science and Applications Division. A major activity in 1987, in addition to the science studies, is AVIRIS data quality assessment, through funding of 17 investigations representing geology, terrestrial ecology, atmospheric radiation studies, oceanography, and snow and ice studies. JPL will be responsible for instrument operation and calibration and data handling during the first 2 years of AVIRIS operations, while NASA/Ames Research Center builds its capability to take over these functions in

1988 or 1989. At that time, full operational responsibility will be shifted to Ames, including data handling, distribution, and archiving.

An example of an AVIRIS image appears on the cover of this report.
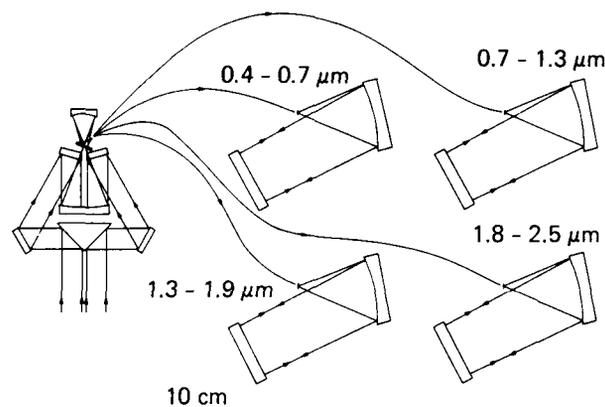
Figure 7. Schematic diagram of the AVIRIS sensor showing four spectrometers connected to the scanning head with optical fibers.

8

II. SPECTRAL REMOTE SENSING BACKGROUND

GEOLOGY

Extensive use of satellite measurements for geologic investigations began in 1972 with the successful launch of Landsat 1 with the MSS. Two important capabilities soon became apparent: (1) analysis of regional- to continental-scale tectonic, magmatic, and depositional features benefits from the synoptic view provided by Landsat MSS images, and (2) many lithologic units can be distinguished through proper digital processing of image spectral radiance data of rocks, soils, and vegetation.

These capabilities have been used to augment the conventional field approach to a variety of geologic investigations, especially geologic mapping. In poorly mapped, reasonably well-exposed areas the distribution of spectrally distinctive lithologies can be analyzed to delineate major folds, fracture systems, volcanic constructs, and some nonconformities. Where geologic mapping is more complete, locally documented features are commonly extended for large distances, and in many areas new features have been discovered. However, extensive field evaluation is needed for verifying these interpretations, especially in identifying the composition of spectrally contrasting rock units. The only rock material that can be identified from MSS data on the basis of a spectral feature is limonite, a combination of Fe^{3+} minerals. Although this capability has been used extensively for mapping hydrothermally altered rocks, identification of other minerals that lead to determination of lithologic composition cannot be obtained from the MSS radiance measurements.

In Landsat TM images more rock types can be distinguished, and somewhat narrower limits can be placed on their mineralogic composition. The additional 1.6 μm and 2.2 μm bands provide a means of detecting and mapping minerals that have OH, HOH, and CO_3 absorption features. The 30 m resolution and high geometric quality also contribute to the high geologic value of TM images.

Figure 8 illustrates the use of a TM color-ratio composite image for mapping hydrothermally altered rocks in southern Nevada. An MSS color-ratio composite image is shown in Figure 9 for comparison. In the TM composite image, limonitic altered rocks containing the OH-bearing minerals kaolinite, alunite, sericite, and jarosite appear white and yellow. Rocks containing HOH-bearing minerals such as gypsum and zeolites are white and magenta, respectively. These colors are related to Fe^{3+} absorption in the short-wavelength region, and OH and HOH absorption in the long-wavelength region; subtle color differences reflect variations in absorption intensity.

Although the presence of OH and HOH, as well as Fe^{3+} minerals, can be deduced from the colors in the TM color-ratio composite image, mineral identification using this spectral reflectance information alone was not possible. The mineral identifications were made through laboratory x-ray diffraction studies. However, *in situ* reflectance spectra representing some of these rock types exhibit absorption features that permit definition of compositional limits. For example, an absorption minimum centered near 2.17 μm is indicative of alunite, dickite, or pyrophyllite. A feature at 2.20 μm can be caused by sericite or kaolinite, although with adequate spectral resolution these minerals can be separated. The reflectances of HOH-bearing zeolites decrease markedly from 1.6 μm to 2.2 μm, but distinct absorption features are lacking in this wavelength region. Unaltered andesite lacks OH and HOH absorption features.

The use of high spectral resolution remote sensing for the identification of minerals began in the last few years with the advent of remote sensing instruments that have improved spectral resolution. Chin and Collins (1978) and Collins *et al.* (1983) developed an aircraft spectroradiometer with which they demonstrated the presence of overtone bands for direct identification of clay minerals. It was recognized, based on field and laboratory as well as aircraft measurements, that imaging systems with higher spectral resolution than either the MSS or TM would be necessary to advance remote sensing to the point where mineral identification could be made (as opposed to the TM- and MSS-based technique of separating cover types into classes based on their broadband spectral characteristics) (Goetz and Rowan, 1981; Goetz *et al.*, 1983).

The first measurements confirming the possibility of direct identification of mineral types from orbit were made by Goetz *et al.* (1982) with SMIRR. SMIRR was an instrument designed to test narrow-band channels in the 0.5 to 2.4 μm wavelength region as a means of identifying minerals from Earth orbit. The instrument was carried during the second flight of the shuttle spacecraft in November 1981 and produced several hundred thousand cloud-free spectra, each containing 10 radiance values for a 100 m diameter spot on the ground. Five channels were placed between 2.0 to 2.4 μm. Their center wavelengths and half-widths in micrometers were 2.10/0.10, 2.17/0.02, 2.20/0.02, 2.22/0.02, and 2.35/0.06. These bands were chosen to allow identification of the minerals alunite, kaolinite, montmorillonite, and calcite provided no other interfering minerals were present. For instance, serpentine contains a 2.32 μm absorption feature which is indistinguishable from the CO_3 absorption feature. At the time of the development of the instrument, it was not

Figure 8. Landsat TM ratio composite of southern Nevada. Band ratios 5/7, 5/4 and 3/1 are displayed as red, green, and blue, respectively.
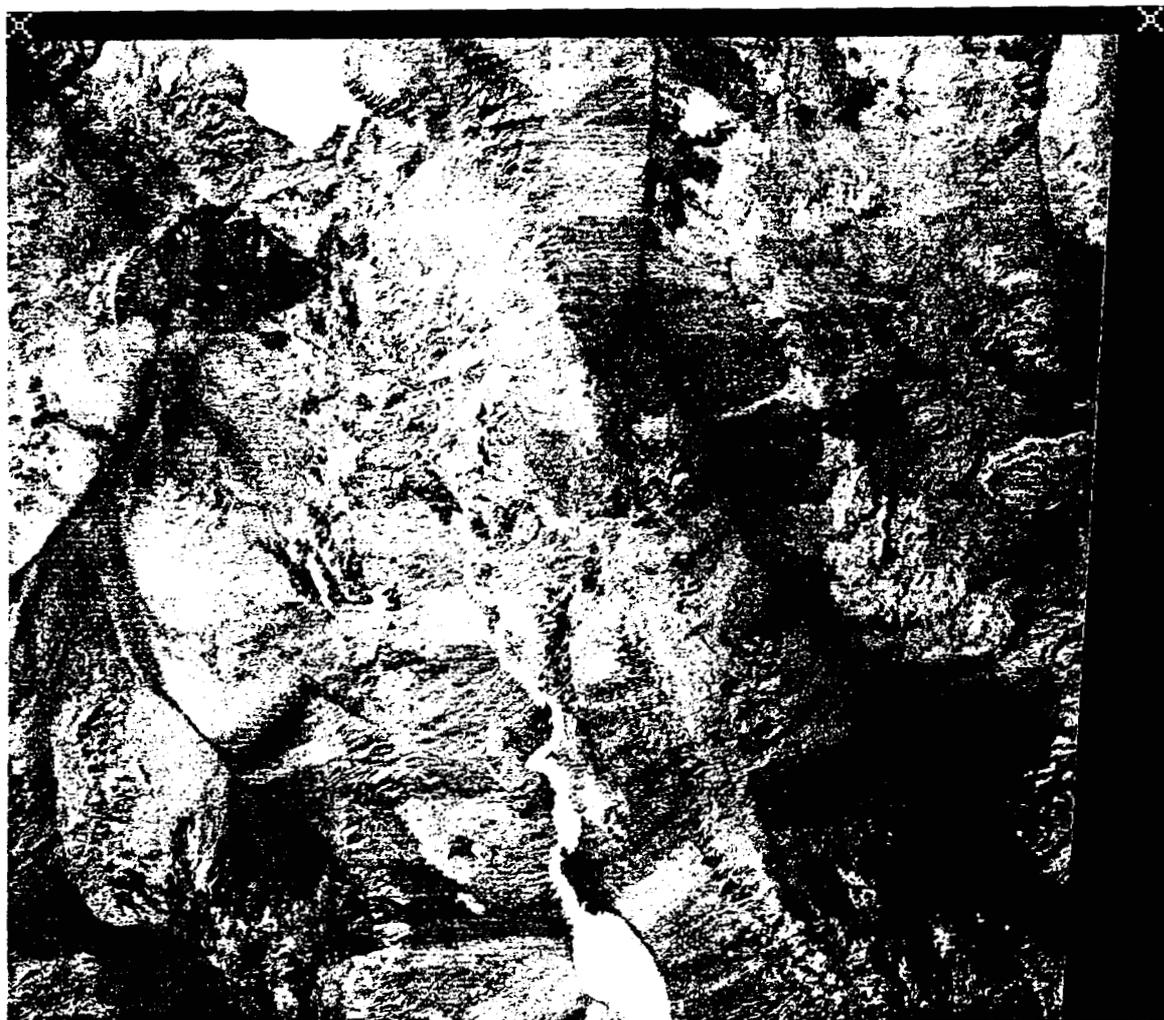
Figure 9. Landsat MSS ratio composite of southern Nevada. Band radios 4/5, 6/7, and 5/6 are displayed as red, green, and blue, respectively.

possible to add more than five channels in the 2.1 to 2.4 μm region without compromising other objectives for the instrument. Subsequent to the initial identification of kaolinite and carbonate from spectra taken over Egypt (Goetz *et al.*, 1982), an alteration zone in Baja California was identified on the basis of the presence of iron oxide minerals, clay minerals, and possibly alunite (Rowan *et al.*, 1983). Laboratory spectral reflectance of samples acquired in the area show the presence of pyrophyllite and/or dickite plus kaolinite and K-mica in addition to dia-

spore. The assemblages of aluminous OH-bearing minerals in the altered rocks result in complex reflectance spectra. Such spectra may be interpreted for sample mineralogy, but higher spectral resolution than available with the three contiguous narrow bands sampled with SMIRR is necessary. The 2.17 μm band produced by pyrophyllite is broadened when other OH minerals are abundant. The broadened 2.17 μm feature strongly resembles the characteristic spectral reflectance of alunite, even though no alunite is present. This example points to the need

11

for sufficiently high spectral resolution and proper contiguous sampling in remote sensing instruments in order to correctly identify mineralogy.

Imaging spectrometry offers the possibility of directly identifying minerals containing iron or other transition elements with electronic transitions in the visible and near infrared, as well as minerals bearing OH, CO_3, and SO_4 that exhibit vibrational features beyond 1.0 μm. Another important advance will be the ability to identify components of mixtures of minerals as well as minerals and vegetation. These advances provide new vistas in the application of remote sensing techniques to geologic problems.

OCEANS AND INLAND WATERS

Oceans

Ocean color data have been collected since late 1978 from the Coastal Zone Color Scanner (CZCS) on the Nimbus-7 satellite (Hovis et al., 1980). The data have been primarily used for studies of meso-scale processes in the ocean (Abbott and Zion, 1985; Brown et al., 1985). Using the four spectral bands that are available, the CZCS data are corrected for atmospheric radiance (Gordon et al., 1983) and are then used to estimate near-surface phytoplankton pigment concentrations (Figure 10). Recent work has focused on the estimation of water column primary productivity using the pigment concentration (Eppley et al., 1985).

The spatial resolution of CZCS (nominally 1 km) is particularly useful for studies of mesoscale processes in the ocean. Early studies tended to focus on the relationship of particular images to ship-derived maps of pigment (Smith et al., 1982). These and other ship studies of phytoplankton variability showed that, given the characteristic scales of temporal and spatial variability, maps of phytoplankton abundance derived from satellite data would fill a large gap in the existing data sets. Later studies began to examine time series of CZCS imagery to study phenomena that have considerable temporal variability such as the spring bloom (Brown et al., 1985) and upwelling events in the coastal ocean (Abbott and Zion, 1985). CZCS data have also been used successfully in the study of fish distributions (Laurs et al., 1984) and in the identification of coccolith blooms (Holligan et al., 1983), which may be important in carbon cycling.

As much as 90 percent of the radiance received by a satellite viewing the ocean is due to light scattered by molecules (Rayleigh scattering) and aerosols (aerosol scattering) in the atmosphere. This means that the atmospheric contribution to the radiance received by CZCS or future water-viewing satellite sensors must be accurately evaluated in order for the residual water-leaving radiance to be determined correctly.

Present CZCS algorithms estimate the atmospheric radiance fraction of the total radiance to accuracies of better than 1 percent for scan angles within 25° of nadir. This accuracy is thought to be limited by instrument calibration relative to the solar constant. Gordon (1981), however, has pointed out that even this accuracy can be significantly improved by the use of a diffuser plate to view the sun in diffuse reflection. Rayleigh scattering, the largest atmospheric scattering component, is computed a priori from theory, while aerosol scattering is estimated by using a 670 nm channel in the near infrared where ocean waters with low-pigment concentration (less than 1 mg chlorophyll/m^3) appear essentially black (Gordon et al., 1983).

HIRIS offers the possibility of dramatic improvements over such algorithms. A variety of channels in the longer near-infrared wavelengths can be utilized as a basis for atmospheric correction over waters with higher sediment or pigment concentration than are presently addressable with CZCS. The fine spectral resolution and numerous channels of the imaging spectrometer also permit mapping of the aerosol selectivity in the near-infrared and longer visible wavelengths over clear water for various continental and maritime aerosols. This should enable improvement of atmospheric correction methodologies for data over the ocean and land. The status of the present atmospheric correction methodology is that it is sufficiently accurate for the purposes required by near solar zenith applications using an imaging spectrometer. Modifications of these algorithms will probably be required in order to accommodate zenith angles corresponding to times earlier in the morning or later in the afternoon.

After atmospheric effects have been removed from the radiance values received by the satellite, the semi-empirical relationships between inherent and apparent optical properties can be used to extract significant information about phytoplankton pigment concentration, detritus, and gelbstoff in the ocean. The water-leaving radiance of the top attenuation depth (e.g., about 20 m for clear ocean water) can be described by a model (Morel and Prieur, 1977; Carder and Steward, 1985) that includes parameterization for the backscattering coefficients for water molecules (known) and particle constituents (e.g., phytoplankton, detritus, and suspended sediments), and the absorption coefficients due to water (known), gelbstoff (dissolved yellow matter), and particles (mostly phytoplankton).

For most open ocean waters with low suspended sediment concentration (Case I waters) the non-water terms of the equation covary with chlorophyll-like pigment concentration (chlorophyll a). Figure 11 depicts the variation of the spectral slope of water-leaving radiance in the blue-green portion of the spectrum with increasing chlorophyll pigments. Estimation of chlorophyll contained in the top attenuation depth has been found to be accurate for CZCS data for Case I waters to within 30 to 40 percent. Since phytoplankton doubling rates range from about 0.3 to more than twice per day, this level

Figure 10. Phytoplankton chlorophyll distribution in the western North Atlantic. This image was produced by compositing eight CZCS passes made over 5 days from May 3-7, 1981. A few small areas of persistent cloud cover are shown in white. Areas rich in phytoplankton are shown as red (>1 mg chlorophyll/m^3) progressing through orange, yellow, green, and blue, with purple representing the lowest chlorophyll concentrations (<0.01 mg/m^3).

of accuracy is very useful for assessing regional or global stocks of phytoplankton or observing the dynamics of a bloom (population explosion) with time. However, errors resulting from the effects of phytoplankton cell size and non-covarying gelbstoff and detritus can significantly affect the accuracy, even for offshore waters (Carder and Steward, 1985; Carder et al., 1986).
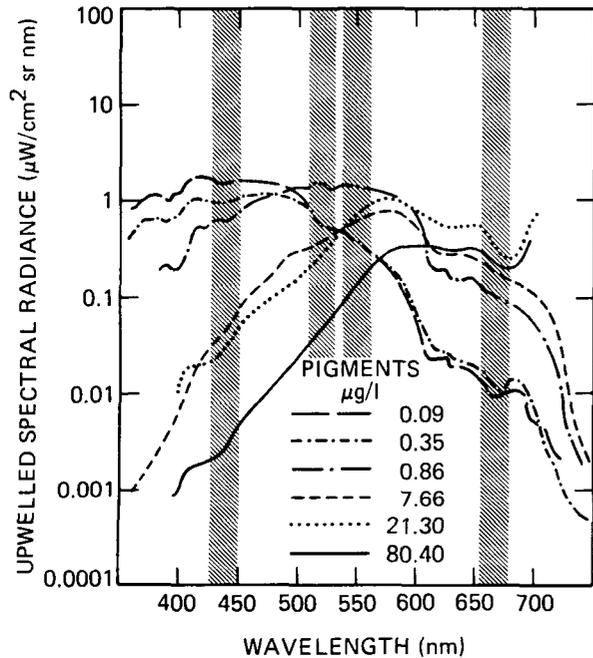
Figure 11. Upwelled spectral radiance as a function of chlorophyll pigment concentration for various ocean waters. Shaded bars represent CZCS bands.

To address near-shore or inland waters (Case II waters) that can visibly fluoresce and contain suspended sediments and gelbstoff not covarying with chlorophyll pigments, increased spectral resolution and numbers of channels relative to the CZCS configuration are required (Figure 12). This permits quantification of gelbstoff, detritus, or suspended sediments, and for high chlorophyll regions, fluorescence efficiency, which can be indicative of nutrient stress or high light adaptation (Carder and Steward, 1985; Carder et al., 1986).

Inland Waters

Inland waters have several distinctive characteristics, which require special attention if remote sensing of those ecosystems is to succeed:

- Sizes are moderate to small (e.g., 100 km to < 1 km in length).

- Long, complex interfaces between land and water occur.

- A very wide range of optical conditions occur and can change over a range of time scales from seconds to months.

- Strong horizontal and vertical gradients in biological and physicochemical conditions are common.

Current remote-sensing methodology has had only modest success in the examination of inland waters (Hilton, 1984). Identification of open water is relatively simple, and lakes and rivers have been located and counted and their bathymetry determined using aircraft and spaceborne sensors (Lemoalle, 1978; Boland et al., 1979). Sediment plumes associated with rivers entering lakes and sediments resuspended within lakes are also conspicuous (Abiodun, 1976; Holyer, 1978; Marks and Melack, 1982). Whiting, the precipitation of calcium carbonate in the open water region of lakes and in shallow tropical seawater, has been observed (Strong and Eadie, 1978). Spatial heterogeneity of phytoplankton abundance has been recognized on some images obtained from aircraft and satellites (Strong, 1974; Horne and Wrigley, 1975; Lindell, 1981; Almanza and Melack, 1985).

MSS has been the primary satellite-borne radiometer used for observing inland waters. This broadband system permits only limited discrimination of chlorophyll present in phytoplankton (Bukata et al., 1974; Boland, 1976; Lemoalle, 1979; Lindell, 1981; Almanza and Melack, 1985). This modest success stems in part from the spectral characteristics of MSS, the complex and variable optical properties of inland waters, and the influence of the atmosphere and specular reflection from the water's surface on the signal received by MSS.
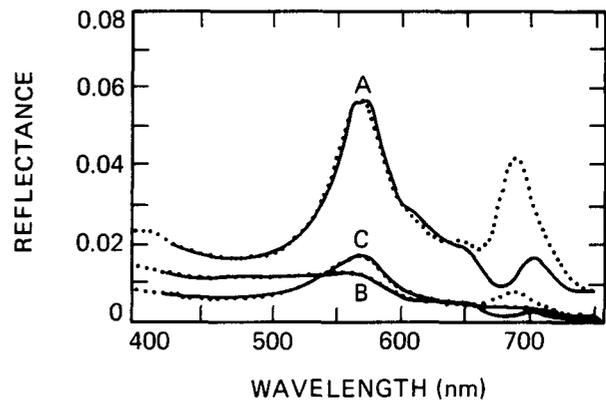
Figure 12. Comparison of modeled (——) and measured (· · · ·) spectral remote-sensing reflectance data at three stations (A, B, and C) off the west coast of Florida during a red tide bloom with chlorophyll pigment concentrations ranging from 7 to 77 mg/m³, and varying concentrations of gelbstoff and detritus. The difference between the measured and modeled curve at about 685 nm is due to fluorescence. This difference is exploited to determine quantum fluorescence efficiency, a variable indicative of nutrient stress (Carder et al., 1985).

14

Spatial and Spectral Limitations with Present Satellite Systems

CZCS retrieval validity is limited by a lack of knowledge of the role of subpixel scale (<800 m) cloudiness, pigment/sediment variability, and various instrumental electronic problems. HIRIS addresses these problem areas by increased spatial resolution and improved response characteristics. The present spatial resolutions have limited use of CZCS to the study of oceanic features with spatial scales of 5 km or larger. Thus, study of many aspects of spatial variability in the phytoplankton has been limited to rather gross characterization of large-scale events such as a spring bloom or upwelling off coastal capes. The imaging spectrometer should attain similar levels of performance at scales of 100 to 200 m, which are more easily validated by surface measurements. In addition, the large-scale aspects of the various applications of HIRIS should permit regional and global studies of biological variability on these smaller scales. These studies are simply not possible with Landsat MSS and TM systems, which have provided adequate spatial resolution for inland waters (circa 80 m and 30 m) by sacrificing spectral definition and sensitivity. HIRIS will offer the flexibility of combining spectral bands or combining pixels to increase radiometric resolution.

Of the four CZCS visible spectral bands, one band is required for determining the aerosol concentration. This leaves two or at most three bands for inferring concentrations of oceanic constituents. The number and distribution of spectral bands on the Landsat satellites were not optimized for the range of conditions expected for inland waters, and therefore do not permit discrimination of the aerosols common over lakes and rivers. Since the presence of gelbstoff, suspended sediment, and specularly reflected sun glint can all contribute to errors in satellite determinations of chlorophyll, quantification of their effects on the water-leaving radiance is important not only for improving the accuracy of chlorophyll retrievals from coastal and inland waters, but also for sediment and humic acid transport studies. Each of these water components has a spectrally recognizable remote-sensing reflectance signature, so their contributions are separable, given an adequate number of spectral bands in the visible and near-infrared wavelengths (Carder and Steward, 1985).

SOILS

Aerial photography has been a standard tool for mapping soils since its introduction more than 50 years ago (Bushnell, 1951). Photographs increased the speed and accuracy of soil mapping because of the wealth of ground detail shown, the accessibility to areas of rugged terrain, and the synoptic view of the soil in the landscape. Tonal characteristics of the photographs permitted the delineation of soil boundaries, but photointerpretation of film products

cannot adequately discriminate soils (Cihlar and Protz, 1972). In the 1960s optical-mechanical scanner systems, along with computer pattern-recognition techniques, introduced a new dimension for studying soils. Soil surface conditions could be mapped with reasonable accuracy by computer-aided analysis of multispectral scanner data (Kristof, 1971; Weismiller and Kaminsky, 1978; Westin and Frazee, 1976).

In a cooperative research effort between Purdue University and the U.S. Soil Conservation Service (SCS), the soil survey of Jasper County, Indiana, was the first to use Landsat MSS data to aid the soil scientists in delineating soil boundaries (Weismiller and Kaminsky, 1978; Weismiller et al., 1979). Map sheets were prepared for the soil survey by first partitioning the county into different parent-material areas based on photointerpretation of Landsat imagery and then identifying soils within each parent material with computer-aided classification of the multispectral data.

One of the major obstacles facing soil scientists in using remotely sensed data is defining the spectral characteristics of soils under a wide range of environmental conditions. A quantitative approach to spectral characterization of soils should lead to improvements in soil information systems and in models of management and productivity (Baumgardner and Stoner, 1982).

Soil reflectance is a cumulative property, which derives from inherent spectral behavior of the heterogeneous combination of mineral and organic matter and soil water. Numerous studies have described the relative contributions of soil parameters, such as organic matter, soil moisture, particle-size distribution, soil structure, iron oxide content, soil mineralogy, and parent material to the reflectance of naturally occurring soils (Baumgardner et al., 1985; Bowers and Hanks, 1965; Bowers and Smith, 1972; Karmanov, 1970; Myers and Allen, 1968; Obukhov and Orlov, 1964; Planet, 1970; Stoner et al., 1980).

Extensive literature exists describing the characteristic variations in visible and near-infrared reflectance of minerals and rocks (Hunt, 1977; Hunt and Salisbury, 1970, 1971, 1976a, 1976b; Hunt et al., 1971a, 1971b, 1972, 1973a, 1973b, 1973c, 1974). Hunt's studies reveal the intrinsic spectral features that appear in the form of bands and slopes in the bidirectional reflectance spectra of minerals as caused by a variety of electronic and vibrational processes. Reflectance measurements of 160 soil samples from 36 states are the basis for an investigation by Condit (1970, 1972) that classifies all soil spectral curve types in relation to soil characteristics or soil classification. Cipra et al. (1971) conducted field spectroradiometric studies and described the properties and classification of seven soil series in terms of Condit's spectral curve types.

Stoner's (1979) work revealed the existence of five distinct soil reflectance curve forms identified by curve shape and the presence or absence of absorp-

tion bands. In addition, these five soil spectral reflectance curve forms could be distinguished by differentiating characteristics caused by the organic content and the iron oxide content. Reflectance spectra representative of the five curve forms are illustrated for five mineral soil samples (Figure 13). Characteristics of these specific surface soils are detailed for comparison of reflectance-related soil properties (Table 3).
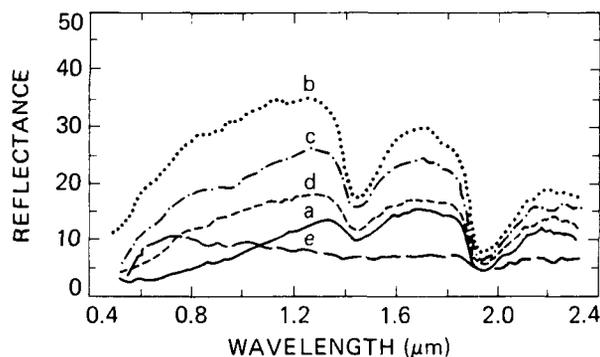
Figure 13. Representative reflectance spectra of surface samples of five mineral soils: (a) organic-dominated (high organic content, moderate fine texture); (b) minimally altered (low organic, low iron content); (c) iron-affected (low organic content, medium iron content); (d) organic-affected (high organic content, moderate coarse texture); and (e) iron-dominated (high iron content, fine texture).

The organic-dominated form (a) exhibits a low overall reflectance with a characteristic concave curve shape from 0.5 to 1.3 μm. Strong water absorption bands are present at 1.45 and 1.95 μm in this and most other curve forms. The broadness of these bands indicates the presence of water molecules in relatively unordered sites, probably as water films on soil particle surfaces (Ångstrom, 1925; Hunt and Salisbury, 1970).

The minimally altered form (b) is characterized by overall high reflectance and a characteristic convex curve shape from 0.5 to 1.3 μm. In addition to the strong water absorption bands at 1.45 and 1.95 μm, weak water absorption bands may be present at 1.2 and 1.77 μm. These weak absorption bands correspond to the absorption bands observed in transmission spectra of relatively thick water films of the type that may be expected to fill the voids between fine sand grains (Lindberg and Snyder, 1972).

The iron-affected form (c) is distinguished by a slight ferric iron absorption band at 0.7 μm together with the stronger 0.9 μm iron absorption band (Hunt et al., 1971a). The 2.2 μm hydroxyl absorption band can be seen in this specific sample, but does not exhibit a consistent relationship with any particular curve form or soil property.

A fourth curve type, labeled the organic-affected form (d), typically has a higher overall reflectance than the organic-dominated form. It exhibits a

Table 3. Characteristics of Surface Samples of Five Mineral Soils

	Reflectance Curve Form				
Soil Attribute	Organic-Dominated	Minimally Altered	Iron-Affected	Organic-Affected	Iron-Dominated
Soil series	Drummer	Jal	Talbott	Onaway	(Not given)
Horizon sampled	Ap	All	Ap	Ap	Ap (0–10 cm)
Soil subgroup	Typic Haplaquoll	Typic Calciorthid	Typic Hapludalf	Alfic Haplorthod	Typic Haplorthox
Sample location	Champaign Co., IL, USA	Lea Co., NM, USA	Rutherford Co., TN, USA	Delta Co., MI, USA	Londrina, Parana, Brazil
Climatic zone	Humid mesic	Semiarid thermic	Humid thermic	Humid frigid	Humid hyperthermic
Parent material	Loess over glacial drift	Fine textured alluvium or lacustrine	Clayey limestone residuum	Glacial drift	Basalt
Drainage class	Poorly drained	Well drained	Well drained	Well drained	Excessively drained
Textural class	Silty clay loam	Loamy fine sand	Silty clay loam	Fine sandy loam	Clay
Munsell color	Black	Brown	Strong brown	Dark brown	Dark red
Contents					
Organic matter	5.61%	0.59%	1.84%	3.3%	2.28%
Iron oxide	0.76%	0.03%	3.68%	0.81%	25.6%
Moisture at 0.1 bar tension	41.1%	17.0%	28.2%	27.3%	33.1%

concave shape from 0.5 to 0.75 μm with a convex shape from 0.75 to 1.3 μm.

The fifth curve type, the iron-dominated form (e), is unique in that reflectance actually decreases with increasing wavelength beyond 0.75 μm. In some soils, such as the one shown here, absorption in the middle infrared wavelengths is so strong that the 1.45 and 1.95 μm water absorption bands are almost obliterated.

Soil parameters characteristic for specific reflectance properties serve to differentiate soil spectral reflectance curve forms (Table 4). Mineral soils with the organic-dominated curve form have high organic matter contents (greater than 2 percent) well dispersed as coatings on the fine to moderately fine soil grains. In the case of organic soils, the decomposition state of plant remains determines the reflectance curve form. Fully decomposed organic fibers reflect in the manner of the organic-dominated form, while well-preserved fibers exhibit the higher reflecting organic-affected form. The high reflectance of fibric soil materials in the infrared region resembles the infrared reflectance of senesced leaves (Gausman et al., 1975). This increased infrared reflectance has been attributed to tissue morphology in which an increased number of air voids provide more air-cell interfaces for enhanced reflection.

The organic-dominated curve form is often associated with montmorillonitic clay mineralogy, while soils with the iron-dominated curve form have been seen to exhibit kaolinitic mineralogy. Inherent spectral properties of clay minerals are not responsible for the character of soil reflectance curves (Lindberg and Snyder, 1972), but mineralogy is interrelated with organic matter content, iron oxide content, and texture, which directly affect soil reflectance.

Soils with the minimally altered curve form are characterized by low organic matter content, low iron oxide content, and good drainage. Texture and mineralogy vary in these soils. Medium iron oxide contents (from 1 to 4 percent) distinguish soils with the iron-affected curve form from those with the minimally altered form. Soils with the iron-dominated curve form have high iron oxide contents (greater than 4 percent) that appear capable of masking out even the effects of high organic matter contents. Mineral soils with the organic-affected curve form differ from those with the organic-dominated form principally because of coarser soil textures.

VEGETATION

Spectral Information

Two conditions must be met if imaging spectrometry is to be useful in the analysis of terrestrial ecosystems. First, there must be strong relationships between canopy characteristics and the rates at which processes important to the biosphere occur. Second, it must be possible to measure these canopy characteristics remotely using high spectral resolution data.

Due to the inherent complexity of biological systems, the field biological sciences have lagged behind many of the physical sciences in identifying the key processes and attributes that control the systems under study. Only in the last several years has information begun to appear at the ecosystem level that suggests that broad generalizations of the type required for biospheric studies may be derivable. These cover the major processes of photosynthesis, primary production, herbivore consumption, and decomposition, as well as the general detection of stress.

The maximum rate of net photosynthesis for the leaf of any C-3 plant is a function of its nitrogen content, regardless of species (Mooney and Gulmon, 1982; Field et al., 1983). The idea that photosynthetic rates can be estimated from leaf chemistry without having to know the species involved is pivotal to estimating photosynthesis of the whole canopy. It is nearly certain that whole canopy chemical parameters will be measured more easily than species composition using high spectral resolution data. The "taxa" of interest in ecosystem studies at the biospheric level may not be species, as recognized by the botanist, but rather much larger groups that share common physiological mechanisms or pathways (e.g., C-3 versus C-4 photosynthesis or nitrogen fixing versus non-fixing).

At a larger scale, total net primary productivity by plant communities may also be strongly related to simple, measurable parameters such as total leaf area or total foliar nitrogen. Linder (1985) found a correlation of net above-ground productivity with annual interception of short-wave radiation, and Kira and Shidei (1967) relate gross photosynthesis to a product of leaf area index (LAI) and length of seasonal leaf display. Agren (1983) has reported strong correlations between total canopy nitrogen content and total annual above-ground productivity. Differences in the slopes and intercepts for these two lines reflect differences in climate, length of growing season, and differences in carbon allocation patterns between different physiological groups (deciduous broad-leaved versus evergreen coniferous).

Plant communities alter their allocation of carbon, and thus the nutrients available for herbivore consumption, between primary products such as cellulose and secondary, woody and defense-related compounds, depending on the relative availability of carbon (through photosynthesis) and nutrients. Of particular importance in temperate systems is lignin, a complex, amorphous polyphenol that is very resistant to insect attack. Recent studies (Waring and Pitman, 1985; Larsson et al., 1983) have shown that reduced tree vigor increases the susceptibility to insect attack and that this can be reversed by thinning or fertilization. The lignin content of foliage may be a sensitive indicator of the carbon status of the community and of the potential for insect outbreak.

It is intriguing, but perhaps not surprising, that the same factors that control photosynthesis, pro-

Table 4. Differentiating Characteristics of Five Soil Spectral Reflectance Curve Forms

Differentiating Characteristics	Reflectance Curve Form				
	Organic–Dominated	Minimally Altered	Iron–Affected	Organic–Affected	Iron–Dominated
Vegetational effects					
Mineral soils[1]	High organic matter content	Low organic matter content	Low organic matter content	High organic matter content	Varied organic matter content
Organic soils	Fully decomposed organic fibers			Organic fibers preserved	
Iron oxide content[2]	Low	Low	Medium[3]	Low	High
Texture	Fine to moderately fine textured soils	Varied	Varied	Medium- to coarse-textured soils	Fine-textured
Natural drainage	Poor to good	Good	Good	Poor to good	Good
Mineralogy	Commonly montmorillonitic	Mixed	Mixed	Mixed	Commonly kaolinitic

[1]Low organic matter content = 0 to 2%, high = 2 + %.
[2]Low iron oxide content = 0 to 1%, medium 1 to 4%, high 4 + %.
[3]Soils with low iron oxide contents occurring as coatings on coarse-textured soil particles exhibit the same curve form.

ductivity, and herbivory in living plants are also crucial in the decomposition process. Decomposition rates are increased in materials that are rich in nitrogen and decreased in materials with high lignin contents (Fogel and Cromack, 1977; Meentemeyer, 1978; Merrill and Cowling, 1966). The decay rate for forest leaf litter can be predicted from the ratio of these two compounds (Melillo et al., 1982). The patterns and quantity of nitrogen immobilization and mineralization are also a function of this ratio (Aber and Melillo, 1982). Thus, if lignin and nitrogen content of leaves can be measured by reflectance at senescence, carbon and nitrogen turnover in decomposition can be estimated.

Unusual soil conditions or high levels of pollution loading can cause stresses in vegetation that are not directly reflected in the nitrogen or lignin contents. Such general stress indicators as the "blue shift" of the red edge of the reflectance curve before the near-infrared plateau, at approximately 700 nm, have been used to indicate the possible presence of heavy metal stress in plants due to either anomalous soil conditions (Collins et al., 1983) or pollution (Rock et al., 1986).

If nitrogen and lignin contents appear to be important characteristics of vegetation canopies, can these be measured remotely? Nitrogen content is already measured routinely in the laboratory by reflectance in the visible part of the spectrum. For example, Tsay et al. (1982) estimated total N content of fresh loblolly pine needles using reflectance at 540 nm. Commercial devices have been developed that estimate N content of dried, ground samples within the repeatability of wet chemical methods, using reflectance between 2.0 and 2.4 μm (10 nm bandwidth, Hooten, 1978; Rotolo, 1979). These devices have become the accepted industrial standard for judging grain quality, and have recently been adapted for measurement of N content in foliage of native tree species (Wessman et al., 1987).

Specific methods for estimating carbon fractions (lignin, cellulose, starch) in actual plant tissues using commercial, laboratory infrared reflectance devices have been suggested in the past and have recently been developed to the application stage for leaves of forest trees (Wessman et al., 1987). Measurements of whole canopy contents in the field from aircraft or satellite have just begun to appear in the literature. Preliminary results suggest that quantitative measurement may be possible, or at least that there is information content at specific wavelengths (Spanner et al., 1985; Fownes and Aber, 1985).

Information from Off–nadir View Angles

Radiative transfer theory provides the mathematical basis for understanding and relating the changes in sensor signal to variations in vegetation and soil characteristics. A number of physical, mechanistic, and radiative transfer models in the short-wave region exist and have been used to increase our understanding of the scattering behavior

of vegetation canopies. Smith (1983) has reviewed these models and studies. These include plane parallel abstractions (Suits, 1972), Monte Carlo simulation (Smith and Oliver, 1972), and additive models (Cooper et al., 1982). These models are one-dimensional in that they treat the spatial variation of canopy components only in the vertical dimension. The model variables include LAI, measure of leaf orientation, spatial dispersion of leaves with height, leaf reflectance and transmittance (Lambertian properties assumed), and soil reflectance (assumed Lambertian). Often these models are used to define the lower boundary layer in atmospheric models, and the combined system is used to predict radiances at satellite levels. Recently, Gerstl and Zardecki (1985) developed a coupled atmosphere/canopy model. Other recent developments include general models that treat the spatial variation of canopy components in three dimensions (Norman and Welles, 1983). Unique variables in these models include leaf orientation and leaf density, which vary in three dimensions. A critical complement to this research will be the modeling of how the chemical constituents of individual leaves and leaf structure control the radiant scattering of the leaf.

These models and the associated analyses of vegetation canopy scattering and properties are examples of a developing body of fundamental knowledge necessary for long-term advancement of our remote sensing and Earth science programs. HIRIS will provide an unprecedented data set of many spectral bands and multiple angles that will serve to validate models and test newly developed techniques.

From these more fundamental studies there is evidence (Gerstl and Simmer, 1986) that off-nadir viewing (as opposed to only nadir viewing) provides additional and superior information about canopy characteristics. The conventional reason to look off-nadir is to increase spatial and temporal coverage of the Earth's surface. Increased temporal coverage is always desired when dealing with the highly dynamic features of vegetation. The difficulty as well as the benefit in looking off-nadir is that the sensor signal can change significantly with changing view angle. A number of individuals have documented the directional reflectance distributions of various vegetation canopies and soils as a function of sun angle (Kirchner et al., 1982; Kimes, 1983). Kimes et al. (1984) have shown that the optimum off-nadir view angles, which minimize the change in sensor response relative to the nadir response, are view angles that are in the azimuth direction perpendicular to the principal plane of the sun for all vegetation surfaces and sun angles. The differences in reflectance between the nadir and off-nadir view angles in this azimuth plane decrease significantly with decreasing solar zenith angle.

Off-nadir measurements document that the directional reflectance of vegetation canopies is very sensitive to the vegetation structure, which includes leaf orientation, leaf density, and plant spacing (Kimes, 1983, 1984). For example, Figure 14 shows how the leaf density can drastically change the directional reflectance distribution of a grass canopy. From basic studies scientists have developed and are testing various techniques for extracting structural information from off-nadir viewing angles. Strahler and Li (1981) obtained information on the distance between trees from short-wave measurements. Jackson et al. (1979) extracted information about the row spacing and row height of agricultural row crops using multiple view angles. Goel et al. (1984) described leaf orientation and leaf density using a short-wave spectral band and multiple view angles. Theoretical studies of Smith and Oliver (1974) indicate that biomass estimates should be best achieved when viewing is with a maximum divergence measured near 55° off-nadir. This prediction is supported by Bunnik (1984), who demonstrated that by viewing vegetation in the hot spot (in the direct solar beam backscatter direction) at 52° off-nadir, the reflectance is insensitive to changes in leaf orientation distributions. Gerstl (1986) has recently predicted similar changes in hot spot variation with leaf size. Thus, this off-nadir viewing geometry as opposed to nadir viewing may provide improved inferences about leaf density or percent cover. Most recently Adams et al. (1986) have employed linear mixing models incorporating a shadow, or bidirectional component, to analyze TM and MSS images that show vegetation texture effects.

In addition to providing information about the structure of vegetation canopies, off-nadir viewing provides superior information about the spectral albedo (hemispherical reflectance) of vegetation canopies and soil important in studying biospheric and atmospheric processes. Kimes and Sellers (1985) analyzed directional reflectance data in the red and near-infrared regions for 11 cover types and solar zenith angles and showed that errors in inferring spectral albedo from nadir reflectance can be as high as 45 percent. For both bands a view angle of 60° off-nadir and +90° from the solar azimuth reduces this error to less than 11 percent for all sun angles and cover types. A technique using two specific view angles reduces this error to less than 6 percent for both bands and for all sun angles and cover types.

ATMOSPHERE

While the main goals of HIRIS pertain to surface observations, it is nevertheless necessary to consider the atmosphere, which for the shorter wavelengths can account for more than 50 percent of the detected radiance. HIRIS measurements are well suited to providing information regarding key parameters of the intervening atmosphere (e.g., aerosol loading, absorptivity, cloud cover), whose determination is of intrinsic scientific value as well as necessary for correcting surface scenes for atmospheric contamination. Due to the increase of path
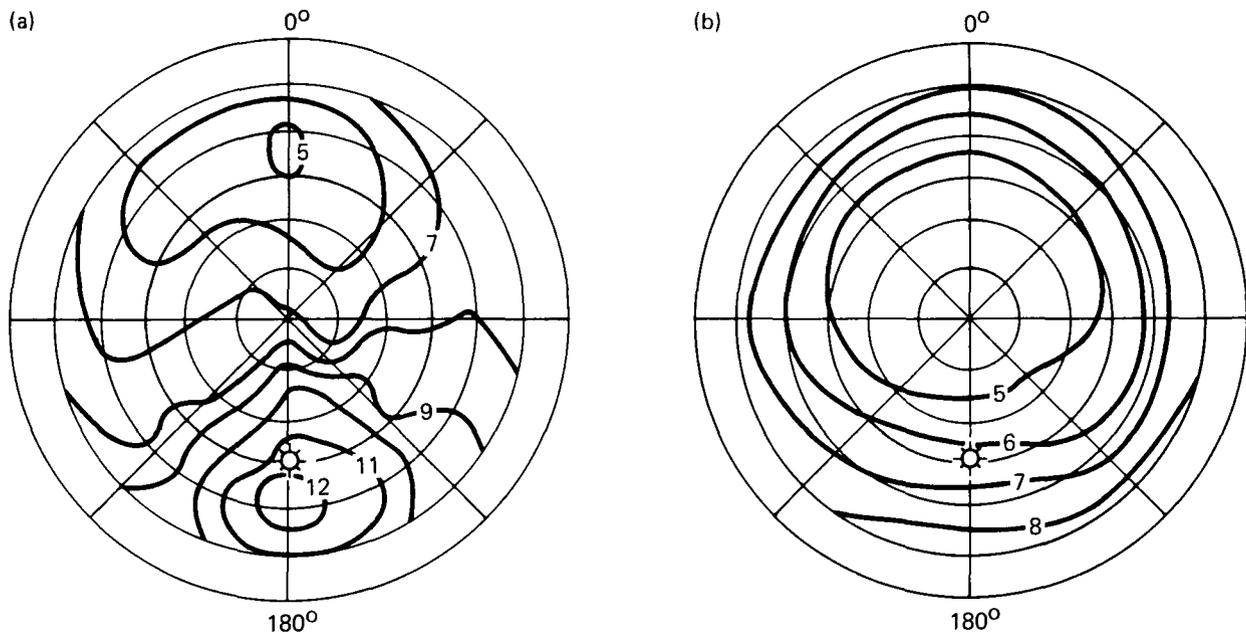
Figure 14. Polar plots of directional reflectance (%) in the Advanced Very High Resolution Radiometer band 1 (0.58 to 0.68 μm) at the ground level for a grass canopy at (a) 50% ground cover and (b) 97% ground cover. The nadir position is represented by the origin. As one moves away from the origin, 15° increments of the off-nadir angle of the sensor are represented by the concentric circles on the polar plot. The azimuth direction on the polar plot represents the sensor's azimuth angle. By convention, the solar azimuth is always 180°. A sensor with 0° azimuth looks into the sun. Thus, an azimuth of 0° and 180° represents forward scattering and backscattering, respectively. Lines of equal percent reflectance were contoured. The solar zenith (shown by a star on each plot) was approximately 45° for both canopies (Kimes, 1983).

length with increasing off-nadir look angle, information about the atmosphere is enhanced. This strategy is best suited to address effects in the troposphere (clouds and aerosols).

Clouds

It has long been known that clouds exert a major influence on the Earth's radiation budget. Studies of cloud bidirectional reflectance-distribution functions, which determine their hemispherical albedos, have been performed using Nimbus-7 Earth Radiation Budget (ERB) and Geosynchronous Operational Environmental Satellite (GOES) data (Stuhlmann et al., 1985). In recent years, it has also been recognized that cloud shape and uniformity are important variables governing the Earth's radiative balance. Theoretical developments in the ability to calculate the bidirectional reflectivity of nonuniform, non-stratified cloud systems (McKee and Cox, 1974) need to be supplemented by high spatial resolution, multiple look-angle experimental data.

Aerosols

Atmospheric aerosols have been measured from space from several satellites using the scattered solar radiation in spectral bands in the visible and near infrared. The technique is more sensitive over ocean surfaces, where most of the radiance is from the atmosphere (due to the low albedo of the ocean), and is

less sensitive over land, where most of the radiance is from the high (and variable) albedo surfaces. Measurements to date have used only one or two spectral bands that have been available on Landsat, GOES, and NOAA (Advanced Very High Resolution Radiometer, AVHRR) satellites. With this limited number of wavelengths, information on the aerosol optical thickness, size distribution, absorptivity, and transport (Lyons and Northouse, 1974) has been derived.

In addition, one of the principal uses of Landsat MSS data for atmospheric studies has been in the determination of aerosol loading. The techniques used generally rely on an assumed model for the aerosol optical properties and correlate satellite measured radiances with aerosol optical depth (Mekler et al., 1977). When the aerosol source can be identified (e.g., windblown dust), the optical depth measurements can be used to estimate the mass of airborne particulates (Fraser, 1976; Griggs, 1975).

Atmospheric Correction

Due to the low albedo of water, atmospheric correction algorithms have been most successful in oceanographic applications (e.g., CZCS data) (Gordon et al., 1983). For instance, when contrast between two large, relatively uniform expanses of differing albedo is present, as near a coastal boundary, Landsat data have been used to study the spatial blurring caused by atmospheric scattering, also

20

known as the adjacency effect (Kaufman and Joseph, 1982). The shape of the atmospheric spread function was used in that analysis to constrain the aerosol optical properties.

Recent theoretical work by Diner and Martonchik (1984a, 1984b, 1985a), Pearce (1977, 1986), and Li et al. (1987) has studied, in more detail, the properties of the atmospheric point-spread function for aerosol-laden atmospheres bounded by a spatially variable reflecting surface. Figure 15 shows the effect of atmospheric blurring on the reflected intensity from a surface with a high albedo contrast. Another theoretical study by Diner and Martonchik (1985b) indicates that aerosol opacity can be estimated from multiple view-angle measurements even over non-Lambertian surfaces. Recent model calculations by

Simmer and Gerstl (1985) simulate the atmospheric effects on off-nadir satellite observations of highly non-Lambertian surfaces such as vegetation. They conclude that some angular signatures are atmosphere-invariant while others can only be retrieved after atmospheric corrections that require some knowledge of the ambient atmospheric parameters. Figure 16 illustrates how the angular reflectance distribution of a non-Lambertian surface is perturbed by atmospheric effects. Note, in particular, the enhancement of the aerosol forward scattering peak when the view direction approaches grazing view zenith angles, ($\theta_v > 60°$) and the view azimuth is toward the sun ($\varphi_v = 0°$). The above results also show some progress in the attempt to arrive at practical atmospheric correction algorithms.
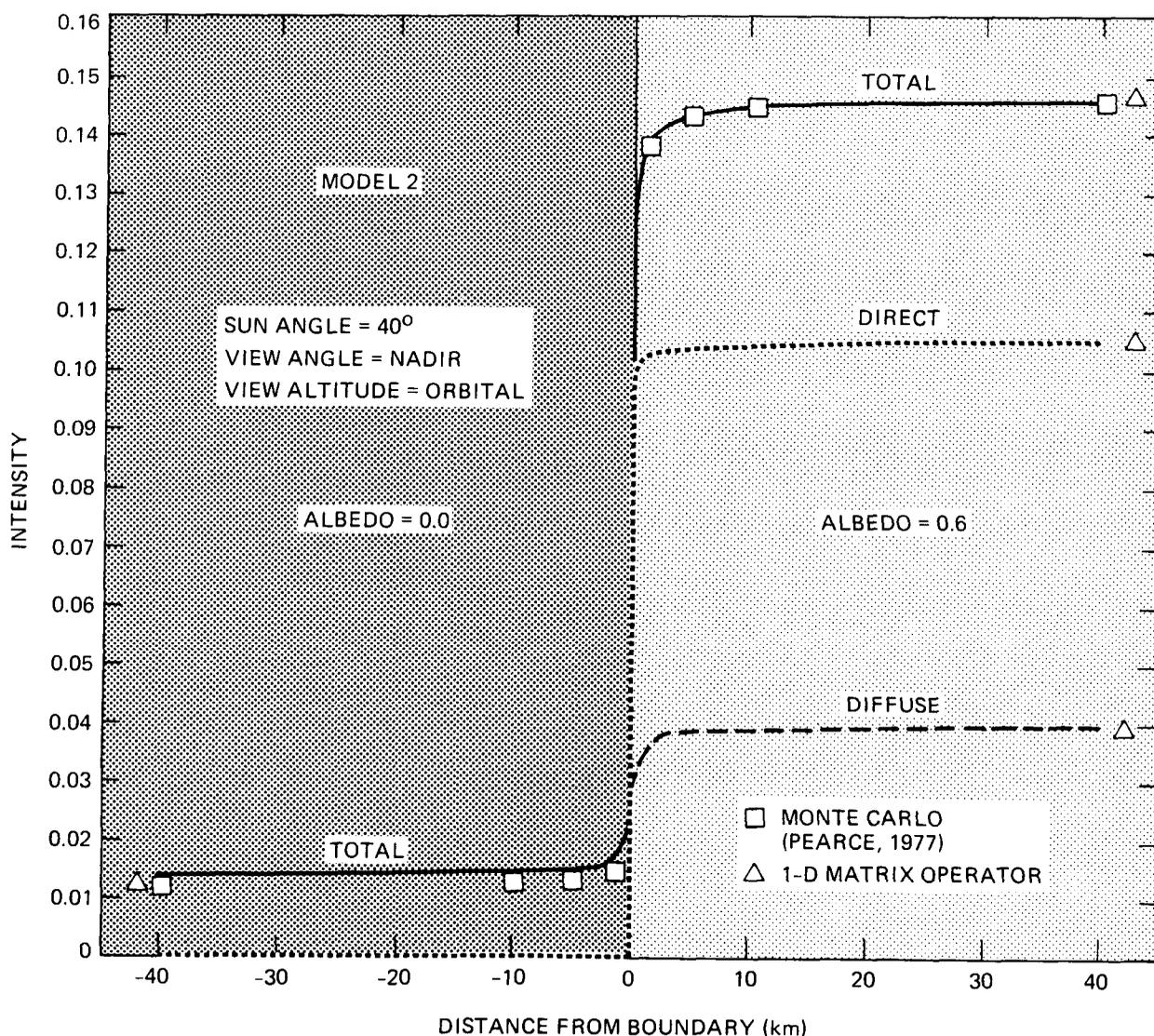
Figure 15. Variations of total intensity and the direct and diffuse components over a surface with high albedo contrast. The atmosphere has two parts: a Rayleigh scattering gas with a scale height of 8 km and an optical depth of 0.1, and a surface-based haze with a scale height of 1 km and an optical depth of 0.212. Intensity is normalized to the exo-atmospheric solar irradiance (Diner and Martonchik, 1984b).
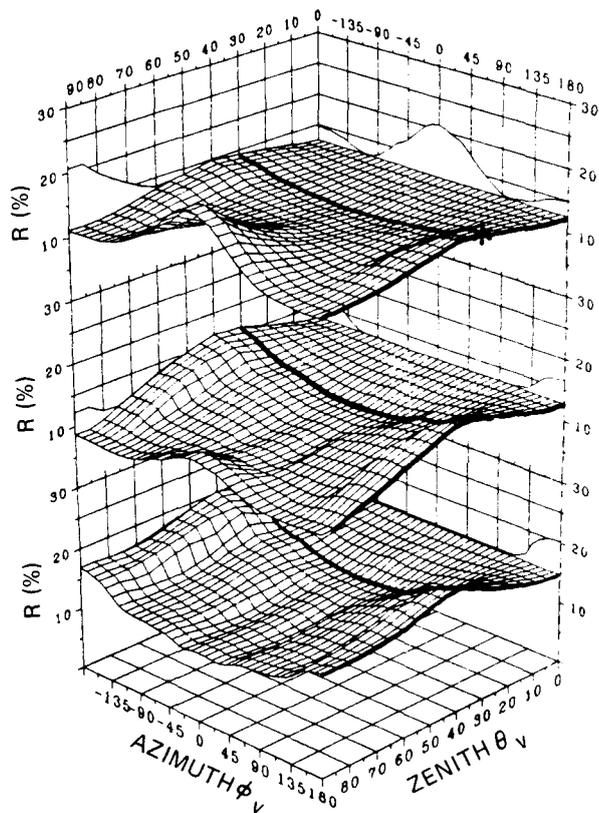
Figure 16. Angular reflectance distributions above Savannah at the surface (bottom data) for a clear atmosphere (aerosol-free), at the top of a mildly aerosol-loaded atmosphere with surface visual range $V_o = 50$ km (middle data), and at the top of a heavier aerosol-loaded atmosphere with $V_o = 10$ km (top data). Hot spot and persistent valley are highlighted. Sun direction is $\theta = 30°$, $\phi = \pm 180°$, $\lambda = 0.85$ μm (Gerstl and Simmer, 1986).

Measurements of angular reflectance signatures from non-Lambertian surfaces require a pointing capability of the sensor for off-nadir viewing combined with high spatial resolution (small GIFOV). Figure 17 illustrates such requirements showing the angular distribution of the vegetation hot spot as computed for a model canopy, assuming single scattering and neglecting the atmosphere. Clearly, multiple scattering within real canopy structures as well as atmospheric effects are expected to broaden these retroreflection peaks. However, radiative transfer calculations through model atmospheres indicate that vegetation identification should still be possible by satellite-based sensors measuring such angular signatures as the canopy hot spot (Gerstl, 1986).

SNOW AND ICE

Spectral Characteristics of Snow and Ice

The most important property of ice that causes spectral variation in the reflectance in visible and near-infrared wavelengths is that the absorption coefficient (i.e., the imaginary part of the refractive index) varies by seven orders of magnitude between 0.4 and 2.5 μm. Figure 18 shows both the real and imaginary parts of the index of refraction for ice and water. The important properties to note are: (1) the variation in the real part of the index of refraction is very small, and the difference between ice and water is not significant; (2) ice and water are optically very similar, except for the region between 1.55 and 1.75 μm, where ice is slightly more absorptive; (3)
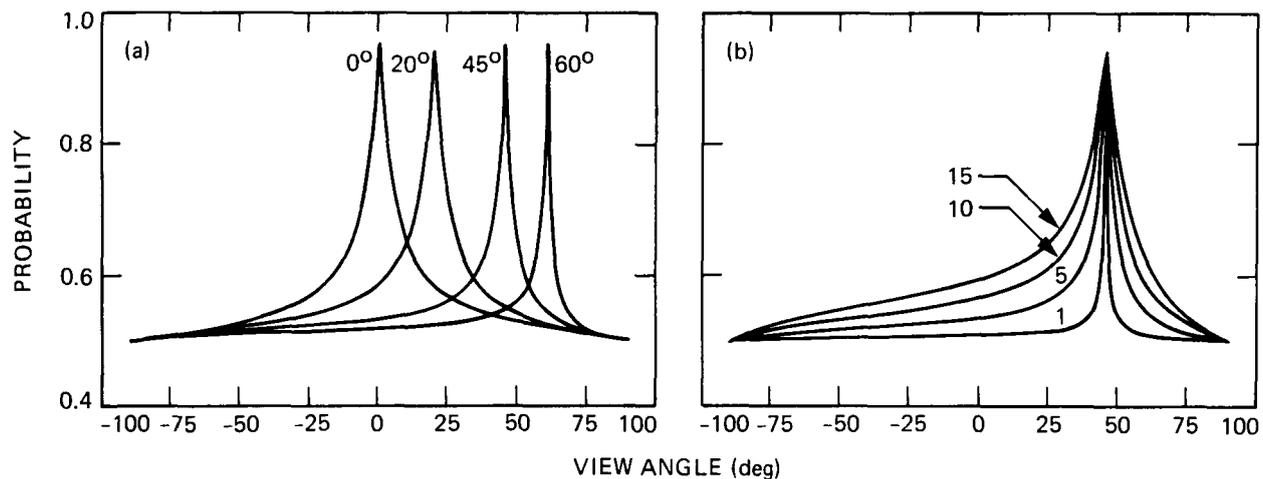
Figure 17. Variation of the canopy hot spot angular signature with (a) solar zenith angle, leaf size = 5 cm, LAI = 3, canopy depth = 1 m; and with (b) leaf size (cm), solar zenith angle = 45°, LAI = 3, for a simplified vegetation canopy model (Gerstl et al., 1986.)

22
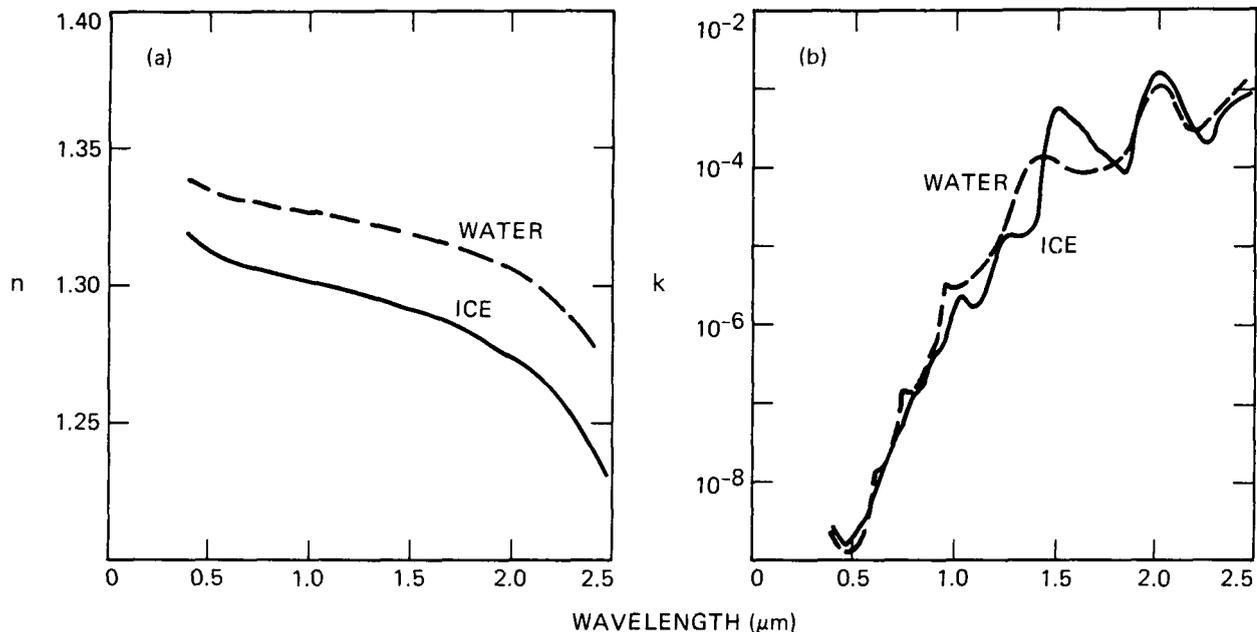
Figure 18. Complex refractive index (n + ik) of ice and water. The real part is (a), the imaginary part is (b). Data for ice are from Warren (1984), data for water are from Hale and Querry (1973).

in the visible wavelengths ice is transparent; and (4) in the near-infrared wavelengths ice is moderately absorptive, and the absorption increases with wavelength.

From the refractive index data, the Mie scattering of ice spheres can be calculated (Wiscombe, 1980; Nussenzveig and Wiscombe, 1980). Alternatively, a geometric optics approximation can be used (Bohren and Barkstrom, 1974; Bohren, 1987). The radiative transfer equation (Chandrasekhar, 1960) can be used to calculate the effects of multiple scattering and absorption on incident irradiance. Wiscombe and Warren (1980) used a delta–Eddington approximation to the radiative transfer equation to calculate the spectral albedo of snow. The delta–Eddington approximation calculates fluxes only, not intensities, so it can calculate albedo but not the bidirectional reflectance-distribution function. Figure 19 shows the spectral albedo of snow for wavelengths 0.3 to 2.7 μm, for snow grain radii from 50 to 1,000 μm (i.e., fine snow to coarse spring snow). Because ice is so transparent in the visible, increasing the grain size does not appreciably affect the albedo. The probability that a photon will be absorbed, once it enters an ice grain, is small, and that probability is not increased very much if the ice grain is larger. In the near infrared, however, ice is moderately absorptive. Therefore, the albedo is sensitive to grain size, and the sensitivity is greatest at 1.0 to 1.3 μm. Because snow is strongly forward-scattering in the near infrared, albedo increases with illumination angle (Figure 20).
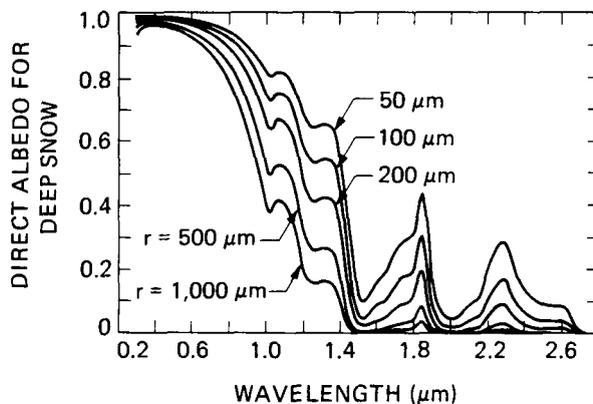
Figure 19. Spectral direct beam albedo of snow of semi-infinite depth, at illumination angle 60°, as a function of wavelength for various grain radii (r) (Wiscombe and Warren, 1980).

The presence of liquid in the snow does not by itself affect the albedo. However, liquid water causes the grains to form clusters (Colbeck, 1979, 1986), and these apparently behave optically as single grains, causing decreased reflectance in near-infrared wavelengths. O'Brien and Munis (1975) observed the spectral albedo of a snow sample to be lower after warm air had been blown over it, but that the albedo did not increase when the snow was refrozen. With data of high spectral resolution, it may be possible to detect the presence of liquid water, using reflectance measurements at 1.03, 1.26, and 1.37 μm (Hyvärinen and Lammasniemi, 1987).
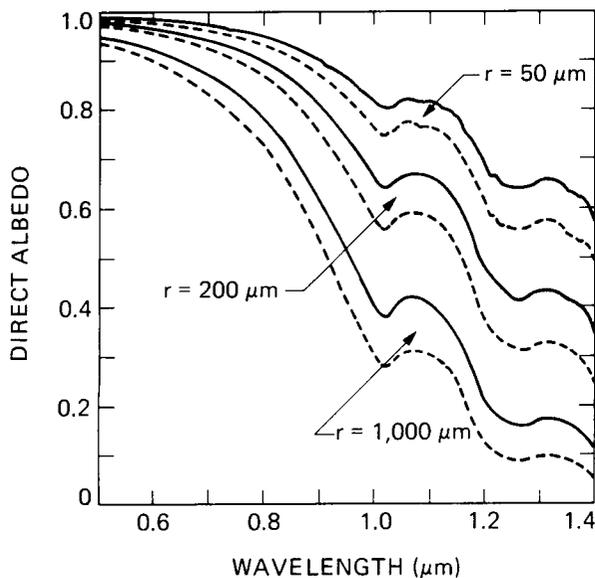
Figure 20. Spectral direct beam albedo of snow of semi–infinite depth, for grain radii 50 μm, 200 μm, and 1,000 μm and solar zenith angles 30° (-------) and 60° (———) (Dozier *et al.*, 1981).

In the visible wavelengths, reflectance is insensitive to grain size, but is affected by two variables, finite depth and the presence of absorbing impurities. The transmission of visible light through snow increases with grain size. Figure 21 shows the relationship of snow albedo to snow depth. For grain radius r = 1,000 μm the albedo is perceptibly reduced when the snow amount is reduced to 100 mm liquid water equivalent.

Warren and Wiscombe (1980) showed that minute amounts of absorbing impurities reduce snow albedo in the visible wavelengths, where ice is highly transparent. Figure 22 shows that soot concentrations as low as 0.1 ppmw (parts per million by weight) are enough to reduce albedo. The effect of the absorbing impurities is apparently enhanced when they are inside the snow grains because refraction focuses the light on the absorbers (Grenfell *et al.*, 1981; Chýlek *et al.*, 1983; Bohren, 1986).

The spectral reflectance of sea ice is somewhat more difficult to model than that of snow because the columnar ice crystals, whose size is related to growth rate, cannot be approximated by "equivalent" spheres. Grenfell (1983) has developed a radiative transfer model for sea ice albedo under conditions where the ice layer is homogeneous. Similar to snow, albedo is higher in the visible wavelengths for thicker sea ice, whereas in the near infrared albedo is insensitive to ice thickness (Figure 23). Albedo increases as ice density decreases, because of multiple scattering off the bubbles, and albedo is higher for faster growing sea ice.
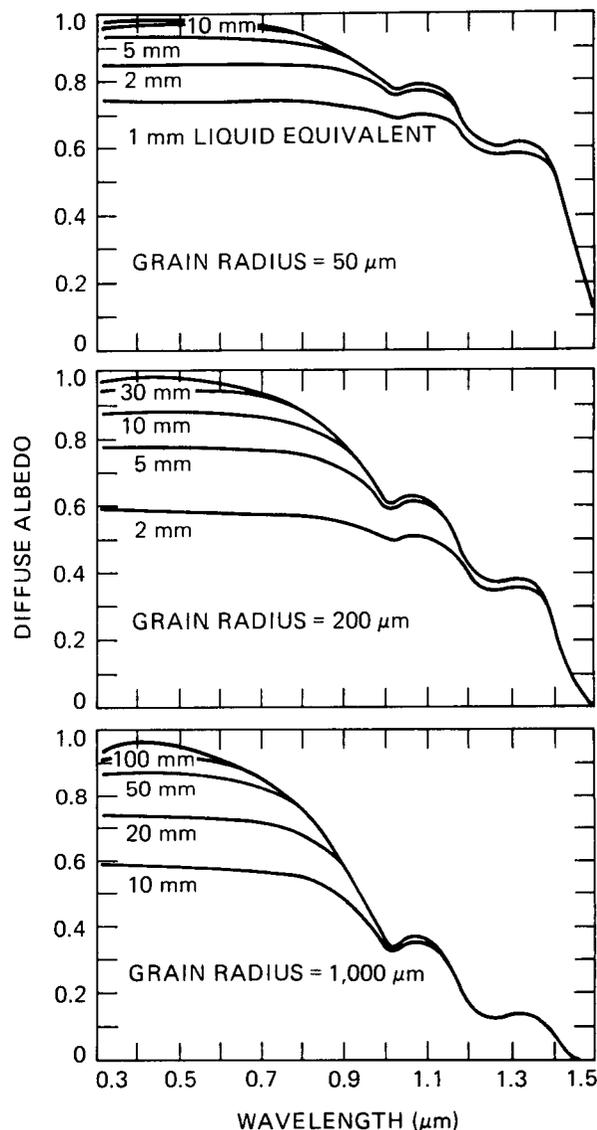
Figure 21. Spectral diffuse albedo of snow versus wavelength for various grain radii, and, for each grain radius, for a variety of snow water equivalences. The top curve in each case is for semi–infinite depth (Wiscombe and Warren, 1980).

Snow Properties from Remote Sensing

The most common use of remote sensing in snow hydrology is to monitor snow covered area (Rango and Itten, 1976; Rango *et al.*, 1977). These efforts have been carried one step further by including satellite–derived measurements of snow covered area as an index in a snowmelt runoff model (Rango *et al.*, 1979; Rango and Martinec, 1979). The next scientific improvement is to use satellite radiometric data to measure or estimate snow surface characteristics that are necessary for calculation of the surface radiation balance (Dozier, 1984).

24
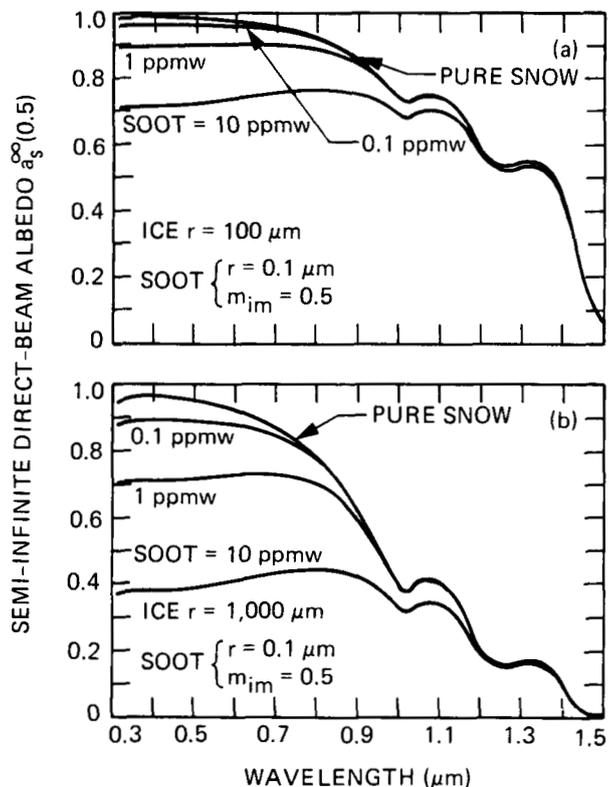
Figure 22. Spectral direct beam albedo of snow versus wavelength for various soot concentrations. (a) $r_{ice} = 100$ μm, (b) $r_{ice} = 1,000$ μm (Warren and Wiscombe, 1980).
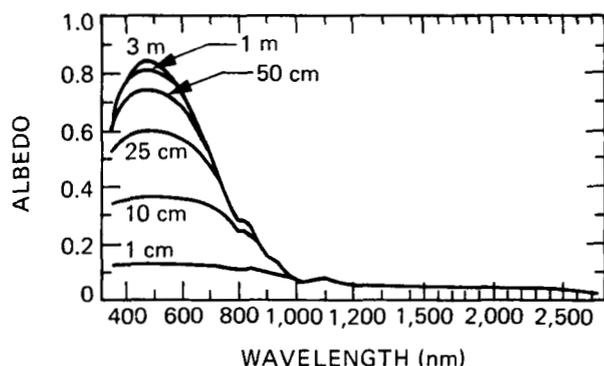
Figure 23. Spectral albedo of young sea ice, for ice density 880 kg/m^3 (Grenfell, 1983).

Figure 24. Traces of reflectance measured from NOAA-6 satellite across three lakes in Saskatchewan on two different days (a) April 12, (b) April 27 in visible channel and near-infrared channel (Dozier et al., 1981).

Dozier et al. (1981) have used the model of Wiscombe and Warren (1980) to calculate snow albedos integrated over the visible and near-infrared bands of the NOAA-6 satellite. They were apparently able to detect the thinning of the snow pack at the end of the melt season on some lakes in subarctic Canada. Figure 24 shows that on April 12 the snow-covered lakes are brighter than the intervening forest in both bands. Two weeks later, much of the snow had melted, so that on April 27 the near-infrared reflectance is much smaller than the visible.

For climate studies, the changing albedo with changing snow cover is the most extensive spatial change that affects global climate. In winter, the maximum snow cover in the northern hemisphere varies between 37×10^6 and 45×10^6 km^2 (Matson and Wiesnet, 1981). Monitoring of the snow and ice cover from NOAA satellites has revealed the interannual variability of the hemispheric snow cover (Barry, 1985).

Remote sensing in the 1.55 to 1.75 μm wavelength region has been used to distinguish snow from clouds. Historically snow/cloud discrimination has been a problem in snow-cover mapping, because in visible and near-infrared wavelengths (up to 1.1 μm) snow and clouds have similar reflected radiance. However, the possibility of such discrimination was noted in the Skylab data (Valovcin, 1976), and the Defense Meteorological Satellite Program's (DMSP) F4 satellite had a channel at 1.53 to 1.62 μm for mapping clouds. Dozier (1984) showed examples of snow/cloud discrimination in mountainous areas (Figure 25). Reflectance of cirrus clouds is greater than that of snow because the mean crystal size is much smaller. Cumulus and stratus clouds have even higher reflectance because of their greater thickness

25
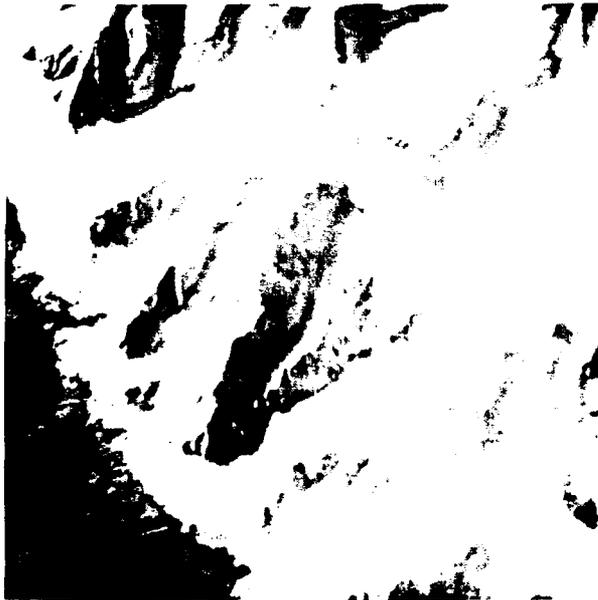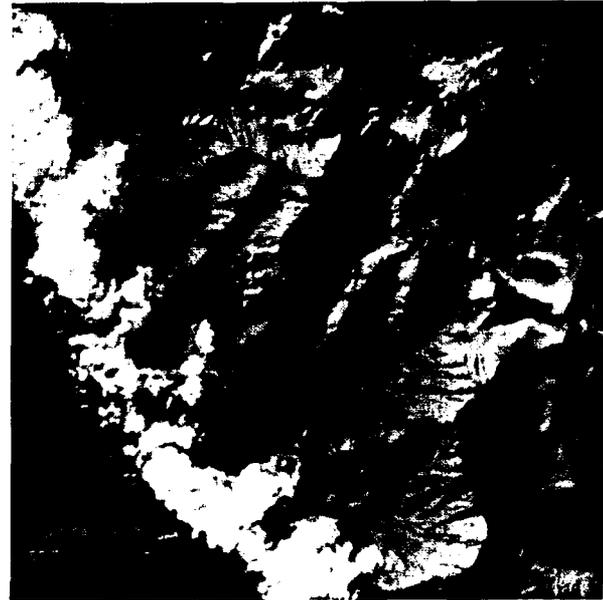
(a)   (b)

Figure 25. Snow/cloud discrimination with the Landsat TM, in the area of Mt. Williamson in the southern Sierra Nevada. Figure (a) is made with TM bands 2, 3, and 4. The clouds on the Sierra front are difficult to identify. Figure (b) is made with TM bands 2, 5, and 7. The clouds are easily distinguished from the snow.

and the lower absorption coefficient of water when compared with ice in this spectral region.

In the thermal infrared region, Dozier and Warren (1982) have shown that snow temperature should be detectable from satellite, provided that the dependence of emissivity on viewing angle and the atmospheric transmittance are accounted for.

Salomonson and Marlatt (1968) showed broad-wavelength data acquired from aircraft for the aniso-tropic reflectance of snow, and Taylor and Stowe (1984) showed similar patterns from the Nimbus ERB Experiment. The only spectral information on the bidirectional reflectance–distribution function of snow are the theoretical calculations of Li (1982), which show that at near–infrared wavelengths snow is significantly non–Lambertian. The signal in these wavelengths would be well correlated with grain size, but the effect of illumination and viewing angle must be accounted for.

Dozier and Marks (1987) have corrected snow reflectance measurements for atmospheric effects and have estimated grain size. The scatter in their results would be considerably reduced if optimally chosen wavelengths were available, as they would be in an imaging spectrometer such as HIRIS.

SUMMARY OF AIS RESULTS TO DATE

Data acquired with AIS represent the first high spectral resolution imagery that has been available to the remote-sensing research community. AIS oper-ates in the near infrared and short–wavelength infra-red using a 32 × 32 element HgCdTe area–array detector to image a ground swath of 32 or 64 pixels in

up to 128 spectral bands. Spectral coverage is at a sampling interval of about 10 nm in either the 0.8 to 1.6 μm or 1.2 to 2.4 μm regions. Since AIS became operational in 1983, data have been collected for about 50 investigators or investigator teams. The locations of the U.S. test sites flown through Fiscal Year 1986 are shown on Figure 26. Additionally, AIS data have been acquired in Australia, Germany, Austria, and Italy. A brief overview of some key results from two AIS workshops (Vane and Goetz, 1985, 1986) follows.

Work in the geological disciplines with AIS clearly confirms that direct mineral identification through imaging spectroscopy is possible and that many fundamental geological problems are now ad-dressable with the new class of information provided by the high spectral resolution data. Many minerals have been identified through spectral signatures derived from AIS imagery, and spectral stratigraphy (the remote analysis of stratigraphic sequences) has been accomplished. Field and lab spectra have been acquired to confirm AIS observations and x–ray dif-fraction analysis has also been done on the field samples. The effects of mineral mixing within a pixel and the spectral contribution of vegetation were also addressed, and the spatial distribution and relative abundance of clays, gypsum, and serpentine associ-ated with the channels and dispersed components of kimberlite and blocks of country rock at the Moses Rock Diatreme, Utah, have been mapped with AIS data.

In the vegetation disciplines, the utilization of imaging spectroscopy has not progressed quite as rapidly, due in part to the fact that vegetation spectra do not exhibit the wealth of infrared spectral absorp-
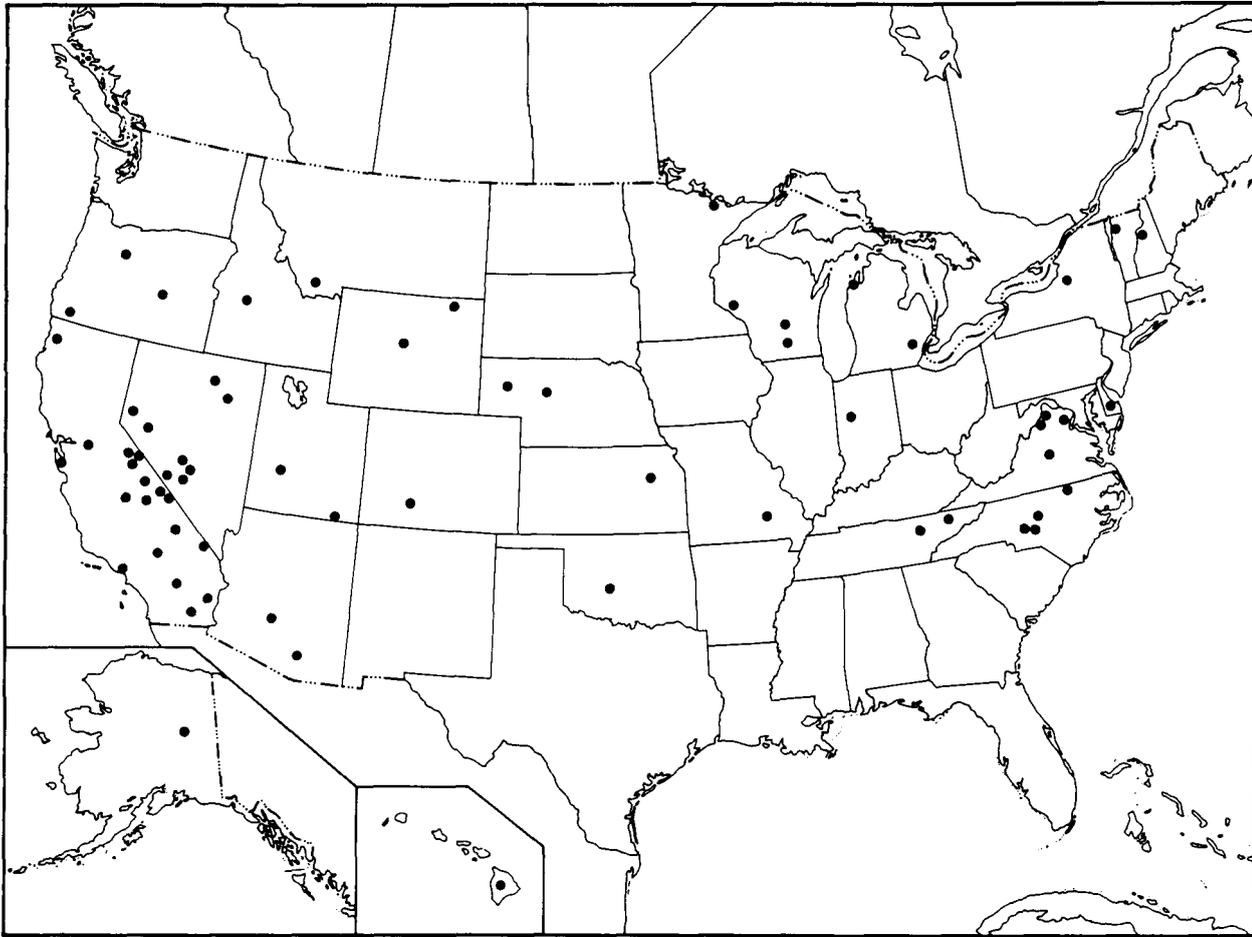
Figure 26. Locations of U.S. test sites flown through Fiscal Year 1986 with AIS-1 and AIS-2. In addition, data were acquired in Australia, Germany, Austria, and Italy.

tion features that are common to so many minerals. Moreover, vegetation spectra are highly variable over time for most species. Therefore, the analytical approaches to information extraction that have been so successful in geological studies are not always directly applicable to vegetation studies. Nevertheless, several studies conducted with AIS have shown the usefulness of high spectral resolution data for addressing key vegetation problems. Absorption at about 1.19 μm is consistently broader and shallower for pine forests than for deciduous forests, and early work with corn, soybeans, and alfalfa indicates that subtle features in the near-infrared plateau, from about 1.18 to 1.31 μm and from 1.6 to 1.78 μm, may be useful for discriminating between these crop types. Variations in the slope of the spectral reflectance curve between 1.4 and 1.9 μm have made it possible to separate among types of wetland vegetation. An important protein absorption feature at 1.5 μm was inferred through a strong negative correlation between the AIS spectra at that wavelength and the nitrogen concentration and total nitrogen. Additional spectral signatures are also related to plant biochemistry. An increase in trace element concentration in plant tissue was found to corres-

pond with an increase in spectral reflectance in the 1.5 to 1.7 μm region.

In geobotanical studies, the ability to discriminate between serpentinized and unserpentinized soils appears to be possible, and spectral differences have been found in the 1.4 to 1.9 μm region related to vegetation cover types in an area of derelict heavy metal mines. A principal factor analysis (PFA) of AIS data from an area with two sagebrush species and montmorillonitic and volcanic soils indicates that there is much information available for material discrimination in high spectral resolution data.

In addition to the spectral analysis manager (SPAM) developed at JPL for spectral feature extraction from AIS data, a number of other analytical techniques are under development. A spectral mixture model has been created at the University of Washington that has been used successfully to identify the origin of spectral variation in AIS images. A technique is under development in Australia for mineral identification making use of the wavelength position, intensity, and shape of diagnostic absorption features. At the U.S. Geological Survey (USGS) in Denver, analysis techniques under development include the normalization of spectra to remove

albedo and illumination effects, and the calculation of reflectance relative to a standard spectrum to identify minerals.

Work in instrument calibration and performance evaluation has been ongoing at JPL since AIS became operational in 1983. Late in 1986 a field calibration experiment was begun jointly between JPL and the University of Arizona over a new test site in the Mojave Desert being developed for AVIRIS calibration.

III. OBJECTIVES, JUSTIFICATION, AND DIRECTION

INTRODUCTION

The following discussions in each discipline are aimed at developing the objectives for high-resolution imaging using HIRIS. Justification is provided based on information presented in the previous section and on additional scientific requirements for each discipline. Another purpose is to highlight the requirements for supporting research to make HIRIS experiments more effective. For instance, in vegetation studies, a library of reflectance spectra of plants undergoing various kinds of stress does not yet exist.

GEOLOGY

Overview

HIRIS data will be of broad utility in many important research areas of solid Earth sciences. The data will be crucially important in two areas of global study: (1) characterizing and mapping sedimentary, igneous, and metamorphic rock units subjected to tectonism and magmatism and exposed by subsequent erosion; and (2) characterizing and mapping surficial materials and landforms that record current and geologically recent processes on the Earth's surface. High spectral and spatial resolution data, even if of limited spatial coverage, can allow the identification of the composition of the components of a scene. The distribution of these components can commonly be mapped over a much larger area with considerable confidence using imagery of lower spectral and spatial resolution by extension of the spatial relations and general color information. For example, a HIRIS strip through a TM image could greatly increase the interpretability of the entire image.

Almost two-thirds of the Earth is covered by oceans, but much of the record of the tectonic and magmatic history of the Earth is largely contained in the nature and geometric configuration of the rock units found in the continental crust. In contrast, ocean crust produced at mid-oceanic ridges is consumed back down into the mantle along subduction zones at typical rates of centimeters per year. Consequently, although the oceanic crust occupies nearly 70 percent of the Earth's surface, it only provides a record for the last 200 million years of geologic time. The continental crust is too buoyant to be subducted, but interaction of the descending ocean slab with the continental margin typically results in extrusion of volcanic rocks, intense folding and faulting, intrusion of magmatic rocks, accretion/obduction of oceanic crustal materials, and uplift of the marginal zone of the continent. As a consequence, the ancient continental margins record a longer history (over 3 billion years) of rifting, collision, downwarping, and uplift associated with plate tectonics and a convecting mantle. This history is recorded in the characteristics (geometry, age distribution, composition) of the rock units that make up the continental crust.

The continental margins with their critical geology are generally mountainous and difficult to access. Due to the difficulty of geologic mapping in such areas, much of our current knowledge is based on extrapolation of localized, detailed geologic mapping using topographic features, aerial photographs, etc. For these areas, HIRIS data will provide major advances in knowledge of the distribution of the sedimentary, igneous, and metamorphic rock units, leading to an understanding of the depositional, folding, faulting, and intrusive history of the area.

The outcrop patterns of rocks produced by various sedimentary, magmatic, and tectonic processes sampled on a worldwide basis are the fundamental record for understanding the Earth's history. In addition, it is important to note that most of the Earth's nonrenewable resources occur within the continental crust. Consequently, a better understanding of the nature and distribution of crustal units will increase our understanding of both the deformational history of the Earth and the location and mode of emplacement of nonrenewable resources.

The long-term record of the climatic history of the Earth is also contained in the geological rock record and in the landforms that make up the continents. A great deal can be learned about climatic variations over the past million years (i.e., Pleistocene) by sampling and mapping on a worldwide basis the types of weathering products and associated landforms that exist on the continental land masses. In principle, the lithological and textural properties of weathering products, together with their ages, provide direct climatic information, since rocks produced by endogenic processes (metamorphism, magmatism, etc.) are unstable at the Earth's surface and weather to a set of products in thermodynamic equilibrium with ambient surface conditions. Likewise, landform evolution is governed by the prevailing ambient climatic conditions.

The degree to which surficial and bedrock units have been mapped on the Earth varies considerably. Most areas in the U.S. and Europe have been mapped in detail, while vast areas elsewhere have only been mapped in a reconnaissance mode or not mapped at all. HIRIS observations, sampled on a worldwide basis, would provide the synoptic view necessary to systematically characterize bedrock lithologies, outcrop patterns, and associated landforms and weathering products for key areas of the Earth's surface. Although Landsat TM data are important precursor data sets for these tasks, the high spectral resolution observations of HIRIS are necessary to identify and to discriminate among the majority of

29

materials exposed at the Earth's surface. In addition, in vegetated regions geological materials are not directly exposed, and other approaches must be used, including use of the reflective and perhaps emissive characteristics of vegetation canopies, to map underlying materials.

Solar radiation (0.4 to 2.5 μm) has sufficiently high energy to provide information on mineral chemistry, since electronic transitions, charge transfers, and molecular vibrations are induced. HIRIS data can be used to identify minerals with transition elements (e.g., Fe, Ti, Mn), minerals having carbonate, sulfate or hydroxyl ions, or minerals that contain bound water. For vegetation, the 0.4 to 0.9 μm region provides information on pigmentation. Responses in the 0.9 to 1.2 μm region are related to cell structure and longer wavelengths to vegetation water content (Goetz et al., 1983). Subtle variations, such as shifts in chlorophyll absorption located near 0.7 μm, have been shown to be related to variations in the amount of base metals found in leaves (Chang and Collins, 1983). Regions with higher base-metal contents also seem to have vegetation that is subject to premature senescence. In addition, the overall reflectance properties of forests vary, in part controlled by underlying materials. For example, flat-topped and oak-hickory canopies are found in the Ozarks (eastern U.S.) in regions with porous or thin soils over rhyolite volcanic rocks. For the first time on a global basis, HIRIS will provide geoscientists with the capability to map surface materials directly using mineral signatures, where soils or rocks are exposed, or canopy optical properties as surrogate measures of underlying materials in regions covered by vegetation.

Field-of-View Mixing

On the scale of tens of meters only a small percentage of the Earth's surface consists of mineral and rock types in pure form. More typically, rocks exhibit some form of weathering that may alter or mask their spectral properties. In arid regions, for example, rocks may develop surface coatings with a manganese-rich varnish. In addition, vegetation and soil commonly contribute to the reflectance measured in individual pixels. Together, weathering products, vegetation, and the natural heterogeneity of the Earth's surface at all scales cause mixed spectral signatures. To identify minerals and rocks remotely using their spectral properties requires methods for isolating the desired signatures from unwanted spectral contributions.

Spectral mixing as applied to minerals has received considerable attention in the last few years, especially from the planetary remote sensing community (Singer, 1981; Johnson et al., 1983; Adams et al., 1986; Cloutis et al., 1986). Powerful methods are evolving that allow the deconvolution of complex spectra in terms of specific diagnostic absorption bands, and in terms of overall shape. High spectral resolution facilitates the process of unmixing, by revealing diagnostic absorption features. Until the development of imaging spectrometers, high-resolution spectra were only available in the laboratory and in telescopic data.

Mineralogy and Compositions of Sedimentary Rocks

Sedimentary rocks account for about 75 percent of the land surface (excluding soil and vegetation) (Pettijohn, 1975). The end-members of the compositional range of the most commonly observed sedimentary rocks are limestone, shale, and sandstone, which form under markedly different depositional environments. Limestone accumulates mainly in seawater from skeletal $CaCO_3$ formed by organisms, whereas sandstone and shale are formed from weathering products sorted and transported to a depositional basin. Each of these end-members implies different environments of deposition (Pettijohn, 1975).

Compositional variations occur both laterally and vertically, and mapping these variations over large areas is especially important for reconstructing the paleo-environments and the influences of changing tectonic, climatic, and other conditions. For example, rapid changes from sandstone to substantially more coarse-grained, heterogeneous material indicate tectonic uplift that resulted in more rapid erosion of landmasses, changes in sea level, or migration of depositional environments. More gradual variations, such as in the proportion of sand and clay particles, implies slow transgression or progression of the sea or again a migrating depositional environment. Mapping the position of reefal limestones that were once barrier reefs separating very different depositional environments has proven useful in oil exploration. In addition, lithologic changes during or after deposition, such as the addition of magnesium to limestone to form dolomite, are important for understanding the rock history.

Conventional methods for studying varying depositional environments involve detailed stratigraphic studies at well-exposed sites, extrapolation of these data to larger regions, and modeling the regional paleo-environment. However, regional maps that accurately portray subtle mineralogical changes are not easily produced today, because laboratory mineralogical analyses are needed to make the necessary mineralogical identifications. This approach is very time-consuming and therefore often impractical.

Calcite and clay minerals, the main constituents of limestone and shale, have diagnostic absorption bands in the short-wave infrared (SWIR) region. Therefore, identification of these end-members and mixtures could be accomplished through analysis of high spectral resolution SWIR measurements. For instance, mineralogical maps showing distribution of many expandable clay minerals, important for understanding landslide potential or petroleum reservoirs, could be compiled from high spectral resolution images. The distinction of limestone from dolo-

mite, which often requires a chemical test in the field, can be achieved remotely by having adequate spectral resolution to detect the 0.02 μm shift in the CO_3 absorption band in the 2.3 μm region. Other important sedimentary deposits that have diagnostic spectral features are gypsum and many evaporite minerals and zeolites.

Continental Margins, Metamorphic Complexes, and Mountain Belts

During the subduction of an oceanic slab under the margin of a continental slab, the sedimentary and volcanic layered rocks in the margin are typically highly deformed, pushed down to great depth, intruded by igneous plutons formed by partial melting at greater depths, and metamorphosed by the resulting high temperature and pressure to create metamorphic rocks, in which new minerals form in the solid state without melting. Typically, dehydration or decarbonation reactions result in the formation of less hydrous minerals than those found in sedimentary rocks. Under such conditions the rocks deform plastically and fold or fracture into complex patterns. Eventually these complex patterns are brought to the Earth's surface by uplift and erosion, typically in mountain belts well covered with vegetation.

Such complexly deformed rocks contain important information on the history of the Earth, if this history can be deciphered. Only a few such belts can be said to be fairly well understood: the Alps, the Appalachians, and the western U.S.; but even these areas seem to grow more complex as we learn more about them. Nevertheless, increased understanding of the general process makes it possible to extrapolate geologic mapping of a few limited areas to interpret the history of a region. Such extrapolation makes use of topographic landforms, showing resistance to erosion, on such maps as are available, of topographic landforms as seen on aerial photographs, of albedo of rock units as seen on aerial photographs, etc. The geologist maps the two-dimensional distribution of rock units on the Earth's surface to infer the third dimension of depth and the fourth dimension of time. In addition, the geologist maps the mineralogic changes due to high temperature and pressure to infer the physical conditions at various depths at various times.

For the first time HIRIS will make it possible to map mineral signatures in the rock units in such complex but important marginal zones on a worldwide basis. It will be possible to begin to achieve an understanding of these important tectonic belts that would otherwise be achieved only after decades of normal geologic mapping.

Mineralogy and Chemistry of Hydrothermally Altered Rocks

The spectral reflectance of hydrothermally altered rocks has been studied in more detail than any other group of rocks. Hydrothermally altered rocks are of economic importance, because they mark the paths of migrating hot fluids that commonly contain base and precious metals. Alteration occurs where invasion of the wall rock by magmatic aqueous solutions causes release of metal cations from minerals that are no longer in equilibrium. A new stable mineral assemblage is formed, whose constituents are controlled by the compositions of the surrounding wall rock and solution, temperature, and pressure.

Alteration intensity is expressed by the mineral assemblage, and most of the key minerals have diagnostic reflectance spectra. Figure 27 shows the reflectance spectra for minerals that characterize four levels of increasing alteration intensity: propylitic, argillic, phyllic, and advanced argillic. Propylitic alteration, the weakest stage, results in the formation of chlorite (or epidote), montmorillonite, and calcite (Figure 27a). In moderately intense argillic alteration, kaolinite, chlorite, and lesser montmorillonite are the characteristic OH minerals (Figure 27b). Phyllic alteration is characterized by sericite (muscovite) (Figure 27c). As alteration intensity progresses to the advanced argillic level, alunite, pyrophyllite, and jarosite form (Figure 27d). Other minerals may form that indicate the presence of significant amounts of other elements or compounds. Buddingtonite, for example, shows that NH_3 was available either in the hydrothermal solutions or the wall rock.

Moderate spectral resolution measurements permit distinction of groups of minerals, such as Al–OH and Mg–OH, but identification within these groups requires resolution that is adequate to delineate subtle diagnostic features. Analysis of SMIRR data showed that two types of Al–OH minerals are present in the Cerro Blanco, Baja California hydrothermally altered area, one with an absorption maximum near 2.17 μm and another with a maximum centered near 2.20 μm (Rowan et al., 1983). X-ray diffraction analysis showed that the 2.17 μm feature is due to pyrophyllite and dickite, whereas kaolinite and muscovite cause the 2.20 μm absorption bands. Continuous high spectral resolution coverage from HIRIS would have allowed these identifications without x-ray diffraction of samples.

In general, hydrothermally altered rocks are more stable than unaltered rocks at the Earth's surface, because the alteration process involves weathering as well as deep–seated magmatic activity (Barnes, 1979). However, the climatic dependence of mineral stability in the unaltered rocks results in different mineralogical contrasts from one region to another. For instance, montmorillonite is the stable phase that develops through weathering in arid and semiarid alkaline environments, such as the Great Basin province of the western United States. In more humid, acid regions, kaolinite, rather than montmorillonite, is stable. Consequently, mineralogical and spectral contrast should be higher in arid and semiarid regions than in more humid regions, because kaoli-
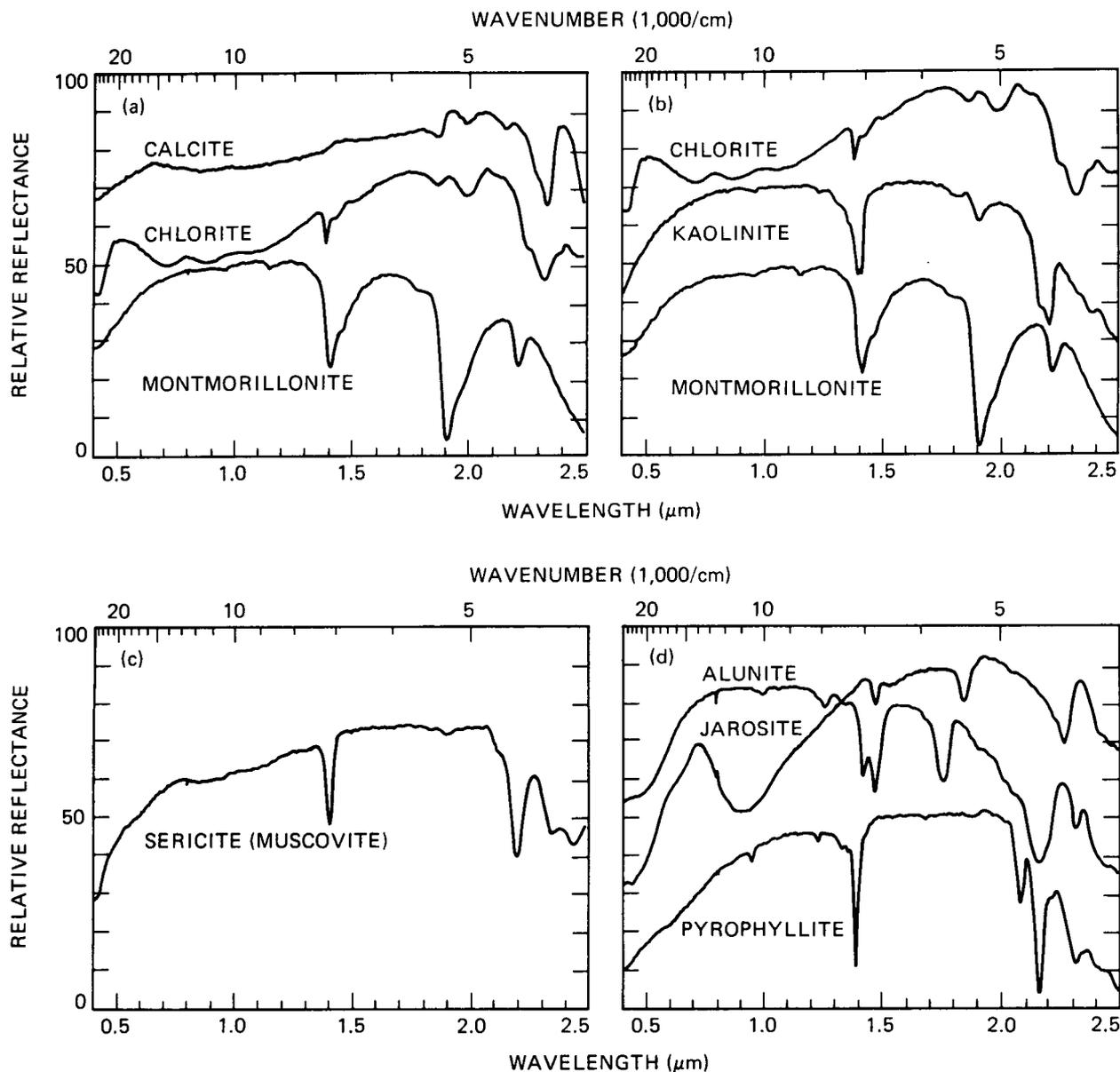
Figures 27. Laboratory reflectance spectra of altered rocks: (a) minerals associated with propylitic alteration, (b) minerals associated with argillic alteration, (c) minerals associated with phyllic alteration, (d) minerals associated with advanced argillic alteration.

nite might be present in both altered and unaltered rocks in the humid regions. These types of relationships are not well understood globally, owing to the lack of mineralogical information at this scale. High spectral resolution images covering portions of climatically and geologically different regions are the only practical approach to studying such weathering phenomena.

Weathering Processes and Landscape Evolution

The rock surfaces exposed in arid and semiarid regions vary widely in the amount and extent of weathering. Fresh rock is typically exposed in

washes, on active parts of fans, and in other areas where fluvial or eolian abrasion continually exposes new surfaces. More stable surfaces are weathered by oxidation and hydration of the exposed minerals or by the development of surface coatings. Surface coatings, such as manganese and clay-rich desert varnish, silica, and ferric oxyhydroxides, are known to be derived from wind-deposited dust through the action of intermittent wetting and drying on rock surfaces. Microorganisms play an important role in dissolving and concentrating materials in some of these coatings.

The mineral phases that are produced by local weathering processes may mask the mineralogy of the host rock. However, laboratory and field spectra

show that the weathering phases often can be identified and distinguished from the unweathered minerals given sufficient spectral resolution. Experiments in the Cuprite, Nevada, area have shown that with high spectral resolution it is possible to deconvolve mixed spectra on the subpixel scale, effectively retrieving characteristic rock spectra from rock surfaces that are partially masked by desert varnish. The development of such unmixing techniques is an essential step in extending remote mineral identification beyond those regions where only fresh rocks are exposed.

The same weathering products that mask fresh rocks can carry important information about the environmental conditions under which the weathering occurred and about the ages of the surfaces affected. Recent studies in the Owens Valley and Mojave Desert of California, Hawaii, and in the Sonoran Desert have correlated the amount of surface weathering products with ages determined by radioisotopes. The types and degrees of weathering appear to have varied with climatic conditions that can be traced at least through the Quaternary period in the United States, and probably back to much earlier geologic times in other places in the world, such as Australia. High-resolution spectral studies may be able to play a key role in extending detailed age-weathering correlations in local areas to the regional landscapes, thereby furthering our understanding of how past and present climates have interacted with geologic processes to shape our environment.

Carbonatites

Carbonatites are carbonate-rich rocks of magmatic derivation that typically contain unusual mineral assemblages (Heinrich, 1980). Calcite, dolomite, and ankerite are the dominant constituents, but many other minerals may also be present, including silicates, phosphates, sulfates, iron oxides, sulfides, fluorides, and various rare earth and niobium-bearing minerals. Carbonatites are commonly associated with alkalic igneous rocks and occur as intrusive bodies of various shapes along continental margins of stable platforms or along major fracture zones within platforms (Kapustin, 1980; Heinrich, 1980).

Since about 1950, scientific and economic interest in carbonatites has increased enormously. As Heinrich (1980) points out:

"The close genetic relationships of carbonatites to subsilicic alkalic igneous rocks point to the necessity of considering the origin of carbonatites in formulating any valid general hypothesis of the genesis of alkalic rocks."

He also notes the genetic link between kimberlites and carbonatites and the carbonatitic affiliation of certain types of explosive volcanism. Economic interests are driven by the presence of exploitable amounts of niobium and rare earth elements (REE),

and locally important sources of thorium, phosphate, uranium, copper, strontium, vermiculite, fluorite, and agricultural lime (Pecora, 1956; Deans, 1966).

Most carbonatite bodies are quite small, ranging in area from a few hundred square meters to several square kilometers. The small size, coupled with the gross compositional and textural similarity of carbonatites to other calcsilicate and calcic metamorphic rocks, has sometimes hampered carbonatite identification. Consequently, most of the known carbonatite complexes have been recognized only during the last 35 years (Deans, 1966; Kapustin, 1980), and many others undoubtedly remain to be discovered.

Spectral reflectance studies of four carbonatite complexes indicate REE absorption bands, particularly neodymium, are present but can be masked by limonite stains. Carbonate absorption bands are conspicuous in nearly all of the carbonate spectra, but the alkalic rocks associated with the carbonatites do not exhibit diagnostic spectral absorption features in the 0.4 to 2.5 μm region (Figure 28).
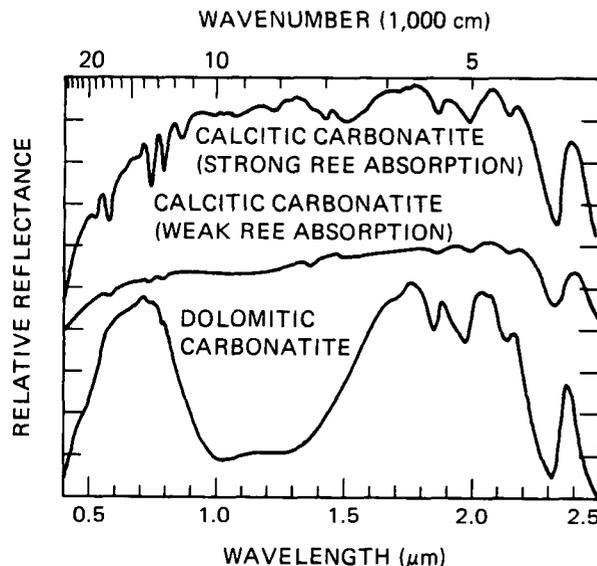
Figure 28. Laboratory reflectance spectra of carbonatites.

Airborne high spectral resolution profile measurements have been used to detect neodymium features, as well as the 2.35 μm CO_3 band, in the rare earth-rich Mountain Pass, California, carbonatite. However, neodymium absorption may not be sufficiently intense to be detectable in many carbonatites. The intense Fe^{2+} absorption in dolomitic carbonatites is also highly diagnostic, because this feature is either absent or weak in sedimentary dolomite. Carbonatites that lack detectable neodymium and Fe^{2+} bands may be distinguishable because of their CO_3 absorption feature and distinguished from sedimentary carbonates by their close association with volcanic rocks.

OCEANS AND INLAND WATERS

Oceanography

One of the key questions in biological oceanography in the next decade concerns the role of primary productivity in the global carbon cycle. Specifically, we wish to understand how fluctuations in the forcing functions affect the fixation of atmospheric carbon and its transfer to the deep marine sediments. In physical oceanography one of the key questions is the response of the upper ocean to atmospheric forcing. In particular we need to understand the transfer of momentum from the atmosphere to the ocean and how this momentum is transferred within the ocean and dissipated. The research will involve a variety of physical and biological measurements from both satellites and *in situ* instruments. One class of measurements will include detailed process studies of a particular phenomenon in a restricted area for a short duration, in contrast to mapping and monitoring types of measurements where data are collected for a large area over a long period of time. HIRIS, given its high spatial and spectral resolution and consequently the long time required for coverage of large areas, is not appropriate for large-scale monitoring, but is ideal for many focused process studies.

There are many process-oriented studies in oceanography in which imaging spectrometry would be extremely useful. For example, large blooms of phytoplankton occasionally occur in coastal areas (e.g., red tides). These blooms usually occupy a small area (from a few tens of square kilometers up to hundreds), last for 10 to 100 days, and are often nearly monospecific. These blooms may represent a significant flux of carbon to deeper waters as they decay and sink. Thus, information on the processes governing the creation and dissipation of such blooms is essential.

Other highly productive areas, such as estuaries, also have fairly short length scales (<1 km) where high spatial resolution in an imaging spectrometer is essential. Similarly, large macrophyte beds occur in coastal regions on scales of a few kilometers. Time series of high spatial resolution data would be useful in understanding the response of these beds to changes in the physical environment. For example, the recent El Niño caused a large mortality among the kelp off southern California. Finally, high spatial resolution imagery will play a useful role in supporting ship measurements in terms of feature location and providing a link between ship-based data and MODIS.

High spatial resolution imagery may also be used in physical oceanographic applications, particularly in the study of small-scale phenomena such as fronts. A specific example would be the study of glint patterns. Photographs from aircraft and the shuttle have shown a wide variety of small-scale features that may arise from interaction of currents with the surface wave field. Certain frontal interactions can also result in the accumulation of surface organic films that result in slicks that are visible in the imagery (Figure 29). The dynamics of these small-scale processes are not well understood, but they may be important in kinetic energy dissipation.

Spectra of upwelling radiance from the sea should allow us to characterize the components suspended in the upper waters of the ocean. Information on the various phytoplankton pigment groups and types of suspended sediments will be very useful. For example, we may begin to understand some of the processes controlling community structure. As this structure greatly affects the processes of carbon fixation and cycling within the marine ecosystem, we will need to develop models of these effects.

Detection of solar-stimulated fluorescence by chlorophyll in phytoplankton may be a valuable technique. Recent work (Kiefer and Mitchell, 1983; Kishino et al., 1984) has shown that fluorescence at 685 nm may be a very good indicator of phytoplankton productivity. Useful measurements of this spectral feature will require high spectral resolution and sensitivity.

Inland Waters

Without adequate supplies of unpolluted freshwater, society as we know it would not exist. The management of inland water is now based largely on empirical relations between forcing functions such as inputs of nutrients, sediments, heat, or toxins and responses of the biological communities such as algal biomass or fish yields. Such models are derived from a very small subsample of inland water lying mainly in northern temperate regions. Vast areas of freshwater comprising diverse natural ecosystems and economically important water bodies occur in arctic, tropical, and southern temperate regions.

Two major scientific problems amenable to remote sensing are measurements of biological productivity and biogeochemical fluxes between inland water and oceans, land, and the atmosphere. Biological productivity should be examined mainly in wetlands and lakes. Fluxes to the ocean are largely via rivers, while exchanges with the atmosphere occur in rivers, lakes, and especially wetlands. Land use in drainage basins and hydrological conditions determine, in part, the fluxes from land to inland waters. Greater elaboration of the rationale and approach to these two scientific problems are provided in Melack (1984) and in the National Academy of Sciences (1986b) publication, *Remote Sensing of the Biosphere.*

The high spatial and spectral resolution provided by imaging spectrometry is essential to examine biological productivity and biogeochemical fluxes in inland waters. To distinguish suspended inorganic and organic materials from the diverse phytoplankton, and to further characterize the major groups of primary producers, requires spectral definition. Both qualitative and quantitative evalua-
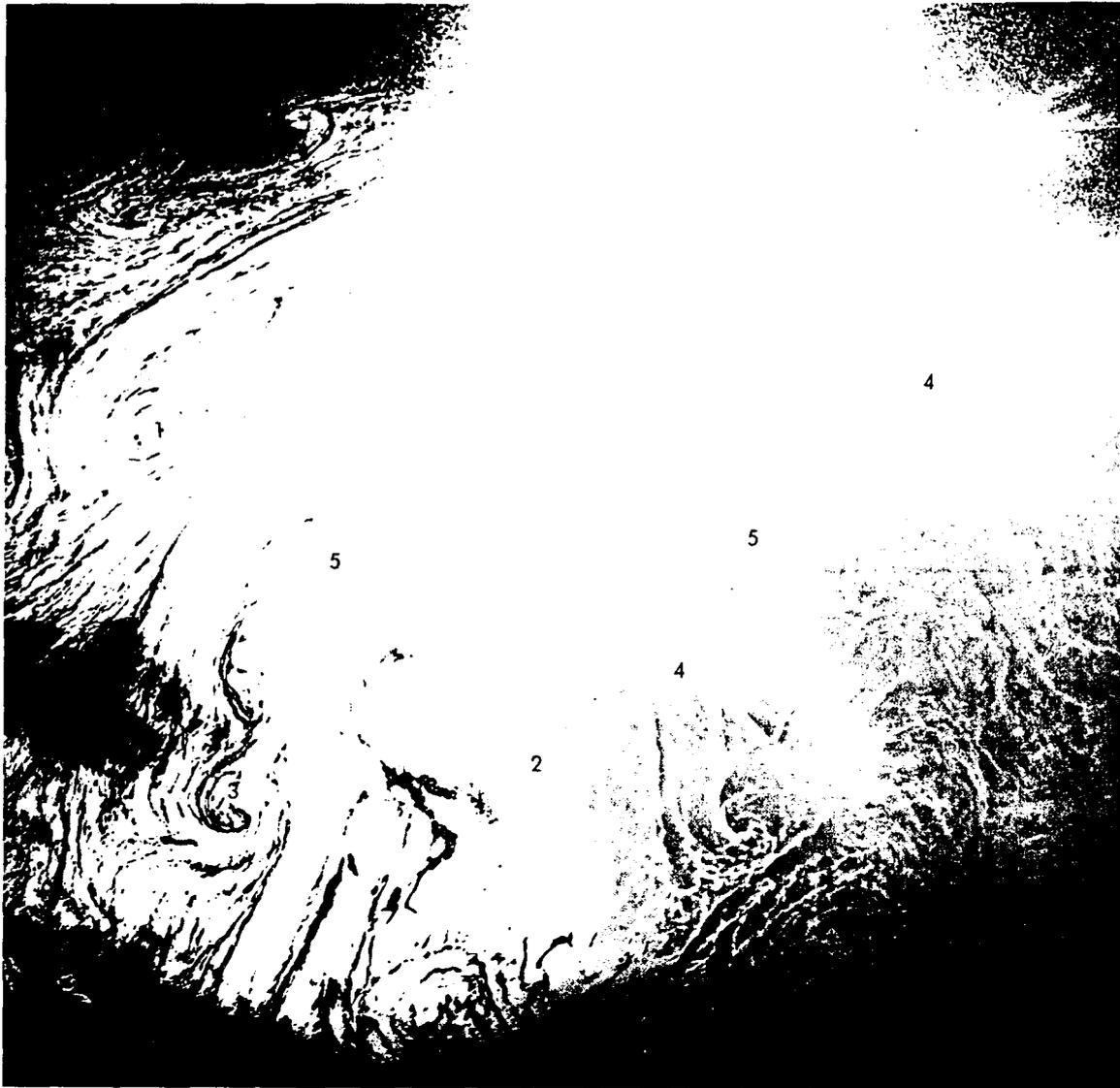
Figure 29. Shuttle hand-held photographic image of spiral eddies in the Mediterranean Sea. In this image the brightness of the sun glint is related to the texture of the ocean surface. In the central portion of the photograph, strongly illuminated by the sun, smooth surfaces reflect light as a mirror and appear bright, while regions roughened by small surface waves appear dark. At the edge of the image the opposite is true. In several places, bright bands wrap in spiral eddies (1, 2, 3). The waves of several ships can be seen as horizontal lines crossing the banded features (4). The waves exhibit marked displacements as they cross certain bands (5), indicating the presence of strong current streams.

tion of the living and dead suspended matter is essential for estimation of carbon fixation and oxygen evolution by aquatic plants. Higher plants in wetlands have recognizable spectral signatures and are usually very spatially heterogeneous. Furthermore, inland waters are intermingled with diverse terrestrial habitats. Therefore, high spatial resolution is necessary to identify aquatic habitats and assess their biogeochemical role.

Inland waters range widely in size, and the larger lakes are amenable to oceanographic approaches as discussed in the previous section. Moreover, process-oriented studies of inland waters, in general as for oceans, are a prime role for imaging

spectrometry. For example, seasonal development of wetland standing crops and changes in reflectance allow estimation of primary productivity, and shifts in pigment composition among phytoplankton permit recognition of successional and nutritional status.

Optical End–Member and Spectral Signature Research

One use for HIRIS is to study representative regions that include high and low concentrations of various aquasols. Such studies will help in developing efficient algorithms for determining constituent concentrations over a wide range of optical settings.

35

(a)

WAVELENGTH (nm)

WATER ABSORPTION COEFFICIENT (M^{-1})

(b)

WAVELENGTH (nm)

WATER ABSORPTION COEFFICIENT (M^{-1})
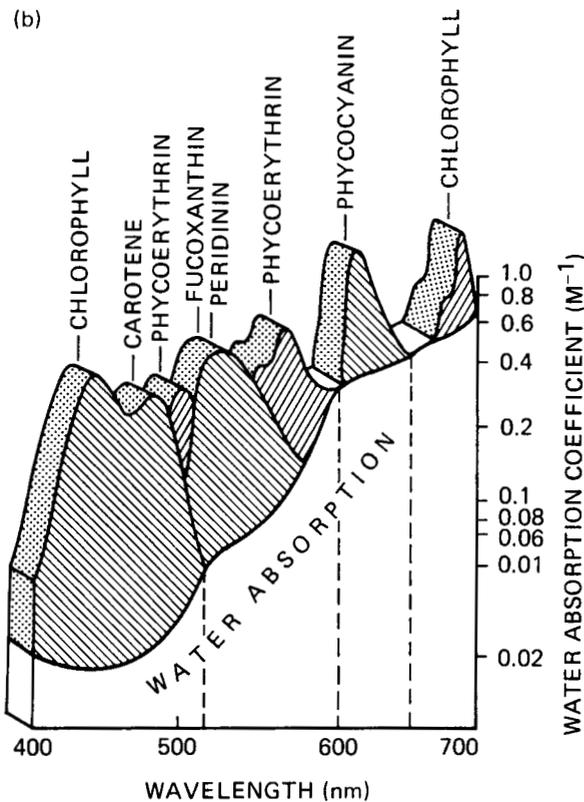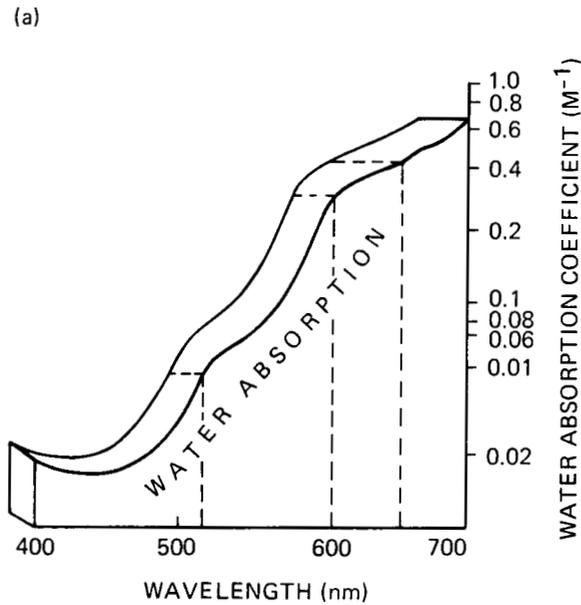
Figure 30. Absorption of light: (a) by water absorption, (b) by different algal pigments in the windows of 'clarity' of water; the spectra for the pigments approximate those measured _in vivo_; fucoxanthin and peridinin are superimposed (Yentsch and Yentsch, 1984).

Candidate sites might include plumes and estuaries of major rivers, like the Mississippi and Amazon, to consider the degree of turbidity tolerable for chlorophyll information extraction, and the Rio Negro for tolerance to gelbstoff. Hypereutrophic lakes could be used for the development of algorithms for extremely high chlorophyll, and lakes at different elevations for development of atmospheric correction algorithms for small bodies of water with highly reflective adjacent pixels. Regions of low-chlorophyll water (e.g., Sargasso Sea) could be examined to determine the number of pixels to be integrated to provide adequate signal-to-noise ratios for the open ocean.

Spectral signatures of plankton permit a variety of ecological and physiological studies. Prezelin and Boczar (1986) provide an excellent up-to-date review of pigment absorption and fluorescence in phytoplankton and a source for much of the following summary. Photosynthetic and nonphotosynthetic pigments in algae can absorb ultraviolet, visible, and near-infrared light, but only visible light (400 to 700 nm) penetrates to appreciable depths in the water column and is absorbed by algal pigments to drive photosynthetic reactions (Figure 30). The absorption capabilities of phytoplankton determine, in part, the spectral quality of the underwater light field. For example, algae that contain both chlorophyll _a_ and chlorophyll _b_ (chlorophytes) usually transmit light in the green region, algae that contain phycocyanin (cyanophyceans) transmit blue light (Figure 31), while algae that contain chlorophyll _a,_ chlorophyll _c_ (diatoms, dinoflagellates, chrysophytes), and phycoerythrin (cyanophyceans) transmit mostly in the yellow.

WAVELENGTH (nm)

ABSORBANCE
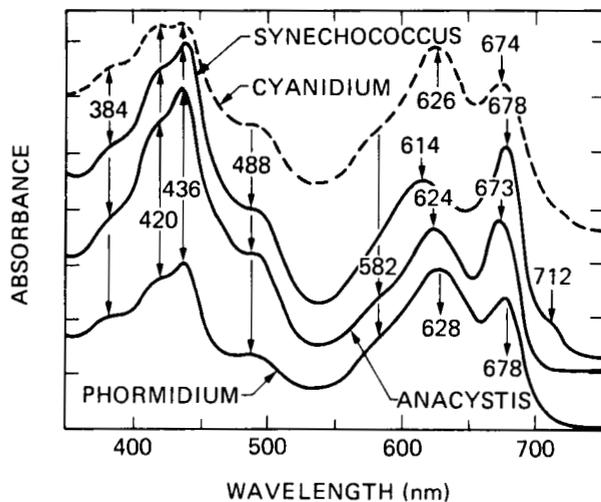
Figure 31. Absorption spectra of several blue-green algae (———) and of _Cyanidium_ (-------). The base line for the different algae were shifted on the ordinate scale (Govindjee and Mohanty, 1972).

36

Light reaching an algal cell may be scattered, transmitted, or absorbed. Algae size, shape, pigment content, and chloroplast arrangement contribute to the spectral quality and quantity of light absorbed by photosynthetic pigments (Kirk, 1983). Once absorbed, the light energy is dissipated as heat, reemitted as luminescence (largely fluorescence) or utilized in photochemical reactions that evolve oxygen and fix carbon. Light that can eventually initiate photosynthesis can be absorbed by chlorophylls, phycobilins, and carotenoids, but only chlorophyll *a* is essential. The other light-harvesting pigments expand the spectral range available. The proportion of these accessory pigments varies, even within one species, as a function of light and nutrient history (Prezelin, 1987). Furthermore, because these other pigments are characteristic of particular algal groups, their recognition aids both estimates of primary productivity and identification of taxonomic or physiological composition.

The absorption spectrum of any pigment is a signature of the energy levels most effectively absorbed and indicates electronic states characteristic of the nuclear structure of the molecule (Sauer, 1975). The proportion of absorbed light utilized for photochemistry or dissipated is highly variable. Fluorescence, one major dissipative route, is a light-emitting process in which the maximum often occurs at slightly longer wavelengths than the longest absorption maximum. A considerable body of literature is devoted to explaining the physiological and ecological significance of fluorescence.

The red (685 nm) fluorescence peak of chlorophyll *a* can be exploited in at least two ways: (1) as a measure of chlorophyll concentration (Kirk, 1983), and (2) as an indicator of physiological state if the chlorophyll has already been determined by another method such as the spectral ratio approach (Carder and Steward, 1985). Estimates of rates of primary productivity are improved when the degree of stress (e.g., light- or nutrient-induced) that a plankton population is undergoing is known. HIRIS will provide data with spectral resolution adequate to address these questions.

## Characteristic Time Scales of Planktonic Features

Variations in the phytoplankton community occur on a broad range of time scales. Of particular interest are those processes that vary on scales of hours to weeks. While larger-scale variations, such as the seasonal cycle and El Niño-type events, have been well documented (Fiedler, 1984), smaller-scale processes are more amenable to the process studies envisioned for high-resolution spectrometry. Denman and Powell (1984) and Mackas et al. (1985) describe many of these small-scale processes that occur in the coastal ocean. On hourly time scales, these processes include internal waves that may expose phytoplankton to a varying light regime (Denman and Gargett, 1983) and can be translated into spatial variations as well (Kahru, 1983). Figure 32 shows a time series of

optical properties in a shallow lake that presumably are a measure of phytoplankton abundance. Pulses of nutrients may occur on time scales of a few tens of hours as wind events cause the entrainment of deeper, nutrient-rich waters into the euphotic zone (Klein and Coste, 1984). Diurnal (or circadian) rhythms in phytoplankton photosynthetic potential have also been documented (Harding et al., 1982).

This spectrum of time-varying processes naturally occurs across a broad range of corresponding spatial scales. The coupling of these time/space variations has proven difficult to study. In essence, it presents an enormous sampling problem, as our methods generally mismatch the scale of the phenomena. For example, we can make very detailed measurements of productivity at a single location for a long period of time in order to resolve some of the dominant temporal scales of fluctuations, but this ignores the spatial extent of these fluctuations. These problems argue for a sampling strategy that is based on a variety of sampling methods, depending on the particular problem under investigation. This aspect is especially acute with remote sensing. While we can obtain high spatial resolution data for a long time period, the data are limited by cloud cover and by the viewing geometry. We cannot sample as frequently as necessary to match the time scale with the sampled space scale (a few tens of meters). In essence, we over-sample in space and under-sample in time. Given that the class of phenomena that we wish to investigate can vary significantly over these time scales, we cannot rely solely on remotely sensed data. Such process studies must also have shipboard and *in situ* (such as moorings) data as part of a complete sampling strategy. In fact, it can be shown for other geophysical phenomena (such as surface winds over the ocean) that the primary limitation to the accuracy of satellite-derived maps is the sampling pattern, not the accuracy of the estimation of the satellite-sensed signal and its associated processing algorithms (Freilich and Chelton, 1985). The severity of this problem depends on the temporal and spatial scale of variation of the phenomenon under study.

Atmospheric Correction for High Contrast Adjacent Pixels

Studies with CZCS have found that on the order of three adjacent pixels may contribute to contamination of a central pixel in cases of high-adjacent pixel contrast (i.e., transition from land to water or from cloud to water). Since an approach similar to the present CZCS algorithms for atmospheric correction will be used with HIRIS, similar sorts of problems are expected to be found. The fine spatial resolution of HIRIS permits study of adjacent pixels, high-contrast radiance contamination near lake and bay shorelines, and around clouds. Use of these high-resolution data over homogeneous waters will permit mapping of the continental aerosol, near-forward scattering function by inversion of the received radiances using appropriate radiative trans-
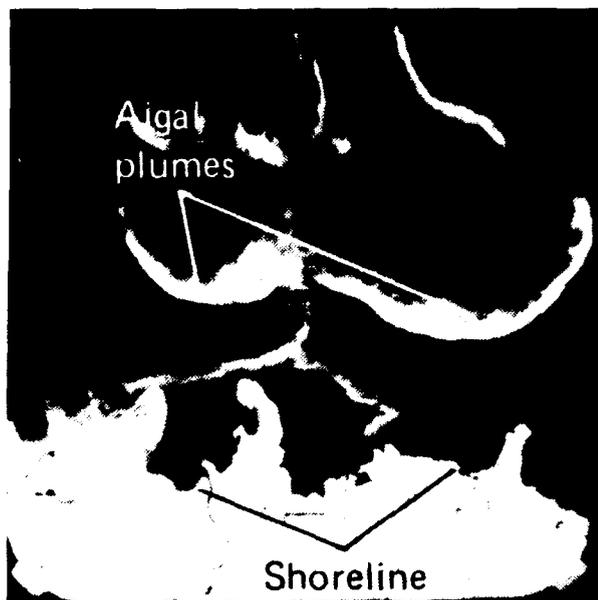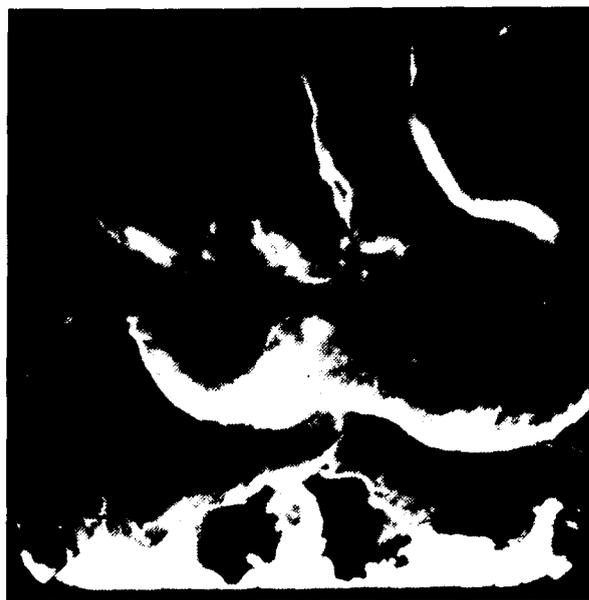
Figure 32. Changes in surface patterns over a 5-hr period in Clear Lake, California, beginning at 7 a.m.: (a) Hour 1, (b) Hour 2, (c) Hour 3, and (d) Hour 5. The large turbulent eddy is outlined by the high reflectance of blue-green algae in the near infrared. Note how the eddy vanished in a few hours, probably due to the setting up of a temporary thermocline. The area shown is 5 km across. There was no inflow to the lake at this time, and there was also no wind. Thus, motion was mostly generated by convection currents due to evaporation (Horne and Wrigley, 1975).

fer codes. Such studies are of particular importance in quantifying the effect of small-scale cloudiness on all visible remote sensors, permitting identification of such problems where they occur, and correction of retrieved radiances near such discontinuities.

Estimation of Primary Productivity

The optical diversity of coastal and inland waters complicates the estimation of chlorophyll concentrations as a measure of phytoplankton bio-

mass. Furthermore, to convert chlorophyll concentrations into estimates of primary productivity requires the rate of photosynthesis per unit chlorophyll at irradiances optimal for photosynthesis, as well as the slope of the light-limited portion of the curve relating photosynthesis per unit chlorophyll to light. These two parameters characterize the photosynthesis versus light curve. In addition, the depth distribution of chlorophyll and light and the incident light are necessary. The numerical model of Fee (1980) provides an example of this approach.

Therefore, estimation of primary productivity of phytoplankton in inland and coastal waters with satellite–sensed reflectances is contingent upon knowing the physiological characteristics of the organisms. The region–to–region and temporal variability of these characteristics must be established as part of the evaluation of the veracity of primary productivity calculations.

Coastal and inland waters can contain submerged and emergent vascular plants and benthic algae. Methods for estimating primary productivity of terrestrial plants can be applied to emergent vascular plants. Submerged aquatic plants are usually very patchy in distribution, and assessment of their abundance will be difficult, but possible under favorable circumstances.

Synergism with AVHRR, MODIS, and SAR

AVHRR

Principal uses of AVHRR observations at the present are for global cloud, sea surface temperature (SST), and vegetation mapping. HIRIS is particularly important in quantifying the role of AVHRR subpixel–scale cloudiness on SST and vegetation retrievals, in improving AVHRR visible calibration, and in giving a better understanding of aerosol selectivity in the near infrared. Although the HIRIS data are limited in spatial extent relative to the AVHRR, use of the two together should permit extrapolation of these results to the global AVHRR data set. While the role for subpixel–scale cloudiness on vegetation index and SST retrieval are fairly easily demonstrated, the improvement in observations of global aerosol radiances in the visible and infrared deserves additional comments. Studies have shown that inclusion of a channel at 1.7 μm (as suggested for future NOAA satellites) can significantly improve AVHRR SST retrieval in regions contaminated by aerosols of volcanic origin. This was a major problem during 1982 in some equatorial regions due to the eruption of El Chichon; SST retrievals were as much as 6°C biased by the volcanic aerosols. HIRIS allows generation of aerosol radiances and selectivity over the oceans from 0.65 to 2.5 μm, and should result in a much better understanding of the role of aerosols in this spectral range and correction of present remote sensing observations in the near infrared.

MODIS

Orbiting HIRIS on the same platform with MODIS provides some major advantages for both systems. The large field coverage of MODIS will provide a means of establishing the atmospheric aerosol type over clear water (Gordon et al., 1983), which is helpful in accurately removing the atmospheric radiance effects for viewing coastal waters. At the same time high spatial resolution HIRIS data will be effective for selected ocean scenes in establishing the gen-

eral size scales for subpixel (MODIS) patches of chlorophyll and clouds. The high spectral resolution of HIRIS data will provide estimates of fluorescence efficiency for key phytoplankton populations, which may help delimit the range of photosynthetic rates for the region. This could yield marked improvements in our estimates of primary productivity, especially for coastal and upwelling regions of the ocean.

SAR

Wetlands are an ecologically and economically important habitat throughout the world, especially in high and low latitudes. These ecosystems are characterized by heterogeneous mixtures of open water and emergent vegetation of varying stature. Two main features of many wetland areas require the combined application of SAR and HIRIS. The extent of flooding is a major environmental factor in wetland ecology, and SAR can penetrate vegetation and recognize flooded areas. Cloud cover is often a severe limitation to observations, and SAR obviates this problem. On the other hand, HIRIS offers superior discrimination of vegetation types and physiological status. As planned by Eos, both HIRIS and SAR will have similar spatial resolutions.

SOILS

Research Needs

Recent field and laboratory studies on the reflectance (visible and infrared) properties of soils have demonstrated the value of narrow–band (10 nm) spectral measurements for characterizing soils and delineating important soil differences (Baumgardner et al., 1985; Karmanov, 1970; Lindberg and Snyder, 1972; Stoner and Baumgardner, 1981; Stoner et al., 1980). The emerging capability to obtain narrow–band spectral measurements over large areas from space platforms calls for a vigorous research program to develop the capability to derive optimum benefit from these new data acquisition systems. To that end these objectives have been formulated for research leading to a more complete understanding and quantitative assessment of our global soil resources:

- To continue the research to define quantitatively the relationships between specific reflectance bands and the physical, chemical, and mineralogical properties of specific soil series and phases within series; to expand this research to include the effects of climate (moisture, temperature) and parent material on the reflectance properties of soils;

- To determine the extent to which radiance measured in narrow spectral bands is affected by the processes of wind erosion, water erosion, salinization, and compaction;

- To identify the spectral regions that can best be used to identify and delineate specific components (minerals, particle sizes, organic residues) and conditions of soils; and

- To generate continuous reflectance curves from narrow-band imaging spectrometer data, and to compare these curves with the five spectal curve forms for soils defined by Stoner and Baumgardner (1981); to determine what soil characteristics can be related to the reflectance curves generated from the imaging spectrometer.

HIRIS will offer the first opportunity to expand narrow-band spectral research on soil resources to a global basis. It should be an excellent catalyst, or common data source, to encourage international cooperation in the area of soil survey research and land resources evaluation. A research effort using HIRIS data should be designed to stratify the land area of the world into relatively homogeneous areas on the basis of climate (moisture regimes, temperature regimes) and geology (parent material). This could turn out to be 50 to 100 different strata or "homogeneous" categories. In each of these test sites strata should be selected that would represent the variation in the soils within that "homogeneous" area.

For each soil sample site within each strata, ground observation data should include the following: (1) description of landscape morphology, (2) soil profile description, (3) precise site location, (4) soil taxonomic designation, (5) climatic regime, (6) spectral (reflectance) data, (7) physical analysis, (8) chemical analysis, and (9) mineralogical analysis.

From these ground observation data a precise quantitative data base will be built with which to compare and interpret the narrow-band HIRIS data obtained over each test site. It will be possible then to compare satellite-derived, narrow-band spectra with the equivalent narrow-band spectra from field and laboratory instruments.

This will be the first opportunity to "globalize" the definition of soils spectra, to relate the variation within these spectra caused by specific components and conditions of the soils, and to quantify the effects of moisture regime, temperature regime, and parent materials on soil reflectance.

This data set will become the basis for defining spectral characteristics of soils under the broadest range of environmental conditions on the Earth. This body of knowledge will be important in using HIRIS-type data in the future to inventory and monitor soil resources of the world.

This basic study of the causes for variations in soil reflectance will also serve as a basis for defining the soil's physical and chemical parameters that can be represented by spectral measurements and predicted through mathematical modeling. The next logical step in this research will be to develop models that can use satellite-derived spectral data and other data sources to develop prediction models for such things as yield prediction, potential soil productivity, and land degradation (wind erosion, water erosion, salinization).

Synergism with MODIS and SAR

The major benefit to be derived from synergism with MODIS and SAR relates to the dynamic short-term changes that occur in soils. The specific areas that would be useful in characterizing current soil conditions include: (1) quantitative assessment of soil moisture conditions, (2) geobotanical studies, (3) tillage operations, (4) climatic events causing changes (wind and water erosion, flooding), and (5) assessment of rates of soil degradation. For the normal use of spectral data as a tool to delineate differences between soils, the synergism with MODIS and SAR is less important.

VEGETATION

Objectives and Justification of Vegetation Remote Sensing Experiments

For vegetated surfaces, imaging spectrometry has the potential to address a host of both basic and applied questions. These range from the fundamental structure and optical properties of plant canopies to the role of the plant-mantled areas of the Earth in maintaining the biosphere. In this section we briefly outline two specific areas in which high spectral and high spatial resolution data will prove most valuable.

Ecosystem Function in the Global Biology Context

There is an increasing awareness in both scientific and lay communities that the Earth functions as a single, integrated biogeochemical system, and that terrestrial ecosystems play a large role in modifying the functioning of this system. Of particular interest are the net inputs and outputs of elements and compounds that may modify climate (e.g., carbon dioxide, nitrous oxide) or enrich or pollute adjacent systems (e.g., nitrate, phosphate, aluminum, heavy metals). Terrestrial ecosystems also act as a major sink for industrial pollutants (e.g., ozone, forms of sulfur), while producing important products such as energy, fiber, food, and usable water.

An important question is whether terrestrial ecosystems will continue to contribute to the maintenance of an acceptable biosphere in a changing global environment. Human manipulation and pollution, along with potential climatic changes, impose stresses on terrestrial systems that may impede their normal functioning. Most natural ecosystems are able to capture and hold essential nutrients so that leakage is low while internal cycling rates are high

(Likens et al., 1977; Henderson et al., 1978). Disturbed, degraded, or severely stressed systems, on the other hand, often exhibit high nutrient loss rates, which may contribute to pollution or eutrophication of adjacent ecosystems (Bormann and Likens, 1979). It thus becomes important to be able to assess the "health," or level of vigor or stress, of terrestrial ecosystems.

The canopy of a plant community contains a wealth of information about the state of the system. Changes in water and nutrient availability are reflected in the degree of canopy development, measured as the amount and seasonal duration of leaf area display (Grier and Running, 1977; Waring et al., 1986), as well as in changes in reflectance characteristics (Tucker et al., 1985; Spanner et al., 1984). Subtle changes in the vigor of vegetation and rates of various ecosystem functions may be apparent through alteration of leaf chemistry well before changes in leaf area and community structure occur (Waring et al., 1986). Of particular interest are shifts in carbon allocation between primary cell constituents such as cellulose, and secondary or defensive compounds such as lignin. The lignin and nitrogen content of leaves are also important in determining rates of decomposition when the leaves become litter (Melillo et al., 1982). Litter decay rates are important determinants of nutrient cycling rates. Total canopy nitrogen and water contents may also be indicative of important system functions, as may changes in leaf morphology and pigment ratios evident in the "blue shift" at the red edge of the chlorophyll absorption (Rock et al., 1986), where the wavelengths at which plant reflectance increases toward the near infrared shifts slightly toward the blue end of the spectrum.

Recent studies of both individual leaf and whole canopy reflectances suggest that it will be possible to measure important canopy chemical characteristics from space using high spectral resolution imagery. Commercial devices are currently being used in analysis of agricultural products (Hooten, 1978; Rotolo, 1979). A preliminary analysis of data from AIS suggests that total canopy nitrogen, water, and lignin will be measurable (Spanner et al., 1985; Fownes and Aber, 1985; Waring et al., 1986). Thus, the development of a satellite imaging spectrometer system should give a new generation of biospheric scientists a better means of assessing how terrestrial ecosystems function and what their contribution is in maintaining the biosphere.

Increased Understanding of the Nature of Vegetated Surfaces

A fundamental understanding of the short-wave energy interactions among various Earth surface scenes is necessary for the intelligent use of remote sensing technology. Most remote sensing studies of the land masses deal in some manner with vegetation cover, whether the vegetation is the primary objective or an impediment to interpreting the underlying soil and geological substrate. In any case, we need to improve our understanding of the physical radiant transfers for various spectral wavelengths that take place within vegetation canopies as a function of (1) geometric structure of the vegetation (e.g., leaf orientation, leaf density, stem size, and plant spacing), (2) optical properties of various components (e.g., leaves, stems, and fruiting bodies), and (3) solar illumination geometry. The geometric structure of vegetation is important information used to discriminate and classify various types and functions of vegetation canopies. The optical properties of the canopy provide further information on chemical composition and physical structure. This growing body of knowledge will ultimately serve the remote sensing and Earth science communities by providing insight and guidance in developing new ways of discriminating important physical and biological processes of the plant system from off-nadir satellite data.

Direction of Imaging Spectrometer Remote Sensing Research

While the potential value of an imaging spectrometer instrument to terrestrial ecosystem research is high, there is much basic research yet to be done to realize this potential. Because of the size and heterogeneity of forest ecosystems, relatively few high-resolution data are available over forest ecosystems. Thus, it is still unclear to what extent structural complexity and non-Lambertian properties might mask subtle reflectance characteristics resulting from differences in canopy chemistry.

For terrestrial ecosystems, it is important that preliminary studies of canopy reflectance be carried out with field and airborne instruments. The purpose of these studies would be to assess the sensitivity of spectra to changes in canopy conditions, which relate to ecosystem function. Thus, the AVIRIS program appears to be an important precursor to the application of HIRIS to the analysis of these complex systems.

As the AVIRIS program builds on the AIS work, a series of well-studied terrestrial systems with well-known canopy characteristics will be identified. These systems must cover long gradients in site quality, pollution impacts, or other important variables of interest in the global biology context. These sites will provide excellent targets, which can be used to demonstrate the feasibility of acquiring and applying high spatial, spectral, and angular resolution data to regional environmental problems, leading to the deployment of HIRIS to continuously sample selected key systems for signs of stress or degradation.

ATMOSPHERE

The main objective of HIRIS, namely surface remote sensing, can only be addressed when there is no, or only sparse, cloud cover. Under these conditions, it is anticipated that atmospheric scattering

and absorption parameters can be measured by HIRIS. However, even under cloudy conditions, which are expected about 50 percent of the time, important information about the cloud cover may be acquired that has considerable influence on the Earth's radiation budget, which plays a major role in climate dynamics.

Clouds

Although there is now a large, ongoing effort to assess the effects of clouds on the Earth's energy budget, imaging spectrometry, through its spectral coverage and resolution, its high spatial resolution, and its multiple-view capabilities, offers unique observing potentials.

HIRIS, operating in the same mode as for surface observations, will provide data on small-scale (tens of kilometers) cloud fields at several angles, thereby testing previous observations and theoretical models for bidirectional reflectivities needed to infer radiative fluxes. Although useful data could be extracted from nadir to 45° view angles, theoretical considerations suggest that an assessment of the sensitivities of bidirectional reflection to cloud geometry requires 60° views. HIRIS could study this sensitivity by obtaining multiple look-angle data at several zenith angles and azimuths with respect to the principal plane. Furthermore, the high spatial resolution allows separation of bidirectional reflectivities into broken and spatially uniform cloud categories.

The effect of pollution on cloud optical properties has yet to be verified. The suspicion is that aerosols, particularly in urban environments, mix with cloud particles and give rise to anomalous absorption at visible wavelengths. In addition, it has long been claimed that given the low absorption by water and ice at visible wavelengths, clouds should reflect more radiation than is often observed. The spectral coverage and resolution, along with the high spatial resolution provided by HIRIS, allow measurement of the reflectivities of cloud elements in various parts of the visible and near-infrared spectrum. Furthermore, the global coverage of space platforms provides sampling in urban and pristine areas to check for systematic differences in spectral signatures of clouds in polluted and clear environments. Such observations would, of course, depend on the relative radiometric calibration among the spectral bands and, in order to assess absorption by clouds, would also require absolute radiometric calibration.

At wavelengths where clouds absorb solar radiation, the reflected radiation is due to low-order scattering that takes place near the cloud surface. Such reflection should provide information that would reveal particle size and, in the case of ice clouds, might indicate crystal structure.

The high spatial resolution provided by imaging spectrometry can be used to probe spatial structure within cloud systems. The spatial structure, along with the meterological environment, provides clues to the physical processes affecting cloud develop-

ment and physical properties. Such studies are not possible with the Landsat TM, but HIRIS would allow the extension of such work. This improved high spatial resolution can also provide a new spatial scale of cloud fields for different synoptic conditions such as a cloud-capped boundary layer in a high pressure region, frontal clouds, and mesoscale convective cloud clusters. Such wide-angle scans would allow the exploration of new objective schemes for obtaining a quantitative measure for cloud cover in broken cloud systems, particularly over continents.

Automated procedures for objectively analyzing cloud properties on a global scale are still under development. A particularly difficult problem is determining cloud-free background radiance for continents under broken cloud conditions. Such a determination is required in order to determine, for example, cloud cover. Imaging spectrometry allows, at least for daytime observations, the ability to explore strategies involving spatial scale, spectral signature, and angular dependence that could be transferred to operational instruments for global monitoring.

Aerosols and Gases

The main perturbations introduced into remotely sensed surface scenes by the atmosphere under cloudless conditions are due to scattering and absorption of solar radiation by aerosols and gaseous constituents, particularly water vapor. In the visible and near-infrared wavelength regions covered by HIRIS, the effects of aerosols are expected to dominate over Rayleigh scattering by the gaseous constituents. However, knowledge of these atmospheric parameters is not only a necessary prerequisite for atmospheric corrections of remotely sensed surface data, but is also needed for climatology and general circulation analysis. The distribution, sources, and sinks of aerosols over urban areas, deserts, large-scale fires, and seas may affect the Earth's climate substantially. Aerosols also participate in the heterogeneous chemistry of atmospheric trace constituents, but the reactions are still poorly understood.

HIRIS provides a unique capability for measuring aerosol properties. In particular, the information content is significantly increased compared to current operational instrumentation, since spectral data are obtained at higher resolution and over a wider spectral range (0.4 to 2.5 μm). Since maximum scattering occurs when the aerosol particle diameter is approximately the same as the radiation wavelength, this spectral range will cover most aerosol sizes of interest in continental and marine atmospheres. Also, the higher spatial resolution of HIRIS will be a significant improvement over the 1 to 4 km resolution of today's operational satellites.

In the most general case of an arbitrary, variegated background (i.e., over land), determination of aerosol content from nadir radiances alone can only be done if the surface bidirectional reflectance properties are known. In this case, a reasonable objective

is to use multitemporal data to measure changes in aerosol loading between successive overflights of a given target, assuming the surface reflection properties have not changed in the interim (Fraser and Kaufman, 1985). The contiguous spectral coverage of HIRIS will be particularly useful, applying this technique to characterize variations in aerosol optical properties. In addition, the ability to obtain off-nadir images enhances the information content due to the increased atmospheric path length (Diner and Martonchik, 1985b). However, since multiple view-angle coverage of the same region using HIRIS can only be obtained on a sporadic and localized basis, useful adjuncts to HIRIS on Eos might be an active lidar to continuously profile atmospheric particulates accompanied by a multiple view-angle imager (Coakley, 1985).

From experience with operational satellites it has been demonstrated that aerosol parameters such as size distribution and mass loading can be meaningfully estimated. This requires that the HIRIS data have a minimum S/N of 200. Precision is more important than absolute accuracy, but a precision and stability of 0.5 percent in reflectance should be maintained.

Determination of aerosol properties, particularly the wavelength dependence of optical depth and absorptivity, is an integral part of any atmospheric correction algorithm. To maximize the information content about atmospheric effects, it is most desirable to obtain symmetric off-nadir scans in the principal plane from about $+65°$ to $-65°$. If this is unattainable, asymmetric scans encompassing 60° forward and 30° aft of nadir would be the next preference for atmospheric effects determinations.

SNOW AND ICE

For research on the climatology and hydrology of snow- and ice-covered areas, we need information that helps us estimate the energy exchange at the surface, the amount of water stored in the snow pack, and the movement of water through and out of the snow pack. For energy exchange we need to know the spectral albedo and emissivity and the surface temperature. Albedo depends on grain size, illumination angle, contaminants, and, when the pack is thin, depth. Emissivity is less sensitive to snow properties. In addition to energy exchange information, we must evaluate the amount of water stored in the snow, and we often want to know the spatial distribution of the movement of water out of the pack.

Table 5 (Warren, 1982) shows which snow parameters are measurable, in principle, in various spectral bands. Except for thermal infrared emissivity, the signals in other wavelength bands are affected by several snow characteristics. Therefore, in order to measure characteristics unambiguously, simultaneous examination at several wavelengths would be necessary. Thus, for the snow and ice community, the combination on Eos of a pointable

instrument with fine spatial and spectral resolution (HIRIS), combined with a sensor with frequent coverage at similar spectral intervals (MODIS), combined with microwave and radar data (AMSR and SAR), would offer unprecedented capability for examining snow and ice processes over the Earth.

In the visible and near-infrared wavelengths, the greatest disadvantages of present satellite systems result from our inability to account for effects of the bidirectional reflectance-distribution function (BRDF), and our inabilities to correct for the atmosphere. A pointable instrument should give us badly needed information on the variation of snow reflectance with the viewing angle, and accumulate the data needed to estimate albedo with nadir-pointing instruments. The multiplicity of spectral bands would provide the redundant information needed to correct for atmospheric components in the signal.

The most promising possible use of HIRIS in the study of snow and ice resources is for investigations of the BRDF and its relation to the spectral albedo. One of the biggest problems in the use of remote sensing to study the climatology of the land surface is that for climatic investigations we are usually interested in the albedo—the reflectance integrated over the entire upwelling hemisphere—whereas the satellite measures the reflectance integrated only over a very small conical angle within this domain.

For large homogeneous surfaces (oceans, sea ice, clouds, the Antarctic snow pack, etc.) the Nimbus-7 ERB Experiment has utilized a broad-wavelength band scanning radiometer to measure typical BRDF values for characteristic surfaces (Taylor and Stowe, 1984). For the land surface, however, and particularly for the snow pack in mountainous areas, the Nimbus-7 ERB scanner has inadequate spatial and spectral resolution. Understanding the surface radiation balance in these areas depends on knowledge of the spatial distribution of surface properties. The HIRIS instrument would give us the only detailed spectral measurements of the BRDF of the snow pack at various elevations and topographic exposures. Thus, it would allow us to understand the variation of the surface climate in these areas.

The high spectral resolution of HIRIS data would allow much better definition of snow characteristics from space. We expect that we will be able to estimate the grain size and the amount of absorbing aerosols incorporated in the surface layers of the snow pack. In addition, if any contaminants have distinctive spectral signatures, it might be possible to identify them.

Synergism with MODIS

HIRIS would be useful for occasional detailed measurements of surface snow characteristics. However, monitoring of the spatial and temporal variation in surface reflectance would require an instrument with more frequent observations. We envision

Table 5. Properties Affecting Albedo and Emissivity of Snow*

	Visible Reflectance	Near–Infrared Reflectance	Thermal–Infrared Emissivity	Microwave Emissivity
Grain size	**	yes	no	yes
Zenith (or nadir) angle	**	yes	yes	yes
Depth	yes	no	no	yes
Contaminants	yes	no	no	no
Liquid water content	no	***	no	yes
Density	no	no	no	yes
Temperature	no	no	no	yes

*Warren, 1982
**Only if snow pack is thin
***Through grain clusters

that the combination of the detailed HIRIS observations with MODIS observations at larger spatial scale two or three times per week would enable an investigator to track the energy balance of the snow pack through time. This would allow accurate estimation of the spatial distribution of snowmelt, which is of importance in analyzing the effect of snow chemistry.

Synergism with HMMR/AMSR and SAR

Two other useful components of the Eos program are HMMR, which will measure passive microwave radiation from 6 to 90 GHz at spatial resolutions from 2 to 10 km, and SAR at 1.4, 6, and 10 GHz with 30 m spatial resolution. In the microwave region, the radiation penetrates the snow to a much greater depth than in the visible (where the signal comes from the top 20 to 50 cm) or the infrared (where the signal comes from the top 20 to 50 mm). Because so many variables influence the signal in the microwave, the relationship between the microwave brightness temperature or the radar backscatter coefficient and such hydrologically useful parameters as snow water equivalence is inexact, but we do know that the microwave radiance and the radar backscatter represent an integrated signal from the whole snow pack and underlying soil. Therefore, the combination of high spectral resolution data to estimate

grain size and thermal infrared data to measure snow temperature would allow us to sort out some of the confounding elements in the microwave and radar signals. The combination of these instruments at wavelengths from the visible to the microwave would allow estimation of snow properties in much better detail than is currently possible with instrumentation in a single spectral region alone.

In particular, it might be possible to estimate the snow water equivalence over entire drainage basins. Currently, our knowledge of distribution is only rudimentary. The usual snow monitoring programs carried out by such agencies at the U.S. Soil Conservation Service or the California Department of Water Resources use snow courses located throughout drainage basins as indices of the amount of snow. Never have we computed a water budget for a basin where the dominant process is snowmelt runoff! Currently in those meterological situations where traditional methods (e.g., degree–day calculations) of forecasting runoff perform badly, we are unable to identify the reasons for the error. The consequences of such uncertainty were vividly demonstrated in California in 1978 and in the Colorado River Basin in 1983, when forecasts were badly in error.

The combination of instruments proposed for the Eos platform—HIRIS, MODIS, HMMR/AMSR, and SAR—would provide valuable information for entirely new methods of monitoring snow resources.

IV. SUMMARY OF SCIENCE REQUIREMENTS

INTRODUCTION

This section synthesizes instrument specifications put forth by each of the disciplines in developing the applications for imaging spectrometry data. The importance of each of the parameters varies among disciplines. Moreover, some disciplines have prior experience with high spectral resolution data and thus can identify requirements in more detail. For example, the requirements for spectral resolution beyond 1.0 μm can be well substantiated for mineralogical mapping but less so for vegetation studies. More work is required to define the requirements more accurately, and the ongoing experiments using AVIRIS data will make the analysis and modeling much easier and far more specific. The following requirements are for a spaceborne imaging spectrometer regardless of altitude, although it is understood that trade-offs may be necessary to comply with platform constraints and constraints imposed by other instruments. Table 6 summarizes the requirements, which are discussed in more detail in the remainder of the chapter.

Table 6. Summary of Science Requirements

Spatial resolution	30 m
Swath width	30 km
Spectral coverage	0.4–2.5 μm
Spectral resolution	10 nm
Coverage frequency	4–5 images possible in 16-day orbit cycle
Pointing	±24° cross-track, +60° to -30° down-track
Calibration	1% absolute, 0.5% stability
Polarization	≤2%
Encoding	Full solar irradiance, 12 bits

SPATIAL RESOLUTION

The quest for ever higher spatial resolution has marked the entire development of spaceborne imaging systems, because more detail has always meant more information. Different kinds of information are available at each scale level down to the submicron resolution of an electron microscope. As an example, Table 7 presents one measure of the scales of features that can be addressed for taxonomic classification of geomorphologic features.

Experience with the Landsat MSS (GIFOV 80 m), Landsat TM (30 m), as well as SPOT (20 m multispectral bands and 10 m panchromatic band) and the Large Format Camera (LFC) (5 m), demonstrates the value of higher resolution for mapping and interpreting landforms. However, given the new spectral dimension provided by imaging spectrometry and the limitations in data transmission, the ISSAG concluded that a 30 m GIFOV was a reasonable compromise. In view of the 500 m GIFOV to be provided by MODIS, and examining experience with Landsat MSS and TM data, it was felt that a TM equivalent pixel size would be adequate to facilitate a multistage sampling approach using combined MODIS and HIRIS data. A better spatial resolution in all bands would extract too large a penalty in data rates, and the disadvantages of a degradation in spectral resolution to overcome this problem would outweigh information gained by smaller pixels.

The requirement for 30 m or smaller pixel size can be quantified in vegetation research. In forest ecosystems, successional changes in vegetation structure and function are linked to the size of gaps created by tree death, windfall, and other forms of disturbance, and also to the spatial scale of change in important environmental drivers. For imaging spectrometers to offer a significant increase in remote sensing capabilities, they must be able to detect these finer spatial-scale patterns.

The 30 m resolution is of the same order as the scale of gap-phase disturbance in forest ecosystems. The largest trees will create openings of this size when they fall. Several functional characteristics, such as nutrient losses—including gaseous fluxes of nitrogen to the atmosphere—show large, nonlinear responses to disturbance. Thus it is important to be able to sense the percentage of an area in gaps at any one time.

Environmental gradients, which determine changes in important processes such as production and evapotranspiration, can also change over short distances. In one study, nitrogen cycling within a plantation of sugar maple of uniform age varied by a factor of three over a distance of 200 m (Lennon et al., 1985). In another study site, used for AIS sampling, changes in soil conditions caused a complete turnover in species composition and a fourfold change in nitrogen cycling in stands less than 1,000 m apart (Pastor et al., 1984). Comparing maps of soils and vegetation changes at this latter study site with an image produced at 30 m resolution from Landsat gives a graphic demonstration of the potential loss of information even at this resolution. Increasing the pixel size would significantly reduce the amount of information available on these fine-scale, nonlinear

Table 7. Scales of Geologic Features*

Order	Surface Size (km²)	Characteristics of Area	Genetic Mechanisms Causing Topography
I	10^7	Continents	Differentiation of core
II	10^6	Great structural units (Tethys)	Crustal movements
III	10^4	Large structural units (basins)	Tectonic units having connection with paleogeography
IV	10^2	Elementary tectonic units (massifs)	Primarily tectonic, secondarily due to lithology
V	10	Tectonic features (anticline)	Predominantly lithology
VI	10^{-2}	Forms of relief Ridges, cirques	Morphodynamic factors
VII	10^{-6}	Microforms Ravines	Morphodynamic factors
VIII	10^{-8}	Microscopic Weathering	Rock texture

*Tricart, 1965

effects, whose understanding is a major goal of the imaging spectrometer program for vegetation studies.

An additional goal of remote sensing of terrestrial ecosystems is to use the data to drive new or existing models of ecosystem dynamics. As an indication of the plot sizes generally used to capture the dynamic state of the system, most models run with plot sizes of around 15 m in diameter (Shugart and West, 1980).

In ice and snow research in mountainous areas, pixels larger than 30 m are invariably mixed and suffer from convolution of multiple slopes and exposures. With a 30 m pixel, one can find at least some that are completely snow covered, with no vegetation, rock, or soil. This helps to sort out the mixed pixel problem over the remainder of the image. At larger pixel sizes, there are fewer pixels that are uncontaminated by vegetation or exposed rock.

SPECTRAL COVERAGE

The choice of spectral coverage is dictated both by the scientific requirements and the technological capabilities. The region 0.4 to 2.5 μm contains almost all possible information that can be derived by passive sensors from reflected solar energy. The only other regions accessible by space remote sensing, and that contain diagnostic information, are the thermal infrared regions, 3 to 5 μm and 8 to 12 μm.

Here, surface temperature information is available and diagnostic spectral features for silicate minerals can be found. From a technological point of view, there is little reason to combine the two regions in one sensor dedicated to high spectral resolution imaging. On the whole, more information can be acquired for more disciplines in the chosen 0.4 to 2.5 μm region than in the thermal infrared. Important correlative data can and should be acquired in the thermal infrared, but with a separate instrument, and perhaps on a separate platform because the ideal acquisition times are not the same as for sensors in the solar spectrum.

SPECTRAL RESOLUTION

The requirements for spectral resolution are driven by the water and vegetation studies in the visible–near–infrared region and by geology in the region beyond 1.0 μm. The spectral resolution requirements of the atmospheric, hydrologic, and glaciologic communities are less severe.

One of the advances in understanding biological activity in water using imaging spectrometry will be to directly identify constituents that affect the optical properties of the water and their concentrations. Absorption spectra of algae pigments such as phycoerythrin and peridinin have spectral features with

full-width, half-depth values of 20 nm. Therefore, a 10 nm resolution will be required to describe these features and separate them from adjacent features in the 0.4 to 0.7 μm region.

Requirements for spectral resolution of imaging spectrometers for vegetation research are less well known. It is clear that the resolution offered by TM has not proven sufficient for high-resolution species identification or for measuring the biogeochemical state of terrestrial ecosystems, beyond general measurements of stress. One goal of imaging spectrometer research is to develop the capability to detect subtle changes in ecosystem biogeochemistry as early indications of coming changes in structure and function. This problem is currently being approached by remote sensing of changes in total canopy content of important constituents such as nitrogen and lignin.

One measurement of stress is the so-called "blue shift" in the red edge of the chlorophyll absorption at 0.68 μm, where the increase in reflectance between the visible and near-infrared (VNIR) wavelengths occurs at a slightly shorter wavelength. Reliable detection of the blue shift requires sampling at 10 nm intervals between 0.5 and 0.75 μm. The detection of the blue shift is not possible at a 20 nm sampling interval.

Spectral features for minerals are associated with electronic transitions in transition elements, mainly iron, in the VNIR region and vibrational modes in the region beyond 1.5 μm. Electronic features are generally broad and thoroughly described at 10 nm sampling. Vibrational features, generally overtone bending-stretching vibrations, are exhibited by minerals bearing Al-OH, Mg-OH, CO_3, and SO_4 constituents. These minerals exhibit features in a few cases as narrow as 10 nm full-width, half-depth, requiring 5 nm sampling for proper description, but the majority of mineral features can be completely described with 10 nm sampling. A significant degradation in identification, particularly in magnesium-bearing minerals and in limestone and dolomite, is seen when the sampling interval is increased to 20 nm.

In general, 10 nm is a critical sampling interval throughout the 0.4 to 2.5 μm wavelength region.

COVERAGE FREQUENCY

Coverage frequency requirements are directly related to the dynamic nature of the problem to be studied. Water studies have the greatest need for frequent measurements; vegetation ranks next, and geological studies a distant third. Geological investigations require data at an optimum time of the year for proper lighting and vegetation cover and absence of cloud cover.

HIRIS will not acquire continuous coverage but rather sample sites at high spatial and spectral resolution. While some water experiments dealing with rapidly changing algae blooms require daily monitoring, a biweekly revisit interval is more realistic based on orbit and instrument constraints.

POINTING

The requirements for pointing are twofold. The first concerns cross-track pointing to acquire data from areas not directly under the spacecraft. Cross-track pointing also allows revisits of the site on subsequent days. Based on requirements for research on algae bloom growth, next-day coverage is required and coverage over a 3-day interval is desirable. Given a 824 km orbital altitude, cross-track pointing of up to $\pm 24°$ is required to allow three to four possible views of an area at the Equator and four to five views at 40° latitude during a 16-day orbit revisit cycle.

Down-track pointing is required to develop BRDFs for surfaces, to evaluate atmospheric extinction and path radiance components, to enable target tracking to increase S/N performance for dark targets, and to avoid sun glint on the ocean surface. The atmospheric measurements have the highest requirements: a $+60°$ and $-30°$ down-track pointing capability.

CALIBRATION

Requirements for calibration are twofold, spectral and radiometric. Spectral calibration entails determining the wavelength falling on each pixel, which can be expected to change with variations in instrument temperature. This calibration must be done onboard and minimally to ± 5 nm.

Radiometric calibration requirements are more difficult to specify. Onboard calibration is required to determine the sensitivity and linearity of each detector element. A general requirement of 0.5 percent channel-to-channel relative response accuracy and absolute accuracy of 5 percent was agreed upon by ISSAG. However, absolute calibration of 1 percent should be achievable and would be useful for energy balance considerations and oceanographic measurements. The use of a solar diffuser on HIRIS, along with a stable sensor and annual lunar calibration, should make these ambitious calibration goals achievable.

Channel-to-channel spectral calibration relative to the solar spectral irradiance curve should be accomplished by viewing the sun in diffuse reflection by use of a diffuser plate at monthly to semiannual intervals (Gordon, 1981) and by annual viewing of the moon. This would alleviate the calibration difficulties encountered at short wavelengths due to outgassing and condensation on the outside mirrors and windows experienced with sensors such as CZCS. Such a scheme is an absolute requirement for HIRIS.

POLARIZATION

Polarization due to the instrument will be convolved with scene polarization, caused both by the surface and by aerosol and Rayleigh scattering in the atmosphere, which varies with solar and viewing geometry and with aerosol type and concentration.

Depolarization of the aperture radiance to less than 2 percent, as done with CZCS, is required to prevent confusion resulting from polarization and to allow removal of atmospheric effects from HIRIS imagery over water bodies.

ENCODING

Requirements for encoding (number of units per pixel) depend on the dynamic range and smallest reflectance interval to be observed.

In the case of snow, a great dynamic range is required. From wavelengths 0.4 to 0.8 μm snow is one of the brightest natural substances, with reflectances near 1.0. Moreover, for estimates of the snow sur-face energy balance, it is important to discriminate between reflectances of, say, 0.92 and 0.90, because the difference represents a 20 percent difference in absorption. Therefore, a dynamic range that encompasses the full solar irradiance is necessary, and the quantization must be fine enough to distinguish minor differences, at least 10 bits.

Because it will be necessary to average pixels to acquire adequate S/N for water studies, 12-bit encoding will be required to take advantage of the potential S/N increase. For other studies, 8-bit quantization should be adequate since S/N varies between 50 and 200 in most regions of the spectrum. Again, more study is required to adequately address the question of encoding requirements.

V. HIRIS SENSOR

Scientific requirements for sensor characteristics are discussed in the preceding chapter and summarized in Table 6. In this section we review the instrument design that will satisfy those requirements.

The rationale for imaging spectrometry is to provide sufficient sampling of the spectrum to resolve features that are diagnostic of a variety of phenomena. Because the required resolution leads to almost 200 bands in the range 0.4 to 2.5 μm, it is not practical to provide individual filters. Instead the spectrometer images the scene through a spectral dispersing system onto a detector array. Figure 33 illustrates the operation of an imaging spectrometer using area-array focal planes. Because the imaging spectrometer provides sampling of the entire spectrum, there will always be more bands than are required for any specific experiment. For this reason, spectral editing is part of the overall data handling scheme.
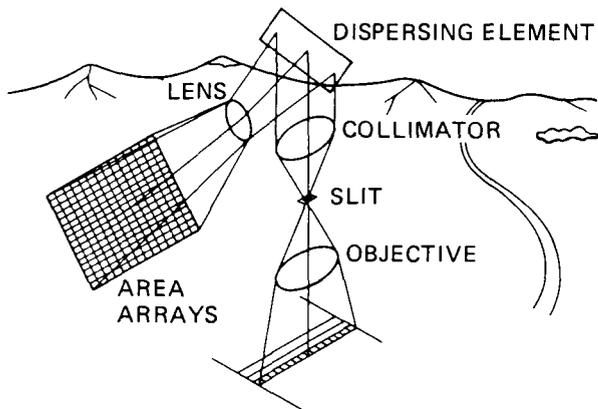

Figure 33. Imaging spectrometer concept using area-array detectors.

INSTRUMENT DESCRIPTION

The HIRIS instrument is a pushbroom imaging spectrometer that uses area-array detectors to provide simultaneous and inherently registered imaging. The GIFOV of 30 m provides the same spatial resolution as the Landsat TM. Cross-track and down-track pointing are provided for target acquisition, multiple look angles, and atmospheric correction. The down-track pointing capability is also used to allow image motion compensation (IMC), which increases the effective integration time and therefore increases S/N.

The instrument parameters are summarized in Table 8.

The instrument will be mounted on the Eos platform main structure with the optical axis aligned with the flight direction. Down-track pointing is provided by a mirror oriented at a nominal 45° angle to the instrument line of sight. Cross-track pointing

Table 8. HIRIS Functional Parameters

Nominal altitude	824 km
GIFOV	30 m
Swath width	30.0 km
Spectral coverage	0.4–2.5 μm
Average spectral sample interval	
0.4–1 μm	9.4 nm
1–2.5 μm	11.7 nm
Pointing	
Down-track	+60°/–30°
Cross-track	+24°/–24°
Encoding	12 bits/pixel
Maximum internal data rate	512 Mbits/sec
Maximum output data rate	300 Mbits/sec
Image motion compensation	Gain states of 1 (off), 2, 4, and 8

is provided by a two-axis mirror. Figure 34 illustrates the conceptual layout of the instrument.

Orbit

The Eos orbit is sun-synchronous, daytime ascending. The orbital repeat cycle is 16 days. Adjacent ground tracks at the Equator are separated by 5 days and 176 km. Additional orbit parameters are given in Table 9 and shown in Figure 35. More detail on the interaction of these orbital parameters with instrument pointing is given in the later section on *Pointing and Image Motion Compensation* in this chapter.

Optical System

The first-order parameters for the HIRIS optical system are shown in Table 10 and the layout of the optical system is shown in Figure 36.

The HIRIS optics consist of an unobstructed, all-reflecting, off-axis fore-optic and an off-axis, unobstructed, two-band, double-pass spectrometer. The optical system aperture stop is located at the telescope corrector and has a diameter of 37.6 cm. The slit, located at the focus of the fore-optic telescope, is a field stop and limits the instrument field-of-view to 0.036 mrad by 2.1°. The optical system has an effective focal length (EFL) of 142.8 cm and covers the spectral range of 0.4 to 2.5 μm.
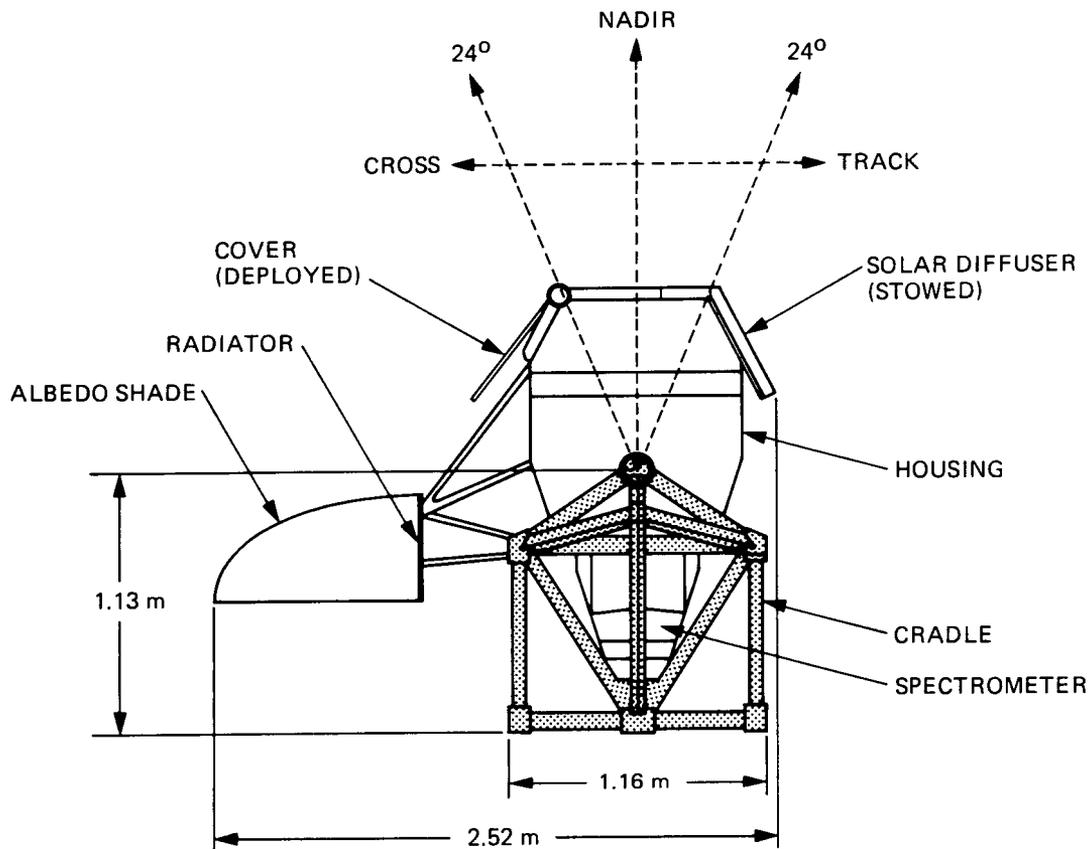
Figure 34. Conceptual layout of HIRIS, phase–A baseline.

Table 9. Eos Orbit Parameters

Nominal altitude	824 km
Altitude range	824 to 845 km
Inclination	98.7°
Ascending node crossing	1:30 p.m. LMT
Orbital period	101.38 min
Revolutions per day	14.2
Successive orbit ground-track spacing	2,824.7 km
Track sequence	1, 6, 11, 16, 5, 10, 15, 4, 9, 14, 3, 8, 13, 2, 7, 12
Adjacent track separation at Equator	176.5 km
Ground-track speed at Equator	6.67 km/sec
Ground-track direction at Equator	12.6°W of North
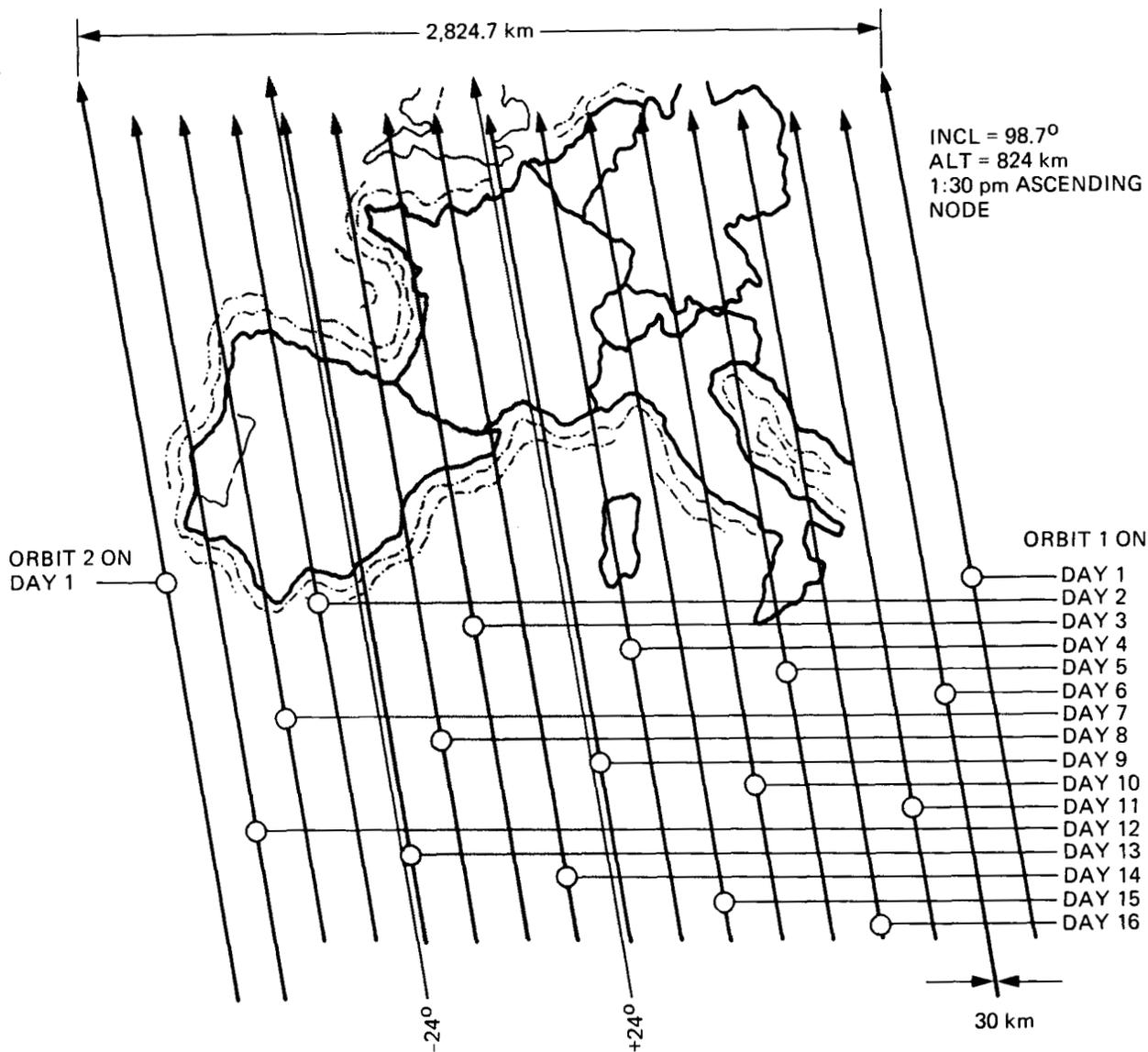
Figure 35. HIRIS orbital coverage pattern. Shaded area represents possible coverage on a given orbit.

Table 10. Optical System Parameters

IFOV	0.036 mrad
Aperture	37.6 cm
Focal ratio	f/3.8
Instrument EFL	142.8 cm
Fore–optics EFL	157.7 cm
Spectrometer	
Collimator EFL	43.0 cm
Camera EFL	40.0 cm
Magnification	0.931
Field–of–view	2.1°

The radiation passing through the slit from the fore–optic is collimated, separated into two bands, dispersed and reimaged onto separate Si and HgCdTe detector arrays by the optics in the spectrometer portion of the instrument. The dichroic beam splitter separates the radiation into the two bands at a wavelength of 1.0 μm. This approach has two major advantages. First, the VNIR and SWIR detectors can be physically separate in the focal plane, while still providing contiguous spectral coverage. Second, the dispersing prisms can be optimized for each wavelength interval, providing more uniform dispersion than provided by a single prism. A single–element prism in the SWIR band and a three–element prism in the VNIR band are used to disperse the radiation and to provide the nominal 10 nm sampling interval. The curved focal surface of the optical system is flattened by the convex reflecting field flattener immediately following the slit.

FORE-OPTICS
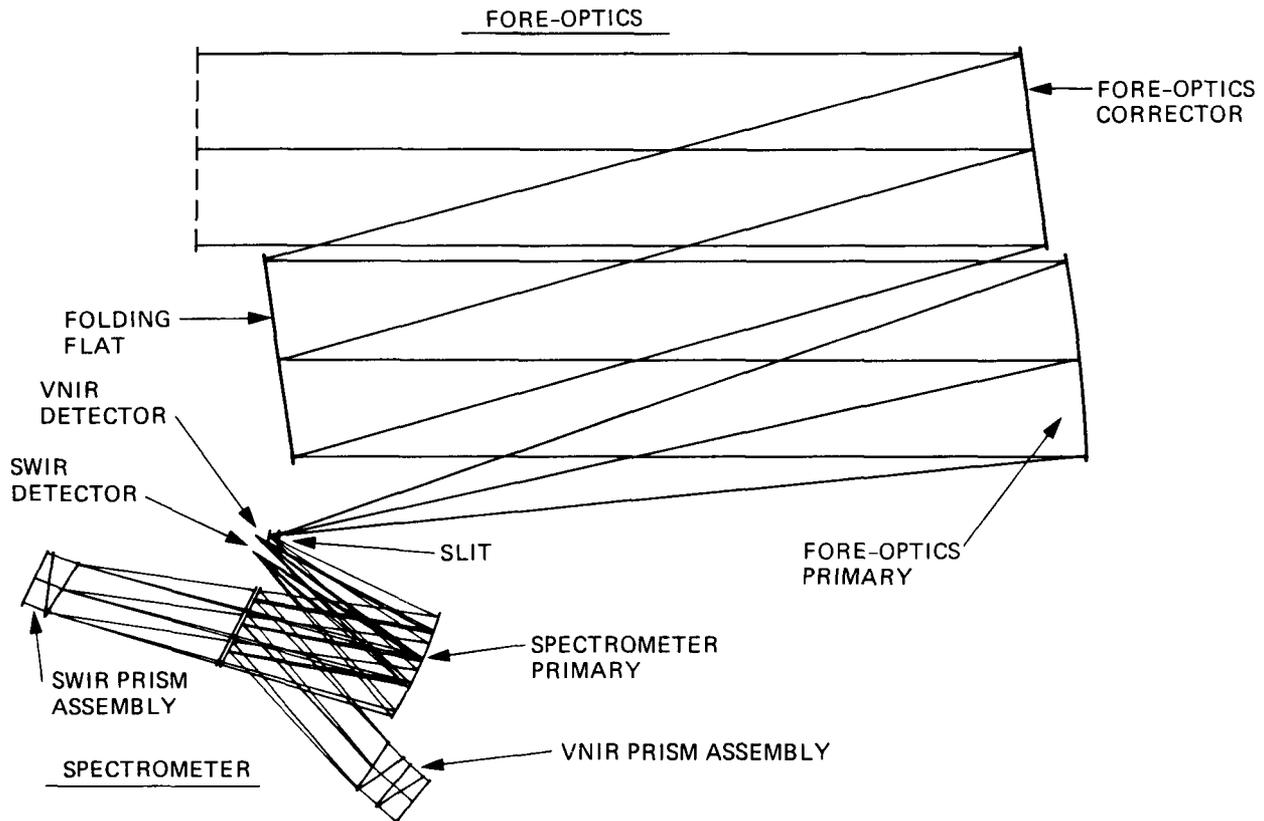
Figure 36. HIRIS optical layout.

Focal Plane

The focal plane assembly includes the spectrometer entrance slit, field flattener, and the VNIR and SWIR detectors. These components are all operated at 130 K and are mounted in the focal plane housing using a suspension band system that provides structural support and thermal isolation.

VNIR Detector

The VNIR detector is a back-side illuminated, buried-channel frame transfer CCD on epitaxial silicon thinned to achieve the required modulation transfer function (MTF) response at $\lambda = 1.0$ μm. Quantitative design and performance parameters of the VNIR CCD are listed in Table 11.

In operation, the image from a line on the ground is spectrally distributed over the 64 rows of the image area by the spectrometer. At the end of one line-integration period, the photon-generated charge on each line is rapidly shifted vertically into a storage area that is covered by aluminization to prevent exposure. Each line in the storage area is subsequently parallel shifted up into registers that are serially shifted out and read through on-chip amplifiers. Since readout is limited to between 3 and 4 Mpixels/sec, due to amplifier bandwidth, approximately four serial registers are used to read out simultaneously to the external circuitry.

SWIR Detector

The SWIR focal plane consists of a set of element hybrid detector arrays that are mosaicked to provide a $128 \times 1,000$ element format. The butting gap between arrays will be a maximum of 10 pixels. Each pixel is 52 μm square. Each hybrid consists of a 2.5 μm cutoff photovoltaic HgCdTe detector array, which is mated, via indium columns, to a multiplexer. The SWIR focal plane will cover the 1.0 to 2.5 μm spectral region with a nominal 10 nm spectral sampling interval. In operation, photon-generated charge is accumulated on the HgCdTe diodes. At the end of the integration time, the accumulated charge is switched to the multiplexed common video line for readout. Table 12 summarizes the physical and operational SWIR focal plane parameters.

Thermal Control

There are three temperature zones on the HIRIS instrument. These are: (1) the electronics, which require a temperature range of -20°C to 40°C; (2) the spectrometer optics, which require a temperature of 270 K; and (3) the focal plane, which requires a temperature of 130 K or less.

The electronics are controlled by standard temperature control techniques; namely radiator plates, multilayer insulation, and louvers.

Table 11. VNIR Detector Parameters

Image format	
Spatial	1,000 pixels
Spectral	128 rows (64 in imaging section, and 64 in storage section)
Pixel size	$52 \times 52 \ \mu m$
Full well capacity (FWC)	
Parallel	2.5×10^6 electrons
Serial register	5×10^6 electrons
Quantum efficiency	>40%, 400–800 nm; >20%, 800–900 nm; >10%, 900–1,000 nm
Readout noise	<300 electrons rms
Linearity	<1% departure from linearity up to 90% of FWC
Resolution	MTF response >42% at the Nyquist frequency
Dark current	Negligible
Vertical transfer rate	>1 Mpixels/sec

Note: Detector parameters are expressed in terms of electrons of signal (or noise). The quantum efficiency is the ratio of the number of electrons of signal to the number of input photons to the detector.

Table 12. SWIR Focal Plane Parameters

Mosaic array size	$128 \times 1,000$
Butting gap	10 pixels maximum
Pixel size	$52 \times 52 \ \mu m$
Detector material	Photovoltaic HgCdTe
Multiplex–type	FET–switch
Wavelength range	$1.0–2.5 \ \mu m$
Detector temperature	130 K
Full well capacity	2.5×10^6 electrons
Dark current	1.2×10^6 electrons/sec
Read noise	<1,000 electrons rms

The spectrometer optics are thermally isolated from the other parts of HIRIS to minimize the temperature gradients and to facilitate the temperature control to 270 K. The thermal isolation of the spectrometer optics consists of enclosing it, to the greatest extent possible, with a blanket of insulation and using mounting supports with minimum thermal conductance.

Cooling of the detectors is accomplished by the use of a radiative cooler, with a surface area of about 1 m².

Electronics

The electronics module will contain the power supplies, detector signal chain, digital processor, command processor, and mechanism drivers. The power supplies will receive the primary spacecraft power and convert it to the required power for the various functions in the electronics, and the detector signal chain will amplify the detector signals and convert them to their digital equivalent. The digital processor will process this digitized detector signal and perform the necessary editing, averaging, and formatting of the science data. It will also process the instrument engineering data to be incorporated into the data stream, and it will control the input to the mechanism drivers from the input received from the command processor, which receives the commands from the spacecraft and decodes them and directs them to the digital processor for the correct response by the instrument. The mechanism drivers will con-

trol the cross-track and along-track motions as well as the cover mechanisms. All electronics will be contained in a single module and can be serviced on-orbit.

Pointing and Image Motion Compensation

The pointing parameters are listed in Table 13. Down-track pointing is required for several reasons: avoidance of sun glint in measurements over water, observations through varying atmospheric path lengths, studies of surface BRDF, and IMC.

Cross-track pointing is required for studies of surface BRDF, but perhaps more importantly it allows multiple views of an area during an orbit revisit cycle. The current baseline, $\pm 24°$ cross-track pointing capability, limited by the passive cooling radiator, will allow a site to be viewed four times at the Equator and five times at 40° latitude within the 16-day orbit repeat period. Figure 37 shows coverage possibilities and down- and cross-track pixel sizes as they relate to pointing angle.

Table 13. Pointing Parameters

	Down-track	Cross-track
Total range	+60°/-30°	+24°/-24°
Resolution	0.070°	0.070°
Stability (jitter)	0.74 arcsec (0.1 pixel)	0.74 arcsec (0.1 pixel)
Slew rate (max)	5°/sec	2°/sec
Settling time (after slew)	0.5 sec	0.5 sec

IMC is implemented using the down-track pointing mirror. The IMC is used in four specific gain states: 1 (off), 2, 4, and 8. In each mode the line time (integration time) is multiplied by the gain, and the down-track mirror is moved at a rate that maintains the 30 m down-track sampling interval.
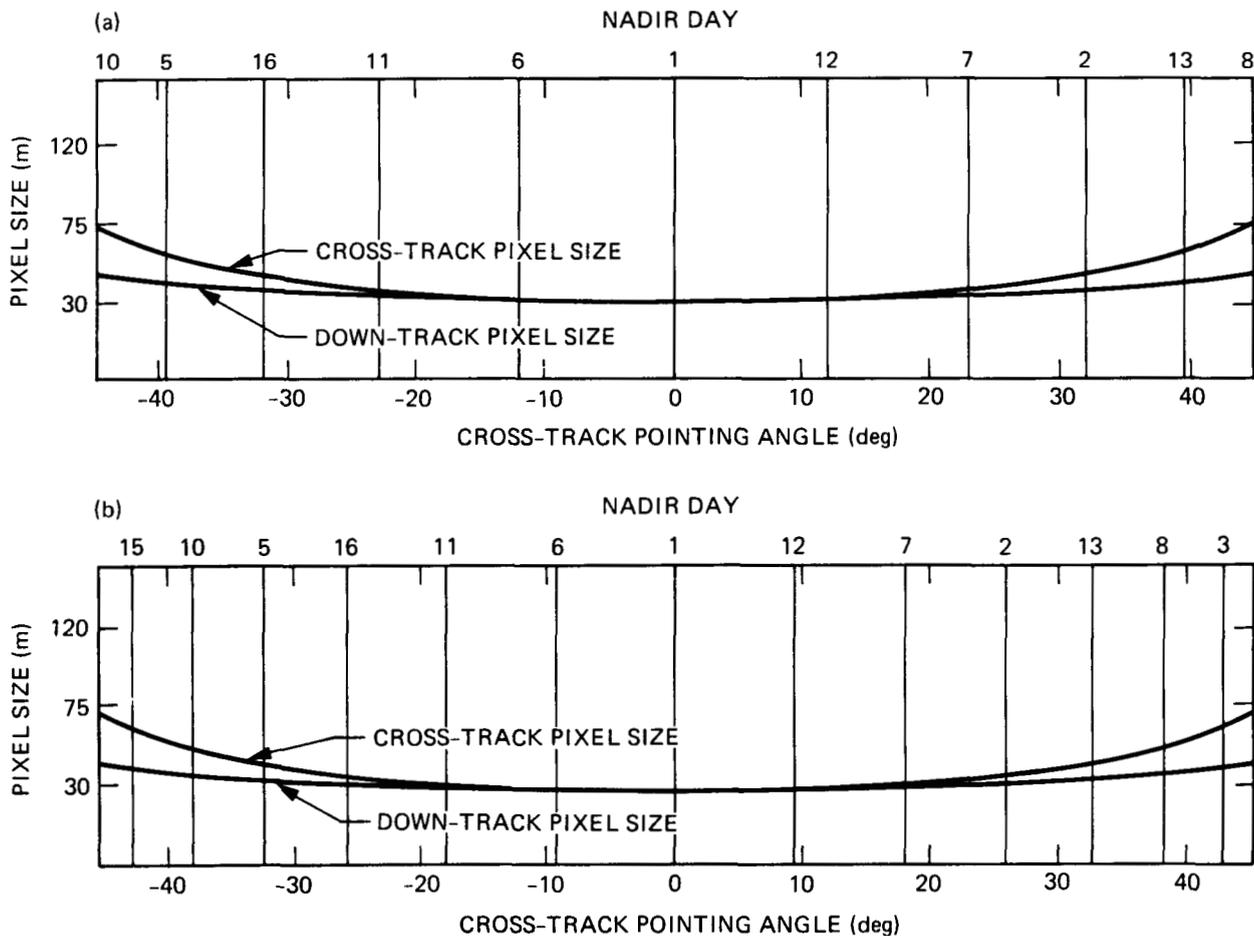

Figure 37. HIRIS observation geometry for (a) Equator and (b) 40° latitude. Plotted are cross-track pixel size versus cross-track angle, down-track pixel size versus cross-track angle, and nadir tracks for orbits within cross-track angles of 45°.

Table 14 lists some of the imaging parameters when using IMC.

Onboard Calibration

Two forms of onboard calibration are provided: spectral and radiometric.

Onboard spectral calibration is accomplished by diffusely reflecting narrow-band light from the back side of the spectrometer entrance slit. At the focal plane, this will result in a bright field with a single dark row of pixels that represents the spectral position of the slit. In addition, a pattern of reflecting spots on the back of the slit will be used to create a bright pattern of spots on the focal plane, which will define the spectral slit position. This calibration method will also provide spatial registration monitoring of the VNIR and SWIR focal planes.

Onboard radiometric calibration is provided by the use of a diffuse reflector, which can be positioned to reflect sunlight into the instrument aperture. A radiometer will be used to monitor the reflecting properties of this target over time.

PERFORMANCE ANALYSIS

The HIRIS system performance has been modeled based on the system parameters defined earlier, and the following additional assumptions: (1) aluminum mirror surfaces, (2) 5° instrument look angle, (3) 25° sun zenith angle, and (4) standard atmosphere with 23 km visual range.

Baseline S/N calculated for albedos 1.0, 0.1, and 0.01 show that the VNIR baseline performance progresses from shot-noise limited performance at high albedos to read-noise limited performance at mid to low albedos. The SWIR channels are read-noise limited. The relatively low S/N for 0.1 and 0.01 albedos can be improved through the use of IMC, which increases the pixel integration time by a factor of two, four, or eight. Table 15 gives the factor by which S/N increases as a function of IMC for 0.1 and 0.01 albedos.

MODES OF OPERATION

The instrument has four basic operational modes, which are listed below with descriptions and subcategories.

1. Service
   Cover closed, purge gas on

2. Standby
   Aperture covered

3. Data Acquisition
   Nadir/off-nadir pointing
   Image motion compensated

4. Calibration
   Solar diffuser
   Spectral line source
   Lunar
   Ground targets

For the "Service" mode the instrument will have all power off and mechanisms stowed essentially as for launch. The optics cover will be closed to prevent contamination by propulsion and life support effluents. In the "Standby" mode, power will be on to critical electronics and replacement heaters, as necessary, to enable rapid initiation of data acquisition or calibration. A submode may be necessary with the optics cover closed, particularly during the nightside part of the orbit.

In the "Data Acquisition" modes the instrument may be used to scan a swath at either the spacecraft ground-track speed of 6.67 km/sec or at reduced effective ground speeds of 1/2, 1/4, or 1/8 of the spacecraft track speed, generated by the IMC scan of the down-track mirror. The center of the spatial swath line may be placed anywhere within the instrument pointing range, which is given in Table 13.

The pixel integration time corresponding to the 6.67 km/sec spacecraft track speed and 30 m pixel is 4.5 msec. For a 1,000 pixel swath width and 192 spectral bands digitized to 12 bits, the corresponding data rate is approximately 512 Mbits/sec. In the following discussion it is assumed that telemetry overhead and

Table 14. IMC Imaging Parameters

	Gain			
	1	2	4	8
Cross-track smear (pixels)	0.07	0.14	0.28	0.56
Maximum pixel size (m)	30.0	30.0	30.1	30.6
Coverage duty cycle	1.0	0.43	0.23	0.12

Table 15. S/N Increase Versus IMC

IMC Gain	S/N Increase[1]			
	Albedo = 0.1		Albedo = 0.01	
	VNIR	SWIR	VNIR	SWIR
1	1.00	1.00	1.00	1.00
2	1.79	1.93	1.92	1.97
4	3.02	3.61	3.55	3.84
8	4.82	6.44	6.25	7.29

[1]The ratio of S/N with IMC to S/N without IMC.

possibly error correction encoding will result in a bandwidth reduction of approximately 20 percent. The full 300 Mbits/sec capacity of the Eos Data and Information System (EosDIS) is also assumed, yielding 240 Mbits/sec for HIRIS data. The baseline design does not include data compression, thus a reduction in the HIRIS output data rate will be necessary at all times when IMC is not in use.

A number of data editing methods, to be effected by ground command, are under consideration to achieve the necessary reduction in data volume. Some possible data modes are described below.

- Spectral Selection—This is expected to be one of the most used editing functions. Deletion of approximately 50 percent of the spectral channels will allow a full-width swath to be acquired.

- Selectable Encoding—By choosing 8-bit or 10-bit rather than the full 12-bit digitizing, it will be possible to select wider spectral or spatial coverage. Logarithmic encoding or some form of truncation may also be implemented.

- Spatial Editing—This form of editing includes two subcategories, adjustable swath width and deletion of samples. The former case refers to simply deleting samples from some contiguous spatial range of pixels, for example, the outermost pixels, to yield a narrower than normal swath. In the latter case, pixels may be deleted in a two-dimensional pattern.

- Pixel Averaging—Pixels may be averaged along either the cross-track or down-track axis. The mechanization of pixel averaging depends upon both the selected axis (cross- or down-track) and the detector chip architecture. For example, the CCD VNIR detector allows noise-free, on-chip summing, whereas the architecture of the short-wave infrared detector requires that it be done off-chip. For down-track averaging the longer integration times that are used in conjunction with IMC may be used, but with no mirror motion to maintain the 30 m IFOV. In this mode, the down-track pixel length will increase in accord with the selected integration time.

Special calibration will be required for each of these modes.

VI. SYNERGISM WITH OTHER Eos INSTRUMENTS

HIRIS will provide detailed spectral resolution from 0.4 to 2.5 μm at a spatial resolution equal to that of the Landsat TM, down- and cross-track pointing capability to examine the surface BRDF, opportunistic coverage of specific areas, and increased probability of obtaining cloud-free images during a 16-day revisit cycle. It will have excellent absolute calibration, and a dynamic range and sensitivity suitable for both bright and dark targets. The amount of information HIRIS would provide about a specific area on the Earth's surface is unmatched by any other instrument.

However, the extraordinary rate at which HIRIS will produce data precludes its use as an instrument for repetitive mapping of large areas. Moreover, its spectral coverage is not complete, as some features of interest in Earth System Science have distinctive electromagnetic properties in the thermal infrared or microwave portions of the spectrum. HIRIS is therefore a research instrument to be used for interpretation and analysis of smaller areas and for detailed subsampling within scenes produced by instruments with lower spatial or spectral resolution or different spectral coverage. In Eos the important synergistic data will be provided by MODIS, HMMR, SAR, GLRS, and LASA.

MODIS is divided into two packages, MODIS-N (nadir) and MODIS-T (tilt). MODIS-N will provide global coverage at 2-day intervals from the visible through thermal infrared wavelengths in 52 bands at 0.5 to 1.0 km resolution. MODIS-T will be capable of +60° rotation about the optical axis and will provide data in 64 bands from 0.4 to 1.0 μm at 1 km resolution. HMMR is a passive microwave instrument in three packages: AMSU (Advanced Microwave Sounding Unit), AMSR (Advanced Mechanically Scanned Radiometer), and ESTAR (Electronically Scanned Thinned Array Radiometer). AMSU will provide atmospheric sounding of temperature and water vapor. AMSR is a six-frequency microwave imager with bands at 6, 10, 18, 21, 37, and 90 GHz, each with dual polarization, which will have a variety of applications in hydrology, soils, vegetation, and oceanography. ESTAR is a 1.4 GHz imaging radiometer designed specifically to measure soil moisture. SAR will have three frequencies, 3, 6, and 12 GHz, with a spatial resolution of 30 m; it will provide radar images of land, ice, and ocean surfaces. LASA will provide atmospheric data helpful in applying atmospheric correction algorithms to HIRIS and MODIS data and surface altimetry profiles helpful for correcting for topographic effects.

While HIRIS will provide an unprecedented high spectral resolution data set for many science applications, it must be complemented with data from these other Eos instruments. In some cases, simultaneous data acquisition is strongly required;

this is particularly true for experiments dealing with dynamic phenomena that change on a short time scale, such as estimating vegetation canopy parameters, or studies of atmospheric conditions and characteristics. For other experiments, simulataneous data acquisition is not required; time constraints can be relaxed to days or weeks between acquisition of data sets from different instruments.

HIRIS and MODIS have similar spectral coverage but dissimilar spatial characteristics. HIRIS has finer spectral resolution and more spectral bands, and covers the SWIR region more completely, while MODIS-N has bands in the thermal infrared. The swath width of MODIS is 1,500 km, with repeat coverage every 2 days. Simultaneous imaging by HIRIS and MODIS will present a unique and important capability for terrestrial remote sensing by the Eos system and will provide an invaluable data set for a wide range of studies. The justification for simultaneous coverage from these two instruments lies primarily in our need to fully understand the scene radiance of the low-resolution data and thereby improve our interpretations. The spectral response from a 0.5 to 1.0 km pixel is produced by the weighted average reflectance from a diversity of surfaces. At this spatial resolution, very few places on the Earth's surface, if any, will have uniform ground characteristics. To date our calibration of low-resolution sensors has been hampered by the difficulty of locating sites of surface sampling on the image. Simultaneous high-resolution data would provide an important intermediate spatial and spectral link between ground measurements and the low-resolution data. The diurnal variations in atmospheric, surface, and illumination conditions are large enough to warrant truly simultaneous imaging from both instruments. HIRIS will reveal the inhomogeneity and structure within MODIS pixels.

In addition to contributing to our understanding of scene radiation characteristics, simultaneous 30 m and 0.5 to 1.0 km data will allow a multilevel sampling approach for a wide variety of applications, with detailed spatial information available in its regional context. Such multilevel sampling has been used in applications in forest and agricultural remote sensing, but the difficulties in coordinating, obtaining, and registering data from different platforms has proved difficult, hence we recommend that MODIS and HIRIS should fly on the same spacecraft.

In this synergistic relationship, HIRIS could be used to more closely investigate dynamic surface phenomena observed on MODIS images. Examples would include insect infestations, oceanic productivity, volcanic eruptions, and floods. With its cross-track pointing capability, HIRIS will have four opportunities in every 16-day orbit cycle to observe any location.

MODIS data will also benefit HIRIS users. MODIS provides data on the mesoscale variability surrounding the HIRIS scene and allows temporal interpolation between HIRIS images. The context of the HIRIS interpretation within the broader region and temporal period is therefore possible.

Instruments operating in the passive or active microwave do not depend on the sun for their illumination source, so the requirements for simultaneity with HIRIS observations are not severe. In spatial coverage HMMR is similar to MODIS, but the spectral coverage is completely different. Thus surface properties affect the electromagnetic signal in different ways, but the spatial relationships between HIRIS and HMMR are similar to those between HIRIS and MODIS. Data from HIRIS and HMMR would allow interpretations that would be difficult or impossible with either sensor alone. For example, studies of vegetation with HIRIS involving photosynthesis and net primary production would be enhanced by measurements of soil moisture from HMMR. Similarly, measurement of snow properties with both instruments would allow estimations of depth, density, grain size, and free liquid water content.

SAR has spatial characteristics similar to HIRIS but completely different electromagnetic characteristics. Combined analysis using VNIR and SWIR and radar wavelengths would, for example, help to determine biomass in vegetated areas and would help to identify areas of saturated soil and standing water. SAR would also make it possible to study the effects of topography on the HIRIS signal.

For each of the six scientific disciplines reported in previous sections, a summary of the benefits, requirements, and constraints of synergism with other Eos instruments is presented in the following sections.

GEOLOGY

Most geologic mapping problems involve studies of areas much larger than a single or even several HIRIS swaths. Tectonic problems related to continental evolution, such as the evolution of the Tibetan Plateau, require mapping of millions of square kilometers. HIRIS data will be used in a "profiling" sense for determination of lithologic composition. To extend these results areally will require integration with other types of imagery such as TM, SPOT, or SAR, and extrapolation of geologic contacts from the coregistered HIRIS data to these other data sets. Integration of topographic information and orbitally acquired geophysical measurements provides critical complementary data. Simultaneity is not required, because topography and gravity/magnetic fields change very slowly (times scales of years).

Studies involved with active tectonism, such as mapping of fault offsets and determination of rate of displacement, require the synergistic use of SAR and

Geodynamics Laser Ranging System (GLRS) data. Due to SAR's sensitivity to small-scale topographic relief and its variable incidence angle (illumination) capability, SAR data can provide local as well as regional structural information. Simultaneous data acquisition is not required; time offsets of weeks to months should be adequate to provide the necessary data (Table 16). More dynamic phenomena, such as volcanic eruptions, place a stronger requirement on simultaneous data acquisition. The time scale of these events is on the order of hours to weeks; in order to properly study and monitor eruptions, near-simultaneous data acquisition is mandatory. Synergistic experiments with HIRIS, SAR, and LASA provide the necessary data for analysis of flow dynamics, morphology, and time history. The cross-track pointing capabilities of the instruments are necessary to provide temporal coverage beyond the 16-day nadir repeat coverage.

OCEANS AND INLAND WATERS

Synergism with other Eos instruments is mandatory for oceanographic studies. AVHRR presently provides information relating to global cloud cover and SST. HIRIS is particularly important in quantifying the role of AVHRR subpixel scale cloudiness on SST, in improving AVHRR visible calibration, and in gaining a better understanding of aerosol selectivity in the near infrared. Although HIRIS data are limited in spatial extent, the use of the two together should permit extrapolation of the results to the global AVHRR data set. Simultaneous acquisition of HIRIS and MODIS data should provide some unique advantages for both systems. The large areal coverage of MODIS will provide a means of establishing the atmospheric aerosol type over clear water. At the same time, the high spatial resolution HIRIS data will be effective for selected ocean scenes in establishing the size scales for subpixel (MODIS) patches of chlorophyll and clouds. The high spectral resolution of HIRIS data will provide estimates of fluorescence efficiency for key phytoplankton populations, which can be extended areally using MODIS data.

Wetlands are an ecologically important habitat throughout the world, characterized by mixtures of open water and vegetation. Two features of wetlands require the combined use of HIRIS and SAR data: the extent of flooding is a major environmental factor, and SAR can penetrate vegetation and recognize flooded areas; cloud cover is often a limitation, and SAR data obviates this problem. On the other hand, HIRIS provides superior discrimination of vegetation types and physiological status.

Simultaneity constraints for synergistic observations are different depending on the particular application. A summary of these parameters is shown in Table 17.

Table 16. Simultaneous Data Acquisition for Geology

	Crustal Structure and Tectonics	Lithologic Mapping/Soils	Volcanic Events
Eos instruments	SAR, LASA, GLRS	SAR, MODIS	SAR
Simultaneity requirements	Weeks to years	Days to weeks	Hours

Table 17. Simultaneity Requirements for Oceanography and Inland Waters

Application	Time Scale	Synergistic Instruments	Required Simultaneity
Wetlands mapping	Days	SAR	1 Day
Surface state	Hours	SCAT, SAR	2 Hours
Phytoplankton	Hours	MODIS, AVHRR	Hours
Currents	Days	SAR, MODIS, SCAT	2 Days

SOILS

Soils studies, from a methodological viewpoint, are similar to lithologic mapping in geology. The major benefits to be derived from synergism with MODIS, SAR, and HMMR relate to the study of dynamic short-term changes that occur in soils. These changes include soil moisture conditions, tillage operations and cultural impacts on land use, climatic events (wind and flood erosion, for example), and assessment of rates of soil degradation. Simultaneous data acquisition is required for most of these applications, as the phenomena have very short time-scales.

VEGETATION

The potential exists for significant synergism with SAR data to determine either the mass or the height of vegetation. Total net productivity in forested areas is often not a direct function of canopy parameters because of variability in the respiring biomass present. In addition, HIRIS and SAR instruments have distinctly different penetration capacities in a nonhomogeneous medium like a vegetation canopy; the reflected energy measured by HIRIS comes from a higher level of the canopy than the backscattered energy measured by SAR. Besides these general observations, and a few studies to evaluate the combined use of optical and radar data for crop identification, there are no definitive studies to establish the quantitative improvement from synergistic use of

these instruments for vegetation monitoring. The use of Eos data will provide the needed data to develop models and algorithms for estimating canopy parameters and determining the simultaneity requirements.

The synergistic use of MODIS is twofold. MODIS will provide the areal coverage (in selected spectral bands) with which to extend the mapping capabilities of HIRIS data. MODIS and HIRIS used together will also allow investigation of the effects of grossly different spatial resolutions on differentiating vegetation types, and the effects of mixed-pixels on spectral signatures at different scales. MODIS has more frequent coverage and thus is better at detecting temporal variation.

ATMOSPHERES

Although the main objective for HIRIS is to provide surface observations, some information about atmospheric parameters can also be obtained from HIRIS data. However, to perform atmospheric corrections on HIRIS surface scenes, additional data about the relevant atmospheric parameters above such scenes are required. Due to the temporal and spatial variability of atmospheric constituents (mainly aerosols and water droplets) such auxiliary data must be acquired truly simultaneously, i.e., at the same time of the HIRIS acquisition viewing the same surface area in the same direction. Such stringent simultaneity requirements are best met by other Eos instruments (on the same platform) that are dedicated to atmospheric observations, such as LASA.

59

Since, for the acquisition of atmospheric parameters, a 1-km spatial resolution is sufficient, simultaneously acquired MODIS data should also be used for atmospheric corrections of HIRIS data.

SNOW AND ICE

HIRIS provides the high-resolution data for detailed measurements of surface snow characteristics. However, monitoring the spatial and temporal variation in surface reflectance requires an instrument with more frequent observations. Synergism with MODIS at larger spatial scales two or three times per week would enable an investigation to track the energy balance of the snow packs through time. This would allow accurate estimation of the spatial distribution of snowmelt and improved determination of runoff as it effects the hydrological cycle. The presence of HIRIS and MODIS on the same platform makes simultaneous data acquisition fairly simple, within the constraints of the Eos platform data handling capacity.

The synergistic use of these two instruments, together with the cloud-penetrating capability of SAR, has a major impact on the improvement in mapping and monitoring sea ice. Particular areas of study that will benefit include determination of pack ice edge, temporal variation of ice concentration, floe size distribution, ice motion, determination of variations in ice composition, and ice thickness.

HMMR/AMSR and SAR data provide information complementary to HIRIS due to the difference in penetration depth. Visible and infrared signals come from the top 20 to 50 cm of the snow pack, while microwave radiation penetrates the snow to a much greater depth. The combination of the three data sets will allow improved determination of grain size and snow water equivalence. Estimation of the latter property over an entire drainage basin has not as yet been effectively accomplished using present instruments. The combination of Eos instruments promises a major improvement in the ability to perform such studies and contribute to our understanding of runoff input to hydrology.

VII. DATA HANDLING AND PROCESSING

INTRODUCTION

The HIRIS mission will acquire data for research into the application of spaceborne imaging spectrometers. The measurements made by this instrument are sampled spectra of the radiance entering the instrument from each pixel in the image. Because the primary application for the data is to investigate the ability of imaging spectrometer data to uniquely characterize the Earth's surface material, it is important that the accuracy of the data not be contaminated by the transmission process. Therefore, this chapter makes the basic assumption that any data transmission scheme used for HIRIS must preserve the full accuracy of the data that are sent.

HIRIS ONBOARD PROCESSING

HIRIS is projected to produce data at a rate of 512 Mbits/sec, and have access to a downlink and/or onboard recorders with a capacity of 300 Mbits/sec.

Three general classes of onboard data processing are contemplated: (1) amplitude compression, (2) data editing, and (3) source coding for bandwidth compression. With HIRIS it will probably be necessary to employ some combination of these techniques in order to be able to transmit the required amount of data. Because of the requirement to preserve the accuracy of all data transmitted, only those coding schemes that completely preserve information will be considered. In addition, the editing and amplitude compression functions will be programmable so that a variety of different editing/amplitude compression schemes can be employed. This will allow the experimenters to choose those combinations of editing and amplitude compression schemes that best suit their particular needs.

Amplitude Compression

The basic instrument employs a 12-bit quantizer. Therefore, the data entering the amplitude compression step consists of 12-bit samples of all the spectral bands for each pixel on the scan line. The basic function of the amplitude compressor is to transform each 12-bit number into an 8-bit number according to a predetermined transfer function. Because of the need for some applications to transmit 12-bit data, a full 12-bit linear mode (i.e., no compression) must be provided. In this case it will be necessary to perform more severe editing of the data in order to maintain the output data rate at an acceptable level, thereby trading off spectral information and/or spatial coverage for increased amplitude resolution and dynamic range.

Because it is envisioned that the amplitude compression step will be implemented using lookup table techniques, any nonlinear transformation from 12 to 8 bits is theoretically possible, however, only five selectable modes are contemplated: (1) 12-bit linear mode (no compression), (2) 10-bit logarithmic compression, (3) 10-bit linear (10 selected contiguous bits), (4) 8-bit logarithmic compression, and (5) 8-bit linear (8 selected contiguous bits).

Data Editing

Three classes of data editing will be considered: (1) band elimination, (2) swath selection, and (3) band combination. This capability will be programmable so that the spectral configuration of the instrument can be changed rapidly and programmed for each site acquisition to give each investigator a data set that is maximally useful within the limitations of the system.

Band elimination involves the deletion of selected spectral bands from the data stream. Swath selection allows selection of an arbitrary subswath instead of transmitting data from the full 30-km swath width covered by the HIRIS instrument. These two techniques, used in combination, will allow the user to trade-off the amount of spectral information received with the swath width. Thus, if a complete spectrum is required, the swath width will have to be reduced. The instrument pointing must be precise to acquire data from the specified area on the ground. On the other hand, if a wider area is to be covered it will be necessary to select a smaller number of spectral bands. This trade-off between swath width and the number of available spectral bands fits with a typical investigative scenario, where detailed initial studies involving essentially full spectra are done on well-defined, relatively small test sites. After analyzing the results of such work, full-swath data sets can be acquired with a restricted set of spectral bands. Figure 38 shows typical examples of the trade-offs between swath width and spectral coverage that can be achieved for available downlink bandwidths of 25 Mbits/sec, 100 Mbits/sec, and 300 Mbits/sec.

As an illustration of band combination, consider the following example. For geological applications, the spectral regions with the greatest requirement for high spectral resolution are 2.15 to 2.33 μm to capture the overtone vibrational absorption feature for Al-OH, Mg-OH, and CO_3, and 0.67 to 0.77 μm to capture subtle changes on the "red edge" of the vegetation spectrum. In addition, moderate resolution is desirable in the 0.87 to 0.96 μm region to capture the Fe^{3+} absorption features, and the 0.40 to 0.67 μm region to pin down the chlorophyll features in plant spectra. Assuming an instrument with a basic sampling interval of 10 nm covering a spectral range from 0.4 to 2.5 μm (approximately 200 channels), the configuration of spectral channels output

12 BIT DATA, IMC GAIN = 1

8 BIT DATA, IMC GAIN = 1

12 BIT DATA, IMC GAIN = 2

8 BIT DATA, IMC GAIN = 2
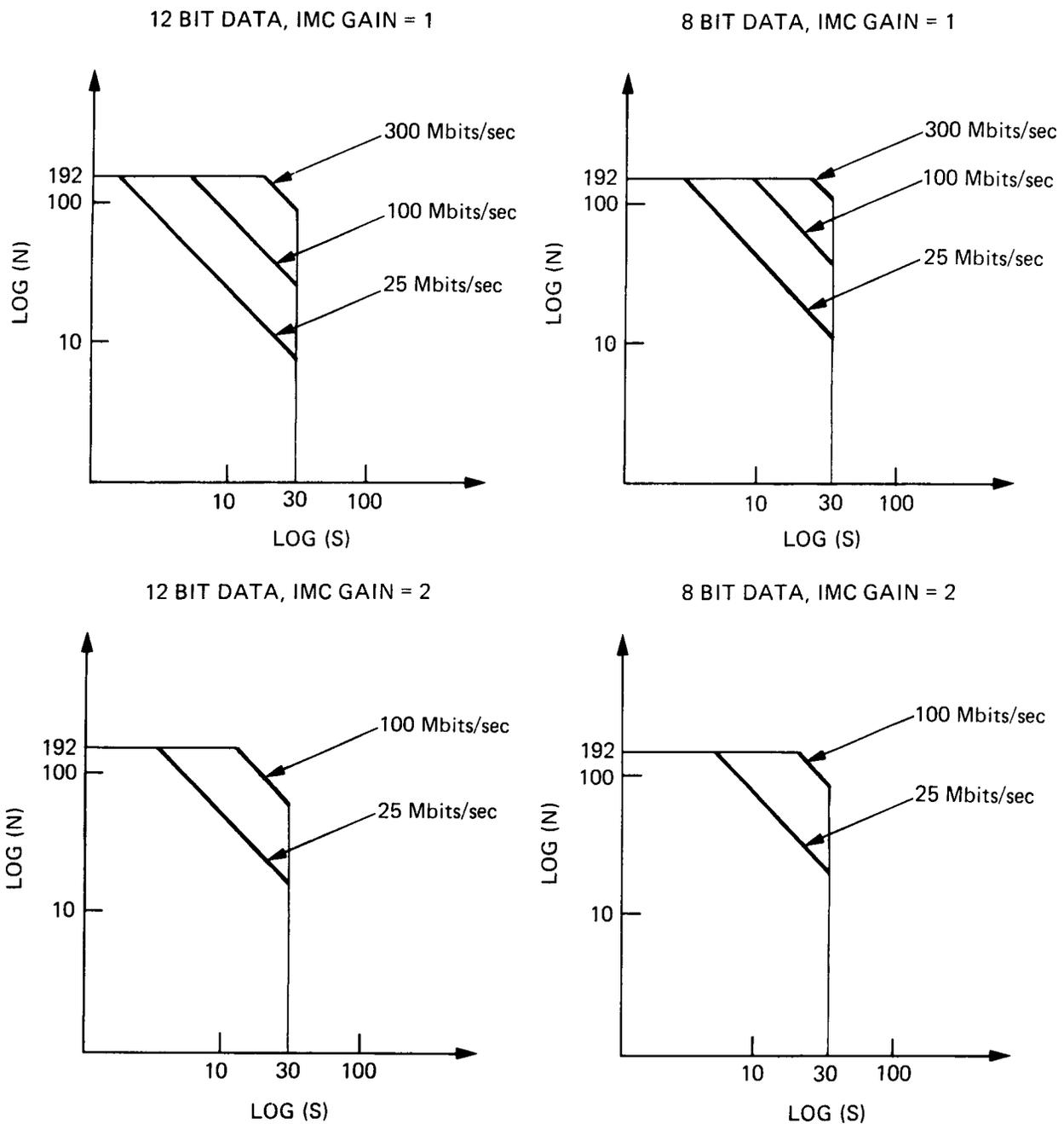
Figure 38. The trade-offs between swath width (S) and the number of spectral channels (N) that can be achieved for available downlink bandwidths of 25 Mbits/sec, 100 Mbits/sec, and 300 Mbits/sec.

from the Band Configuration Module shown in Table 18 would serve most geological needs.

In order to successfully combine bands in this way, it is necessary to equalize the output of all the sensing elements so that equal radiance falling on each element produces an equal output from the system. Digital pre-equalization of the VNIR focal plane sensor is expected to be straightforward. However, the characterization of the SWIR focal plane sensor is not understood sufficiently well at this time to be sure of being able to implement a simple and

straightforward pre-equalization scheme onboard the spacecraft. In addition, currently, there is also some doubt as to the stability of the calibration of the SWIR focal plane. For these reasons, it will be necessary to do considerably more research into the characteristics of the focal plane sensors and their stability before a design involving onboard band combination can be committed to for the SWIR spectral region. In addition, the performance of a band combination scheme depends on the accuracy of the calibration system that is ultimately employed.

62

Table 18. Band Configuration Example

Spectral Range (μm)	Number of Bands	Width/Band (nm)
0.40–0.67	9	30
0.67–0.77	10	10
0.77–0.87	2	50
0.87–0.96	3	30
0.96–1.24	4	70
1.50–1.75	5	50
2.00–2.15	5	30
2.15–2.33	18	10
2.33–2.50	2	40
Total	58	

In the above example, the regions 1.24–1.50 μm and 1.75–2.00 μm have been eliminated entirely since they contain large water vapor absorption features.

Source Coding for Bandwidth Compression

As mentioned above, compression schemes used in this system must be of the data-preserving type. It may or may not be possible to devise such a scheme to transmit the whole data set, depending on the statistical properties of the spectrometer output signal. If the spectrometer data can be coded in such a way that information is preserved and the average information rate is less than the bit-rate capabilities of the transmission channel, then the basic system will transmit the data with no loss of information. Buffer overflow would occur with very low probability, and when it did, the system would simply shorten the scan line resulting in a small loss of data, but preserving the fidelity of the data that are transmitted. Since the most important statistical property of the data source is that it have low entropy, it will be necessary to pre-equalize the sensor data prior to compression in order to avoid the introduction of entropy into the data from the sensor itself. As with the band combination method, it will be necessary to establish that the focal plane sensors can be pre-equalized with sufficient accuracy and have sufficient long-term stability before coding schemes such as those suggested here can be implemented.

The success of source coding schemes for compressing the data as proposed hinges entirely on the question of whether the entropy of imaging spectrometer data is sufficiently low to permit the degree of compression that is required. At this point in time, very little is known about the statistical properties of imaging spectrometer data. For this reason it is essential that experiments be carried out using both AIS and AVIRIS to answer this question using real data. In addition, work should also begin to develop coding techniques that take advantage of the statistical properties of imaging spectrometer data and that have the desired information-preserving proper-

ties to determine the operational feasibility of coding for data compression at an early date.

HIRIS GROUND DATA PROCESSING

Archival Processing

Archival processing of HIRIS data consists of decommutating the telemetry data stream and separating it into engineering, calibration, platform, and image data. The reformatted data stream is then written directly to the archival medium. Provisions should also be made for automatically entering image data information into a data base for use in the retrieval operation. Although the current standard archive medium for image data is magnetic tape, the total volume of HIRIS data to be archived strongly suggests the necessity of using optical storage technology for this task. Investigators who desire to work with "raw" data should be able to obtain copies of the appropriate segments of archival data.

The volume of HIRIS data will require a disciplined approach to data handling. The design of the HIRIS downlink and telemetry formats should be such that the required ancillary data from the spacecraft can be recorded directly on an archival medium as the image data are received. In addition, attitude and ephemeris data should be readily available and of sufficient accuracy to permit precise cartographic correction of the images to be carried out by routine processing from the archival medium. In other words, the archival medium should contain all of the information necessary to produce fully geocoded images with the addition of a minimum of ground control information.

Data Flow and User Interaction

Data Take Requests

It is expected that the investigators will be able to request data takes from their home institutions via an online user interface. The user will be prompted for all pertinent information that is needed to acquire the data take, including specification of the bands to be acquired and the precise swath to be covered.

Output Product Requests

The investigators will also be able to request output products via an online catalog by inputting the longitude and latitude of the desired site. A chart will then appear on the user's screen showing the date and time of each acquisition over his site as well as other information such as look angle, sun angle, percent cloud cover, IMC, swath width, encoding, spectral bands acquired, etc. Users will then be able to order the data set they need at the processing level they desire. Users will also be able to search the cata-

log to see if a certain site has been flown; if not they can then request a data take.

Data Products' Descriptions

The following data products will be available to HIRIS investigators from the HIRIS Ground Data Processing System. The normal product will be Level 1B data. The availability of higher-level products will be determined after potential demand is identified. Possibly, the HIRIS ground data processing system will distribute coded algorithms so that users can create higher-level products on their own computer systems.

Level 0—Basic telemetry stream and archive format, as received from HIRIS. These are normally not available as a data product.

Level 1A—HIRIS instrument data augmented with ancillary data necessary to compute geographic locations and translate data into radiometric units, i.e., radiometric and geometric calibration information, satellite ephemeris, attitude, time, and sensor information.

Level 1B—Level 1A HIRIS data in orbit-sequential format that have been converted to radiometric units, including equalization between detectors. Data are geometrically raw but are augmented with ancillary data necessary to compute geographic locations.

Level 2—Geophysical or environmental parameters in orbit-sequential format, derived from a Level 1A or 1B image. Desired products and algorithms await specification by community. Some processing could be computationally intensive, for example it could require atmospheric correction. Possible products are identification of specific minerals, surface reflectance corrected for atmospheric scattering and absorption, leaf area index, coastal ocean phytoplankton, terrestrial aerosols, snow cover, and bioluminescence.

Level 3A—Level 2 or Level 1B data mapped to geographic data base, using satellite ephemeris information only. Because resampling is involved, this is not reversible to Level 1B or Level 2.

Level 3B—Level 2 or Level 1B data mapped to geographic data base, using satellite ephemeris information and ground control points. Processing would take considerably longer than for Level 3A data. Because resampling is involved, this is not reversible to Level 1B or Level 2.

Level 4—Model output or results from analyses of lower-level data, not measured by HIRIS but derived from HIRIS data and ancillary data measured at ground surface, multiple HIRIS images, or data from other satellite instruments. Possible examples are surface radiation balance integrated over some time period, and near-surface atmospheric water vapor. The distinction between Levels 2 and 4 is that Level 2 (and 3) products are derived from a single multispectral image, without the necessity for additional data.

Since it is anticipated that some investigators will have time-critical requirements for field experiments that necessitate quick data turn-around, preliminary-look data products for two spectral bands (0.65 μm and 1.6 μm) must be provided in response to a specific request.

INFORMATION EXTRACTION

The complexity and volume of data that will be generated by HIRIS are far beyond any data sets used by the remote sensing community up to now. Although such an instrument can provide detailed, accurate information on the composition of the Earth's surface cover, current methods for information extraction do not take full advantage of the spectral resolution and radiometric information in the data. Techniques for recognition of known absorption features in spectra of geologic materials have been developed (Goetz et al., 1985), but these typically do not require use of absolute radiometric quantities, atmospheric correction, compensation for effects from terrain, etc. Other Earth surface covers, for example vegetation, water bodies, snow, and soils, have distinctive spectral features associated with changes in their physical properties, but these are not so well characterized. Computational techniques for modeling and recognizing these features await development, and will be required if the full potential of HIRIS is to be realized.

ISSUES AND RECOMMENDATIONS FOR DATA HANDLING

Data handling and processing is an important and often neglected part of any spaceborne remote sensing system. Previously we have outlined some of the approaches that, from a user viewpoint, seem both practical and essential. In summary, the salient points are:

- The bandwidth compression schemes designed for HIRIS must preserve the full accuracy of the data transmitted. Three general classes of such compression techniques include amplitude compression, data editing, and information-preserving source coding.

- To determine the operational feasibility of developing an information-preserving coding technique for HIRIS, it is essential that work be supported immediately to gather and analyze imaging spectrometer data using AIS and AVIRIS to determine their statistical characteristics.

- Research into the characterization of the focal plane sensors to be used in HIRIS is essential to the successful implementation of band combination and/or data compression techniques. This includes consideration of both the calibration and stability of these devices. Such research should be supported immediately.

- The HIRIS spacecraft and data retrieval system should be designed to allow for routine correction of the image data to a cartographic grid (geocoded product), in addition to providing "raw" and sensor-corrected data products.

REFERENCES

Abbott, M.R., and P.M. Zion, Satellite observations of phytoplankton variability during an upwelling event, *Cont. Shelf Res., 4,* 661, 1985.

Aber, J.D., and J.M. Melillo, Nitrogen immobilization in decaying hardwood leaf litter as a function of initial nitrogen and lignin content, *Can. J. Bot., 60,* 2263, 1982.

Abiodun, A.A., Satellite survey of particulate distribution patterns in Lake Kaingi, *Remote Sens. Environ., 5,* 109, 1976.

Abrams, M.J., R.P. Ashley, L.C. Rowan, A.F.H. Goetz, and A.B. Kahle, Mapping of hydrothermal alteration in the Cuprite Mining District, Nevada, using aircraft scanner imagery for the 0.46–2.36 μm spectral region, *Geology, 5,* 713, 1977.

Adams, J.B., M.O. Smith, and P.E. Johnson, Spectral mixture modeling: A new analysis of rock and soil types at Viking Lander 1 site, *J. Geophys. Res., 91,* 8098, 1986.

Agren, G.I., Nitrogen productivity of some conifers, *Can. J. For. Res., 13,* 494, 1983.

Almanza, E., and J.M. Melack, Chlorophyll differences in Mono Lake (California) observable on Landsat imagery, *Hydrobiologia, 122,* 13, 1985.

Ångstrom, A., The albedo of various surfaces of ground, *Geograf. Ann., 7,* 323, 1925.

Barnes, H.L., Solubilities of ore minerals, in *Geochemistry of Hydrothermal Ore Deposits,* 2nd edition, H.L. Barnes, ed., John Wiley and Sons, New York, NY, 1979.

Barry, R.G., The cryosphere and climate change, in *Detecting the Climatic Effects of Increasing Carbon Dioxide,* M.C. MacCracken and F.M. Luther, eds., U.S. Dept. of Energy, Washington, DC, 1985.

Baumgardner, M.F., and E.R. Stoner, Soil mineralogical studies by remote sensing, *Trans. 12th Intl. Congr. Soil Sci., 5,* 419, New Delhi, India, Feb. 8–16, 1982.

Baumgardner, M.F., E.R. Stoner, L.F. Silva, and L.L. Biehl, Reflectance properties of soils, in *Advances in Agronomy, 38,* 1, N. Brady, ed., Academic Press, New York, NY, 1985.

Bohren, C.F., Applicability of effective-medium theories to problems of scattering and absorption by nonhomogeneous atmospheric particles, *J. Atmos. Sci., 43,* 468, 1986.

Bohren, C.F., Multiple scattering of light and some of its observable consequences, *Am. J. Phys., 55,* 524, 1987.

Bohren, C.F., and B.R. Barkstrom, Theory of the optical properties of snow, *J. Geophys. Res., 79,* 4527, 1974.

Boland, D.H.P., Trophic classification using Landsat-1 (ERTS-1) multispectral scanner data, *USEPA 600/3-76-037,* 1976.

Boland, D.H.P., D.S. Schaeffer, D.F. Sefton, R.P. Clarke, and R.J. Blackwell, Trophic classification of selected Illinois water bodies, *EPA-600/3-79-123,* 1979.

Bormann, F.H., and G.E. Likens, *Pattern and Process in a Forested Ecosystem,* Springer-Verlag, New York, NY, 1979.

Bowers, S.A., and R.J. Hanks, Reflection of radiant energy from soils, *Soil Sci., 100,* 130, 1965.

Bowers, S.A., and S.J. Smith, Spectrophotometric determination of soil water content, *Soil Sci. Soc. Am. Proc., 36,* 978, 1972.

Brown, O.B., R.H. Evans, J.W. Brown, H.R. Gordon, R.C. Smith, and K.S. Baker, Phytoplankton blooming off the U.S. east coast: A satellite description, *Science, 299,* 163, 1985.

Bukata, R.P., G.P. Harris, and J.E. Bruton, The detection of suspended solids and chlorophyll *a* utilizing multispectral ERTS-1 data, *2nd Can. Symp. Remote Sens.,* 551, 1974.

Bunnik, N.J.J., Review of models and measurements of multispectral reflectance by plant canopies: Recommendations for future research, *Proc. Soc. Photo-Opt. Engrs., 475,* 2, 1984.

Bushnell, T.M., Use of aerial photography for Indiana land studies, *Photogram. Engrg., 17,* 725, 1951.

Carder, K.L., and R.G. Steward, A remote-sensing reflectance model of red-tide dinoflagellate off west Florida, *Limnol. Oceanogr., 30,* 286, 1985.

Carder, K.L., R.G. Steward, J.H. Paul, and G.A. Vargo, Relationships between chlorophyll and ocean color constituents as they affect remote-sensing reflectance models, *Limnol. Oceanogr., 31,* 403, 1986.

Carder, K.L., R.G. Steward, and P.R. Payne, Solid-state spectral transmissometer and radiometer, *Opt. Engrg., 24,* 863, 1985.

Chandrasekhar, S., *Radiative Transfer,* Dover, New York, NY, 1960.

Chang, S.H., and W. Collins, Confirmation of the airborne biogeophysical mineral exploration technique using laboratory methods, *Econ. Geol., 78,* 723, 1983.

Chin, H.Y., and W. Collins, A spectroradiometer for airborne remote sensing, *Photogram. Engrg. Remote Sens., 44,* 507, 1978.

Chýlek, P., V. Ramaswamy, and V. Srivastava, Albedo of soot-contaminated snow, *J. Geophys. Res., 88,* 10,837, 1983.

Cihlar, J., and R. Protz, Perception of tone differences from film transparencies, *Photogrammetria, 8,* 131, 1972.

Cipra, J.E., M.F. Baumgardner, E.R. Stoner, and R.B. MacDonald, Measuring radiance characteristics of soil with a field spectroradiometer, *Soil Sci. Soc. Am. Proc., 35,* 1014, 1971.

Cloutis, E.A., M.J. Gaffey, T.L. Jackowski, and K.L. Reed, Calibration of phase abundance, composition, and particle size distribution from olivine-orthopyroxene mixtures from reflectance data, *J. Geophys. Res., 91,* 11,641, 1986.

Coakley, J., Earth Science Systems Committee Working Group on Imaging and Tropospheric Sounding, *JPL Intern. Doc. D-2415,* 1985.

Colbeck, S.C., Grain clusters in wet snow, *J. Colloid Interface Sci., 72,* 371, 1979.

Colbeck, S.C., Classification of seasonal snow cover crystals, *Water Resour. Res., 22,* 59S, 1986.

Collins, W., S.H. Chang, G. Raines, F. Canney, and R. Ashley, Airborne biogeochemical mapping of hidden mineral deposits, *Econ. Geol., 78,* 737, 1983.

Condit, H.R., The spectral reflectance of American soils, *Photogram. Engrg., 36,* 955, 1970.

Condit, H.R., Application of characteristic vector analysis to the spectral energy distribution of daylight and the spectral reflectance of American soils, *Appl. Optics, 11,* 74, 1972.

Cooper, K., J.A. Smith, and D. Pitts, Reflectance of a vegetation canopy using the adding method, *Appl. Optics, 21,* 1982.

Deans, T., Economic mineralogy of African carbonatites, in *Carbonatites,* O.F. Tuttle and J. Gittins, eds., Interscience Publishers, New York, NY, 1966.

Denman, K.L., and A.E. Gargett, Time and space scales of vertical mixing and advection of phytoplankton in the upper ocean, *Limnol. Oceanogr., 28,* 801, 1983.

Denman, K.L., and T.M. Powell, Effects of physical processes on planktonic ecosystems in the coastal ocean, *Oceanogr. Mar. Biol. Ann. Rev., 22,* 125, 1984.

Diner, D.J., and J.V. Martonchik, Atmospheric transfer of radiation above an inhomogeneous non-Lambertian reflective ground: I. Theory, *J. Quant. Spectrosc. Rad. Transf., 31,* 97, 1984a.

Diner, D.J., and J.V. Martonchik, Atmospheric transfer of radiation above an inhomogeneous non-Lambertian reflective ground: II. Computational considerations and results, *J. Quant. Spectrosc. Rad. Transf., 32,* 279, 1984b.

Diner, D.J., and J.V. Martonchik, Influence of aerosol scattering on atmospheric blurring of surface features, *IEEE Trans. Geosci. Remote Sens., GE-23,* 618, 1985a.

Diner, D.J., and J.V. Martonchik, Atmospheric transmittance from spacecraft using multiple view angle imagery, *Appl. Optics, 24,* 3503, 1985b.

Dozier, J., Snow reflectance from Landsat-4 Thematic Mapper, *IEEE Trans. Geosci. Remote Sens., GE-22,* 323, 1984.

Dozier, J., and D. Marks, Snow mapping and classification from Landsat Thematic Mapper, *Ann. Glaciol., 9,* 97, 1987.

Dozier, J., S.R. Schneider, and D.F. McGinnis, Jr., Effect of grain size and snow pack water equivalence on visible and near-infrared satellite observations of snow, *Water Resour. Res., 17,* 1213, 1981.

Dozier, J., and S.G. Warren, Effect of viewing angle on the infrared brightness temperature of snow, *Water Resour. Res., 18,* 1424, 1982.

Eppley, R.W., E. Stewart, M.R. Abbott, and U. Heyman, Estimating ocean primary production from satellite chlorophyll: Introduction to regional differences and statistics for the Southern California Bight, *J. Plankton Res., 7,* 57, 1985.

Fee, E.J., Important factors for estimating annual phytoplankton production in the Experimental Lakes Area, *Can. J. Fish. Aquat. Sci., 37,* 513, 1980.

Fiedler, P.C., Satellite observations of the 1982-1983 El Niño along the U.S. Pacific coast, *Science, 224,* 1251, 1984.

Field, C., J. Merino, and H.A. Mooney, Leaf age and seasonal effects on light, water, and nitrogen use efficiency in a California shrub, *Oecologia, 56,* 341, 1983.

Fogel, R., and K. Cromack, Effect of habitat and substrate quality on Douglas fir litter decomposition in western Oregon, *Can. J. Bot., 55,* 1632, 1977.

Fownes, J.H., and J.D. Aber, Forest canopy chemistry from Blackhawk Island, Wisconsin, Proceedings of the Airborne Imaging Spectrometer Data Analysis Workshop, G. Vane and A.F.H. Goetz, eds., *JPL Pub. 85-41,* Jet Propulsion Laboratory, Pasadena, CA, 1985.

Fraser, R.S., Satellite measurement of mass of Sahara dust in the atmosphere, *Appl. Optics, 15,* 2471, 1976.

Fraser, R.S., and Y.J. Kaufman, The relative importance of aerosol scattering and absorption in remote sensing, *IEEE Trans. Geosci. Remote Sens., GE-23,* 625, 1985.

Freilich, M.H., and D.B. Chelton, Wavenumber spectra of Pacific winds measured by the Seasat scatterometer, *J. Phys. Oceanogr., 16,* 742, 1985.

Gausman, H.W., A.H. Gerbermann, C.L. Wiegand, R.W. Leamer, R.R. Rodriguez, and J.R. Noriega, Reflectance differences between crop residues and bare soils, *Soil Sci. Soc. Am. Proc., 39,* 752, 1975.

Gerstl, S.A.W., Off-nadir optical remote sensing from satellites for vegetation identification, *IGARSS '86, 3,* 1457, 1986.

Gerstl, S.A.W., and C. Simmer, Radiation physics and modelling for off-nadir satellite sensing of non-Lambertian surfaces, *Remote Sens. Environ., 20,* 1, 1986.

Gerstl, S.A.W., C. Simmer, and B.J. Powers, The canopy hot spot as crop identifier, Proceedings of the International Symposium on Remote Sensing for Resources Development and Environmental Management, Aug. 25-29, M.C.A. Damen *et al.,* eds., Balkema Publishers, Enschede, The Netherlands, *ISPRS Pub. 26/7/1, ISSN 0256-1840,* 1986.

Gerstl, S.A.W., and A. Zardecki, Discrete-ordinates finite-element method for atmospheric radiative transfer and remote sensing, *Appl. Optics, 24,* 81, 1985.

Goel, N.S., D.E. Strebel, and R.L. Thompson, Inversion of vegetation canopy reflectance models for estimating agronomic variables: Use of angle transforms and error analysis as illustrated by Suits' model, *Remote Sens. Environ., 14,* 77, 1984.

Goetz, A.F.H., F.C. Billingsley, A.R. Gillespie, M.J. Abrams, R.L. Squires, E.M. Shoemaker, I. Lucchitta, and D.P. Elston, Application of ERTS images and image processing to regional geologic problems and geologic mapping in Northern Arizona, *NASA-JPL Tech. Rep. 32-1597,* 1975.

Goetz, A.F.H., B.N. Rock, and L.C. Rowan, Remote sensing for exploration: An overview, *Econ. Geol., 78,* 573, 1983.

Goetz, A.F.H., and L.C. Rowan, Geologic remote sensing, *Science, 211,* 781, 1981.

Goetz, A.F.H., L.C. Rowan, and M.J. Kingston, Mineral identification from orbit: Initial results from the Shuttle Multispectral Infrared Radiometer, *Science, 218,* 1020, 1982.

Goetz, A.F.H., G. Vane, J.E. Solomon, and B.N. Rock, Imaging spectrometry for Earth remote sensing, *Science, 228,* 1147, 1985.

Gordon, H.R., Reduction of error introduced in the processing of Coastal Zone Color Scanner-type imagery resulting from sensor calibration and solar irradiance uncertainty, *Appl. Optics, 20,* 207, 1981.

Gordon, H.R., D.K. Clark, J.W. Brown, O.B. Brown, R.H. Evans, and W.W. Broenkow, Phytoplankton pigment concentrations in the Middle Atlantic Bight: Comparison of ship determinations and satellite estimates, *Appl. Optics, 22,* 20, 1983.

Govindjee, and P.R. Mohanty, Photochemical aspects of photosynthesis in blue-green algae, in *Taxonomy and Biology of Blue-Green Algae,* T.V. Desikachary, ed., Univ. of Madras, Madras, India, 1972.

Grenfell, T.C., A theoretical model of the optical properties of sea ice in the visible and near infrared, *J. Geophys. Res., 88,* 9723, 1983.

Grenfell, T.C., D.K. Perovich, and J.A. Ogren, Spectral albedos of an alpine snow pack, *Cold Regions Sci. Technol., 4,* 121, 1981.

Grier, C.C., and S.W. Running, Leaf area of mature northwestern coniferous forests: Relation to site water balance, *Ecology, 58,* 893, 1977.

Griggs, M., Measurements of atmospheric aerosol optical thickness over water using ERTS-1 data, *J. Air Poll. Contr. Assoc., 25,* 622, 1975.

Hale, G.M., and M.R. Querry, Optical constants of water in the 200-nm to 200-μm wavelength region, *Appl. Optics, 12,* 555, 1973.

Harding, L.W., B.B. Prezelin, B.M. Sweeney, and J.L. Cox, Primary production as influenced by diel periodicity of phytoplankton photosynthesis, *Mar. Biol. 67,* 179, 1982.

Heinrich, E.W., *The Geology of Carbonatites,* Robert E. Krieger Publishing Company, Huntington, NY, 1980.

Henderson, G.S., W.T. Swank, J.B. Waide, and C.C. Grier, Nutrient budgets of Appalachian and Cascade region watersheds: A comparison, *For. Sci., 24,* 385, 1978.

Hilton, J., Airborne remote sensing for freshwater and estuarine monitoring, *Water Res., 18,* 1195, 1984.

Holligan, P.M., M. Viollier, D.S. Harbour, P. Camus, and M. Champagne-Philippe, Satellite and ship studies of coccolithophore production along a continental shelf edge, *Nature, 304,* 339, 1983.

Holyer, R.J., Toward universal multispectral suspended sediment algorithms, *Remote Sens. Environ., 7,* 323, 1978.

Hooten, D.E., The versatility of near-infrared reflectance devices, *Cereal Foods World, 23,* 176, 1978.

Horne, A.J., and R.C. Wrigley, The use of remote sensing to detect how wind influences blue-green algal distributions, *Verh. Int. Ver. Limnol., 19,* 784, 1975.

Hovis, W.A., D.K. Clark, F. Anderson, R.W. Austin, W.H. Wilson, E.T. Baker, D. Ball, H.R. Gordon, J.L. Mueller, S.Y. El Sayed, B. Sturm, R.C. Wrigley, and C.S. Yentsch, Nimbus-7 Coastal Zone Color Scanner, system description and initial imagery, *Science, 210,* 60, 1980.

Hunt, G.R., Spectral signatures of particulate minerals in the visible and near infrared, *Geophysics, 42,* 501, 1977.

Hunt, G.R., and J.W. Salisbury, Visible and near-infrared spectra of minerals and rocks: I. Silicate minerals, *Modern Geol., 1,* 283, 1970.

Hunt, G.R., and J.W. Salisbury, Visible and near-infrared spectra of minerals and rocks: II. Carbonates, *Modern Geol., 2,* 195, 1971.

Hunt, G.R., and J.W. Salisbury, Visible and near-infrared spectra of minerals and rocks: XI. Sedimentary rocks, *Modern Geol., 5,* 211, 1976a.

Hunt, G.R., and J.W. Salisbury, Visible and near-infrared spectra of minerals and rocks: XII. Metamorphic rocks, *Modern Geol., 5,* 219, 1976b.

Hunt, G.R., J.W. Salisbury, and C.J. Lenhoff, Visible and near-infrared spectra of minerals and rocks: III. Oxides and hydroxides, *Modern Geol., 2,* 195, 1971a.

Hunt, G.R., J.W. Salisbury, and C.J. Lenhoff, Visible and near-infrared spectra of minerals and rocks: IV. Sulphides and sulphates, *Modern Geol., 3,* 1, 1971b.

Hunt, G.R., J.W. Salisbury, and C.J. Lenhoff, Visible and near-infrared spectra of minerals and rocks: V. Halides, phosphates, arsenates, vanadates, and borates, *Modern Geol., 3,* 121, 1972.

Hunt, G.R., J.W. Salisbury, and C.J. Lenhoff, Visible and near-infrared spectra of minerals: VI. Additional silicates, *Modern Geol., 4,* 85, 1973a.

Hunt, G.R., J.W. Salisbury, and C.J. Lenhoff, Visible and near-infrared spectra of minerals and rocks: VII. Acidic igneous rocks, *Modern Geol., 4,* 217, 1973b.

Hunt, G.R., J.W. Salisbury, and C.J. Lenhoff, Visible and near-infrared spectra of minerals and rocks: VIII. Intermediate igneous rocks, *Modern Geol., 4,* 237, 1973c.

Hunt, G.R., J.W. Salisbury, and C.J. Lenhoff, Visible and near-infrared spectra of minerals and rocks: IX. Basic and ultrabasic rocks, *Modern Geol., 5,* 15, 1974.

Hyvärinen, T., and J. Lammasniemi, Infrared measurement of free-water content and grain size of snow, *Opt. Engrg., 26,* 342, 1987.

Jackson, R.D., R.J. Reginato, P.J. Pinter, Jr., and S.B. Idso, Plant canopy information extraction from composite scene reflectance of row crops, *Appl. Optics, 18,* 3775, 1979.

Johnson, P.E., M.O. Smith, S. Taylor-George, and J.B. Adams, A semi-empirical method for analysis of the reflectance spectra of binary mineral mixtures, *J. Geophys. Res., 88,* 3557, 1983.

Kahle, A.B., and A.F.H. Goetz, Mineralogic information from a new airborne thermal infrared multispectral scanner, *Science, 222,* 24, 1983.

Kahru, M., Phytoplankton patchiness generated by long internal waves, *Mar. Ecol., 10,* 111, 1983.

Kapustin, Y.L., *Mineralogy of Carbonatites,* Nauka Publishers, Moscow, 1971 (Translated from Russian, Smithsonian Institution and National Science Foundation, Washington, DC, Amerind Foundation Co. Pvt. Ltd., New Delhi, India, 1980).

Karmanov, I.I., Study of soils from the spectral composition of reflected radiation, *Sov. Soil Sci., 4,* 226, 1970.

Kaufman, Y.J., and J.H. Joseph, Determination of surface albedos and aerosol extinction characteristics from satellite imagery, J. *Geophys. Res., 87,* 1287, 1982.

Kiefer, D.A., and B.G. Mitchell, A simple steady state description of phytoplankton growth based on absorption cross section and quantum efficiency, *Limnol. Oceanogr., 28,* 770, 1983.

Kimes, D.S., Dynamics of directional reflectance factor distributions for vegetation canopies, *Appl. Optics, 22,* 1364, 1983.

Kimes, D.S., Modeling the directional reflectance from complete homogeneous vegetation canopies with various leaf-orientation distributions, J. *Opt. Soc. Amer., A1,* 725, 1984.

Kimes, D.S., B.N. Holden, C.J. Tucker, and W.W. Newcomb, Optimal directional view angles for remote sensing missions, *Intl. J. Remote Sens., 5,* 887, 1984.

Kimes, D.S., and P.J. Sellers, Inferring hemispherical reflectance of the Earth's surface for global energy budgets from remotely sensed nadir or directional radiance values, *Remote Sens. Environ., 18,* 205, 1985.

Kira, T., and T. Shidei, Primary production and turn-over of organic matter in different forest ecosystems of the western Pacific, *Japan J. Ecol., 17,* 70, 1967.

Kirchner, J.A., J.A. Smith, and S. Youkhana, Influence of sky radiance distribution on the ratio technique for estimating bidirectional reflectance, *Photogram. Engrg. Remote Sens., 48,* 955, 1982.

Kirk, J.T.G., *Light and Photosynthesis in Aquatic Ecosystems,* Cambridge Univ. Press, Cambridge, England, 1983.

Kishino, M., S. Sugihara, and N. Okami, Estimation of quantum yield of chlorophyll *a* fluorescence from the upward irradiance spectrum in the sea, *La Mer, 22,* 233, 1984.

Klein, P., and B. Coste, Effects of wind–stress variability on nutrient transport into the mixed layer, *Deep-Sea Res., 31,* 21, 1984.

Kristof, S.J., Preliminary multispectral studies of soils, J. *Soil Water Conserv., 26,* 15, 1971.

Larsson, S., R. Oren, R. Waring, and J.W. Barrett, Attacks of mountain pine beetle as related to tree vigor of ponderosa pine, *For. Sci., 29,* 395, 1983.

Laurs, R.M., P.C. Fiedler, and D.R. Montgomery, Albacore tuna catch distributions relative to environmental features observed from satellites, *Deep-Sea Res., 31,* 1085, 1984.

Lemoalle, J., Application des images Landsat a la courbe bathymetrique du Lac Tchad, *Cah. ORSTOM Hydrobiol., 12,* 83, 1978.

Lemoalle, J., Application des donnees Landsat a l'estimation de la production du phytoplankton dans Lac Tchad, *Cah. ORSTOM Hydrobiol., 13,* 1979.

Lennon, J.M., J.D. Aber, and J.M. Melillo, Primary production and nitrogen allocation of field grown sugar maple in relation to nitrogen availability, *Biogeochemistry, 1,* 135, 1985.

Li, S., A model for the anisotropic reflectance of pure snow, *Disc. Pap. 4,* Department of Geography, University of California, Santa Barbara, CA, 1982.

Li, S., Z. Wan, and J. Dozier, A component decomposition model for evaluating atmospheric effects in remote sensing, J. *Electromag. Waves Appl., 1,* 323, 1987.

Likens, G.E., F.H. Bormann, R.S. Pierce, J.S. Eaton, and N.M. Johnson, *Biogeochemistry of a Forested Ecosystem,* Springer-Verlag, New York, NY, 1977.

Lindberg, J.D., and D.G. Snyder, Diffuse reflectance spectra of several clay minerals, *Am. Mineral, 57,* 485, 1972.

Lindell, L.T., Experiences from correlations of Landsat data versus transmission of light and chlorophyll *a, Verh. Int. Ver. Limnol., 21,* 438, 1981.

Linder, S., Potential and actual production in Australian forest stands, in *Research for Forest Management,* Proceedings of Conference Organized by the Director of Forest Research, C.S.I.R.O., Australia, 1985.

Lyons, W.A., and R.A. Northouse, The use of ERTS-1 imaging in air pollution and mesometeorological studies around the Great Lakes, Third Earth Resources Technology Satellite-1 Symposium, *NASA SP-351*, 1974.

Mackas, D.L., K.L. Denman, and M.R. Abbott, Plankton patchiness: Biology in the physical vernacular, *Bull. Mar. Sci., 37,* 652, 1985.

Marks, D., and J.M. Melack, Spectral reflectance properties of water surfaces in the Amazon basin of Brazil, *Eos, Trans. Amer. Geophys. Union, 63,* 936, 1982.

Matson, M., and D.R. Wiesnet, New data base for climate studies, *Nature, 289,* 451, 1981.

McKee, T.B., and S.K. Cox, Scattering of visible radiation by clouds, *J. Atmos. Sci., 31,* 1885, 1974.

Meentemeyer, V., Macroclimate and lignin control of litter decomposition rates, *Ecology, 59,* 465, 1978.

Mekler, Y., H. Quenzel, G. Ohring, and I. Marcus, Relative atmospheric aerosol content from ERTS observations, *J. Geophys. Res., 82,* 967, 1977.

Melack, J.M., Inland aquatic resources and biogeochemical cycles, Science and Mission Requirements Working Group, Earth Observing System, *NASA Tech. Memor. 86129,* Goddard Space Flight Center, 1984.

Melillo, J.M., J.D. Aber, and J.F. Muratore, Nitrogen and lignin control of hardwood leaf litter decomposition dynamics, *Ecology, 63,* 621, 1982.

Merrill, W., and E.B. Cowling, Role of nitrogen in wood deterioration: Amounts and distribution of nitrogen in tree stems, *Can. J. Bot., 44,* 1555, 1966.

Mooney, H.A., and S.L. Gulmon, Constraints on leaf structure and function in reference to herbivory, *BioSci., 32,* 198, 1982.

Morel, A., and L. Prieur, Analysis of variations in ocean color, *Limnol. Oceanogr., 22,* 709, 1977.

Myers, V.I., and W.A. Allen, Electro-optical remote sensing methods as nondestructive testing and measuring techniques in agriculture, *Appl. Optics, 7,* 1819, 1968.

National Academy of Sciences, *A Strategy for Earth Science from Space in the 1980s, Part 1, Solid Earth and Oceans,* National Academy Press, Washington, DC, 1982.

National Academy of Sciences, *A Strategy for Earth Science from Space in the 1980s and 1990s, Part 2, Atmosphere and Interactions with the Solid Earth, Oceans, and Biota,* National Academy Press, Washington, DC, 1985.

National Academy of Sciences, *Global Change in the Geosphere-Biosphere, Initial Priorities for an IGBP,* National Academy Press, Washington, DC, 1986a.

National Academy of Sciences, *Remote Sensing of the Biosphere,* National Academy Press, Washington, DC, 1986b.

National Aeronautics and Space Administration, *Earth System Science: Overview,* Washington, DC, 1986.

Norman, J.M., and J.M. Welles, Radiative transfer in an array of canopies, *Agron. J., 75,* 481, 1983.

Nussenzveig, H.M., and W.J. Wiscombe, Efficiency factors in Mie scattering, *Phys. Rev. Lett., 45,* 1490, 1980.

O'Brien, H.W., and R.W. Munis, Red and near-infrared spectral reflectance of snow, *CRREL Res. Rep. 332,* U.S. Army Cold Regions Research and Engineering Laboratory, Hanover, NH, 1975.

Obukhov, A.I., and D.S. Orlov, Spectral reflectivity of the major soil groups and possibility of using diffuse reflection in soil investigations, *Sov. Soil Sci., 2,* 174, 1964.

Pastor, J., J.D. Aber, C.A. McClaugherty, and J.M. Melillo, Aboveground production and N and P cycling along a nitrogen mineralization gradient on Blackhawk Island, Wisconsin, *Ecology, 65,* 256, 1984.

Pearce, W.A., A study of the effects of the atmosphere on thematic mapper observations, *Report 004-77,* Contract NAS5-23629, EG&G/Washington Analytical Services Center, Inc., Riverdale, MD, 1977.

Pearce, W.A., Monte Carlo study of the atmospheric point spread functions, *Appl. Optics, 25,* 438, 1986.

Pecora, W.T., Carbonatites—A review, *Geol. Soc. Amer. Bull., 67,* 1537, 1956.

Pettijohn, F.J., *Sedimentary Rocks,* Harper and Brothers, New York, NY, 1975.

Planet, W.G., Some comments on reflectance measurements of wet soils, *Remote Sens. Environ., 1,* 127, 1970.

Prezelin, B.B., Photosynthetic physiology of dino-flagellates, in *The Dinoflagellates*, F.J.R. Taylor, ed., Blackwell Publishers, London, England, 1987.

Prezelin, B.B., and B.A. Boczar, Molecular basis of cell absorption and fluorescence in phytoplankton: Potential applications to studies in optical oceanography, in *Progress in Phycological Res.*, 4, F. Round and D. Chapman, eds., 1986.

Rango, A., J.F. Hannaford, R.L. Hall, M. Rosenzweig, and A.J. Brown, Snow covered area utilization in runoff forecasts, *ASCE J. Hydraul. Div.*, 105, 53, 1979.

Rango, A., and K.I. Itten, Satellite potentials in snowcover monitoring and runoff prediction, *Nordic Hydrol.*, 7, 209, 1976.

Rango, A., and J. Martinec, Application of a snowmelt-runoff model using Landsat data, *Nordic Hydrol.*, 10, 225, 1979.

Rango, A., V.V. Salomonson, and J.L. Foster, Seasonal streamflow estimation in the Himalayan region employing meteorological satellite snow cover observations, *Water Resour. Res.*, 14, 359, 1977.

Rock, B.N., J.E. Vogelmann, D.L. Williams, A.F. Vogelmann, and T. Hoshizaki, Remote detection of forest damage, *BioSci.*, 36, 439, 1986.

Rotolo, P., Near infrared reflectance instrumentation, *Cereal Foods World*, 24, 94, 1979.

Rowan, L.C., A.F.H. Goetz, J.K. Crowley, and M.J. Kingston, Identification of hydrothermal mineralization in Baja California, Mexico from orbit using the Shuttle Multispectral Infrared Radiometer, *IGARSS '83*, 1, 3.1, 1983.

Rowan, L.C., P.H. Wetlaufer, A.F.H. Goetz, F.C. Billingsley, and J.H. Stewart, Discrimination of rock types and detection of hydrothermally altered areas in South-Central Nevada by the use of computer-enhanced ERTS images, *U.S. Geol. Survey Prof. Paper 883*, 1974.

Salomonson, V.V., and W.E. Marlatt, Anisotropic solar reflectance over white sand, snow, and stratus clouds, *J. Appl. Meteorol.*, 7, 475, 1968.

Sauer, K., Primary events and the trapping of energy, in *Bioenergetics of Photosynthesis*, Govindjee, ed., Academic Press, New York, NY, 1975.

Shugart, H.H., and D.C. West, Forest succession models, *BioSci.*, 30, 308, 1980.

Simmer, C., and S.A.W. Gerstl, Remote sensing of angular characteristics of canopy reflectances, *IEEE Trans. Geosci. Remote Sens.*, GE-23, 648, 1985.

Singer, R.B., Near-infrared spectral reflectance of mineral mixtures: Systematic combinations of pyroxenes, olivine and iron oxides, *J. Geophys. Res.*, 86, 7967, 1981.

Smith, J.A., Matter-energy interaction in the optical region, in *Manual of Remote Sensing*, R.N. Colwell, ed., Amer. Soc. Photogram. Remote Sens., Falls Church, VA, 1983.

Smith, J.A., and R.E. Oliver, Plant canopy models for stimulating composite scene spectroradiance in the 0.14 to 1.05 μm region, *Proc. Eighth Int. Symp. Remote Sensing Environ.*, 1333, University of Michigan, Ann Arbor, 1972.

Smith, J.A., and R.E. Oliver, Effects of changing canopy directional reflectance on feature selection, *Appl. Optics*, 13, 1559, 1974.

Smith, R.C., R.W. Eppley, and K.S. Baker, Correlation of primary production as measured aboard ship in southern California coastal waters and as estimated from satellite chlorophyll images, *Mar. Biol.*, 66, 281, 1982.

Spanner, M.A., D.L. Peterson, W. Acevedo, and P. Matson, High resolution spectrometry of leaf canopy chemistry for biogeochemical cycling, Proceedings of the Airborne Imaging Spectrometer Data Analysis Workshop, *JPL Pub. 85-41*, G. Vane and A.F.H. Goetz, eds., Jet Propulsion Laboratory, Pasadena, CA, 1985.

Spanner, M.A., K.W. Teuber, W. Acevedo, D.L. Peterson, S.W. Running, D.H. Card, and D.A. Mouat, Remote sensing of the leaf area index of temperate coniferous forests, *Proc. 10th Intl. Symp. Machine Process. Remotely Sensed Data*, 362, Purdue University, West Lafayette, IN, 1984.

Stoner, E.R., Physicochemical, site, and bidirectional reflectance factor characteristics of uniformly moist soils, Ph.D. dissertation, Purdue Univ., West Lafayette, Ind. (Libr. Congr. Card No. Mic. 80-15525) Univ. Microfilms, Ann Arbor, Mich. (Diss. Abstr. 41:22-B), 1979.

Stoner, E.R., and M.F. Baumgardner, Characteristic variations in reflectance of surface soils, *Soil Sci. Soc. Am. J.*, 45, 1161, 1981.

Stoner, E.R., M.F. Baumgardner, R.A. Weismiller, L.L. Biehl, and B.F. Robinson, Extension of laboratory measured soil spectra to field conditions, *Soil Sci. Soc. Am. J.*, 44, 572, 1980.

Strahler, A.H., and X. Li, An invertible coniferous forest canopy reflectance model, *Proc. 15th Intl. Symp. Remote Sens. Environ.*, University of Michigan, Ann Arbor, 1981.

Strong, A.E., Remote sensing of algal blooms on aircraft and satellite in Lake Erie and Utah Lake, *Remote Sens. Environ., 3,* 99, 1974.

Strong, A.E., and B.J. Eadie, Satellite observations of calcium carbonate precipitations in the Great Lakes, *Limnol. Oceanogr., 23,* 877, 1978.

Stuhlmann, R., P. Minnis, and G.L. Smith, Cloud bidirectional reflectance functions: A comparison of experimental and theoretical results, *Appl. Optics, 24,* 396, 1985.

Suits, G.H., The cause of azimuthal variations in directional reflectance of vegetative canopies, *Remote Sens. Environ., 22,* 175, 1972.

Taylor, V.R., and L.L. Stowe, Reflectance characteristics of uniform Earth and cloud surfaces derived from Nimbus-7 ERB, *J. Geophys. Res., 89,* 4987, 1984.

Tsay, M.L., D.H. Gjerstad, and G.R. Glover, Tree leaf reflectance: A promising technique to rapidly determine nitrogen and chlorophyll content, *Can. J. For. Res., 12,* 788, 1982.

Tricart, J., La cartographie géomorphologique detailée, in *Principe et methodes de la geomorphologie,* Paris: Masson, 1965.

Tucker, C.J., J.R.G. Townshend, and T.E. Goff, African land-cover classification using satellite data, *Science, 227,* 369, 1985.

Valovcin, F.R., Snow/cloud discrimination, *Report AFGL-TR-76-0174,* Air Force Geophysics Laboratory, Hanscom Air Force Base, MA, 1976.

Vane, G., M. Chrisp, H. Enmark, S. Macenka, and J. Solomon, Airborne Visible/Infrared Imaging Spectrometer: An advanced tool for Earth remote sensing, *IGARSS '84, SP215,* 751, 1984a.

Vane, G., A.F.H. Goetz, and J.B. Wellman, Airborne Imaging Spectrometer: A new tool for remote sensing, *IEEE Trans. Geosci. Remote Sens., GE-22,* 546, 1984b.

Vane, G., and A.F.H. Goetz, eds., Proceedings of the Airborne Imaging Spectrometer Data Analysis Workshop, *JPL Publication 85-41,* Jet Propulsion Laboratory, Pasadena, CA, 1985.

Vane, G., and A.F.H. Goetz, eds., Proceedings of the Second Airborne Imaging Spectrometer Data Analysis Workshop, *JPL Publication 86-35,* Jet Propulsion Laboratory, Pasadena, CA, 1986.

Waring, R.H., J.D. Aber, J.M. Melillo, and B. Moore III, Precursors of change in terrestrial ecosystems, *BioSci., 36,* 433, 1986.

Waring, R.H., and G.B. Pitman, Modifying lodgepole pine stands to change susceptibility for mountain pine beetle attack, *Ecology, 66,* 889, 1985.

Warren, S.G., Optical properties of snow, *Rev. Geophys. Space Phys., 20,* 67, 1982.

Warren, S.G., Optical constants of ice from the ultraviolet to the microwave, *Appl. Optics, 23,* 1206, 1984.

Warren, S.G., and W.J. Wiscombe, A model for the spectral albedo of snow, II, Snow containing atmospheric aerosols, *J. Atmos. Sci., 37,* 2734, 1980.

Weismiller, R.A., and S.A. Kaminsky, Application of remote sensing technology to soil survey research, *J. Soil Water Conserv., 33,* 287, 1978.

Weismiller, R.A., F.R. Kirschner, S.A. Kaminsky, and E.J. Hinzel, Spectral classification of soil characteristics to aid the soil surface of Jasper County, Indiana, *LARS Technical Report 040179,* Purdue Univ., W. Lafayette, IN, 1979.

Wellman, J., A.F.H. Goetz, M. Herring, and G. Vane, An imaging spectrometer experiment for the Shuttle, *IGARSS '83, 2,* 6.1, 1983.

Wessman, C.A., J.D. Aber, and D.L. Peterson, Estimating key forest ecosystem paramters through remote sensing, *IGARSS '87, 2,* 1189, Ann Arbor, MI, 1987.

Westin, F.C., and C.J. Frazee, Landsat data: Its use in a soil survey program, *Soil Sci. Soc. Am. J., 40,* 81, 1976.

Wiscombe, W.J., Improved Mie scattering algorithms, *Appl. Optics, 19,* 1505, 1980.

Wiscombe, W.J., and S.G. Warren, A model for the spectral albedo of snow, I, Pure snow, *J. Atmos. Sci., 37,* 2712, 1980.

Yentsch, C.M., and C.S. Yentsch, Emergence of optical instrumentation for measuring biological parameters, *Oceanogr. Mar. Bio. Ann. Rev., 22,* 55, 1984.